SAMUELMIKOVINY
DOCTORAL SCHOOL OF EARTH SCIENCES
AND ENGINEERING

Head of Doctoral School:
Dr. h.c.mult, Dr. Ferenc Kovacs
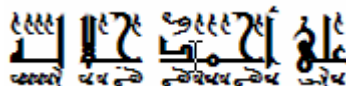Member of the Hungarian Academy of Sciences

Ph.D. DISSERTATION

DETERMINATION AND ANALYSIS OF POROUS ROCK
COMPRESSIBILITY OF HUNGARIAN ROCK SAMPLES

by

ALI AHMED JALALH

Scientific Supervisor
Dr. BÓDI TIBOR

A DISSERTATION PRESENTED TO **MIKOVINY SAMUEL**
DOCTORAL SCHOOL OF EARTH SCIENCES AND ENGINEERING
OF THE UNIVERSITY OF MISKOLC IN PARTIAL FULFILLMENT
OF THE REQUIREMENTS FOR THE DEGREE OF
DOCTOR OF PHILOSOPHY

UNIVERSITY OF MISKOLC

2006

A DISSERTATION PRESENTED TO **MIKOVINY SAMUEL
DOCTORAL SCHOOL OF EARTH SCIENCES AND ENGINEERING**
OF THE UNIVERSITY OF MISKOLC IN PARTIAL FULFILLMENT
OF THE REQUIREMENTS FOR THE DEGREE OF
DOCTOR OF PHILOSOPHY

UNIVERSITY OF MISKOLC

PETROLEUM ENGINEERING

Copyright 2006

by

ALI AHMED JALALH

DEDICATION

This document is dedicated to those who love me more than themselves, my parents.

ACKNOWLEDGMENTS

TABLE OF CONTENTS

LIST OF TABLES

LIST OF FIGURES

XIII

XV

XVI

CHAPTER 1
1. **INTRODUCTION**

1.1 STATEMENT OF PROBLEM

The most important properties of underground gas storage are the mobile and cushion gas and the pick capacity of the producing wells. There is a strong relationship between the actual reservoir pore volume and the volume of injected gas, the amount of mobile gas, and the capacity of gas producing wells. The pressure of the reservoir after injection or production of gas can be determined by the material balance calculation.

The conventional material balance calculation neglects the isothermal compressibility of the reservoir rock and fluids. Neglecting the compressibility will cause incorrect estimation of total gas in place, and the pressure that can be reached after injecting and producing a certain amount of gas. The error in the calculated pressure will result in an incorrect estimation of well capacity. This will mislead the management of cycling operation of underground gas storage.

The consideration of rock compressibility becomes increasingly important for deeper, high-pressure gas reservoirs or underground gas storage. The reservoir characterization process aims at the incorporation into the reservoir models of all data available, so that more realistic models can be generated for improved prediction capabilities.

The use of pore-volume compressibility porosity correlations in engineering calculations is well known. The correlations developed by H. N. Hall [1953] and R. N. Horne [1990] for both sandstone and limestone have been widely distributed. Van der Knaap [1959] published a similar correlation using limestone samples from a single well and correlated the data with net pressure.

Such correlations are attractive because of the simple relationship established. However, those correlations were intended only for well-consolidated samples: correlations for friable and consolidated sandstones have not been published, with the

1

exception of R. N. Horne [1990], who gave correlations of friable, unconsolidated and consolidated reservoir rocks using measurement results of G. H. Newman [1973].

The main object of this work is to measure the compressibility of some limestones and sandstones with a wide range of porosity and varied rock type from underground gas storage in Hungary. This study compares my laboratory data with the published correlations of consolidated limestone samples as well as with values for friable, and consolidated sandstones and investigates the validity of using compressibility data from the literature. This thesis provides a detailed analysis of the use of pore volume compressibility in material balance calculations for oil and gas reservoirs.

The effects of changes of pore volume during the cycling operation of underground gas storage have been investigated. The measured data shows poor agreement with the published correlations by Hall and Horne.

My approach to finding better and more accurate rock compressibility correlation consists of combing all the available data in literature and using the same Horne's formula type. Nonetheless, this attempt does not give a satisfactory fitting result. By using twelve different fitting formulas and professional nonlinear regression programs, I was able to develop new rock compressibility correlations for limestone and sandstone rock with better fitting results. These new correlations can be generalized and used for most; oil and gas reservoirs.

The structure of the thesis is the following. In Chapter 2, some basic concepts of compressibility of porous media that are used in this work are introduced. In the second part, I review the basic concepts of the mathematical expression of compressibility and the relationship between compressibilities in detail. The third part of the chapter explains the effective stress coefficient. The concept of "effective stress" has long been used in rock mechanics. The motivation for this concept is that since the pore pressure and confining pressure tend to have opposite effects on the volumes (as well as on most petrophysical properties, such as permeability, electrical resistivity, etc.), it would be convenient to subtract some fraction of the pore pressure from the confining pressure and then treat the pressure as a single variable. The last part presents an extensive and deep review of previously published literature dealing with rock compressibilities.

Chapter 3 presents an introduction to the poroelasticity theory, which was pioneered by Biot [1941]. The theory of poroelasticity is fundamentally a higher-order theory than that of classical elasticity, in that it involves concepts such as "pore pressure" and "pore strain" that have no analog in classical mechanics. The measurements I performed in this

work on samples of various limestones and sandstones confirmed the theoretical framework of poroelasticity theory.

Chapter 4 introduces the compressibility apparatus that was used to perform the measurements of pore volume compressibility in this study. It also presents all the technical aspects, porosity measurements and calculations. I developed an easier method for equipment correction and calibration than that explained in the manufacturer's user manual. Chapter 5 is dedicated to the analysis of the results obtained from measurements of rock samples. Rock identity cards of the used core samples are also presented.

Two different approaches are addressed in Chapter 6. The first section addresses the Modified Horne's correlation. The second section is dedicated to developing newly pore volume correlations for limestone and sandstone reservoir rocks.

Chapter 7 is focused on use of the pore volume compressibility data in oil and gas calculations for improving reservoir analysis. The final Chapter provides a summary of the main conclusions of the thesis.

CHAPTER 2
2. BACKGROUND AND LITERATURE REVIEW

2.1 COMPRESSIBILITY OF POROUS ROCKS

Compressibility is the parameter that quantifies the relationship between the pressure exerted on a body and the resulting change in its volume. A non-porous material has a single compressibility, C, defined [Collins, 1961] by:

$$C = -\frac{1}{V}\frac{\partial v}{\partial p}$$

(2.1)

where V is the volume of the body, and P is the hydrostatic pressure exerted over its outer surface. In the general definition of compressibility given by Eqn. (2.1), rock compressibility in terms of change to pore volume should be a negative quantity. However, the effect of an increase in pore volume with an increase in pressure can be pictured as an increase in the size of the container holding reservoir fluids. If the volume stain (dε) = -CdP (change in the compressibility with pressure) container volume is held constant, the same effect could be achieved by additional shrinkage of same contained fluids. Thus, the effective rock compressibility may be considered a positive quantity additive to fluid compressibility, which is the usual thermodynamic convention. In the above definition, as well as all of those, which follow, it is implicitly assumed that the temperature is held constant as the pressure is being varied.

As shown in Eqn. 2.2, the bulk volume V_b is defined as the volume that would be measured if the presence of the pores were ignored. The pore volume V_p is defined as that part of the bulk volume which is not occupied by rock minerals. These two volumes are related by

$$V_b - V_p = V_s$$

(2.2)

where V_s is the volume occupied by the mineral grains. Geophysicists and petroleum engineers usually quantify the relative amounts of pore space and minerals in the rock by the porosity ф, defined by

$$\phi = V_p/V_b$$

(2.3)

Civil engineers often use the void ratio e, defined by

$$e = V_p/V_s = \frac{V_p}{V_b - V_p} = \frac{\phi}{1 - \phi} \qquad (2.4)$$

Note that while the porosity is restricted, by definition, to the range $0 \leq \phi < 1$, the void ratio can take on any positive value. Although the void ratios of some uncompacted near-surface soils are greater than unity, since their porosities may exceed 50%, values of e for consolidated sandstones will typically be less than one, since their porosities will be less than 50%.
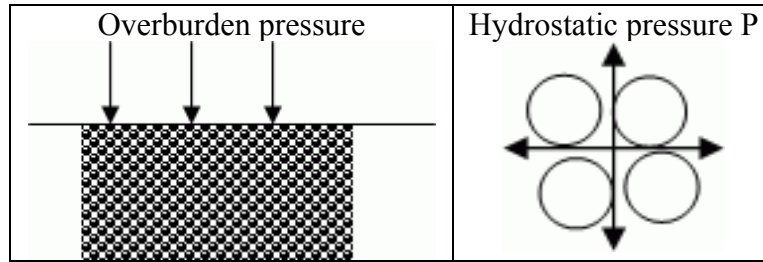
Figure 2.1: Illustration of the two types of stresses.
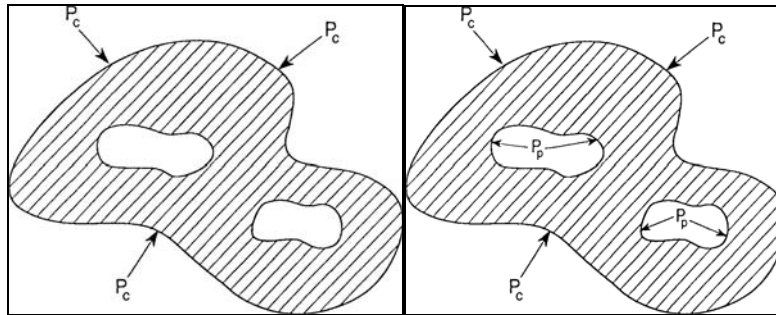
Figure 2.2: Illustration of the overburden confining pressure P_c and internal pore-pressure P_p of porous body

Since experimental observations have a wide scatter, there is little expectation that measurements from one reservoir will necessarily apply to another reservoir or even a different part of the same reservoir. Jalalh and Bódi [2004] have studied and investigated the importance of rock compressibility factor in material balance in gas reservoir. We used data from Hungarian underground gas storage and the new material balance [Fetkovich et al., 1991] to investigate and study the effect of the compressibility on Original Gas In Place (OGIP) calculations [Jalalh & Bódi, 2004]. Detailed results are presented in Chapter 7.

The production of oil or water from underground reservoirs or injection of displacing fluids results in local changes of the stress field because of pressure changes in permeable formations surrounding wells. The resulting reservoir deformations tend to alter porosity of the reservoir rock and can have a pronounced effect on conditions of fluid flow.

Modification of the reservoir effective stress due to production causes volumetric changes in pore space in a reservoir. The engineering parameters quantifying these volumetric variations are compressibilities. Reliable compressibility values are essential for resource estimation, reservoir maintenance and drive assessments, as well as subsidence evaluations [Ruddy et al., 1989; Johnson et al., 1989; Geertsma, 1973]. Production forecasting is intimately related to a total system compressibility combining the compressibilities of liquid and gaseous phases in the pore space, the grain compressibility of the solid portions and the pore volume compressibility, often referred to as formation compressibility.

2.2 MATHEMATICAL EXPRESSIONS FOR COMPRESSIBILITY

Since there are two independent volumes and two pressures that can be varied, four different compressibilities can be associated with a porous rock. Each of these porous rock compressibilities relates changes in either the pore volume V_p or the bulk volume V_b to changes in the pore pressure P_p or the confining pressure P_c. Using a notation in which the first subscript indicates the relevant volume change, and the second subscript indicates the pressure which is varied, the most commonly used definitions of compressibility [Biot, 1941] are as follows,

$$C_{bc} = -\frac{1}{V_b}\left[\frac{\partial V_b}{\partial p_c}\right]_{Pp} \tag{2.5}$$

$$C_{bP} = -\frac{1}{V_b}\left[\frac{\partial V_b}{\partial p_p}\right]_{Pc} \tag{2.6}$$

$$C_{pc} = -\frac{1}{V_p}\left[\frac{\partial V_p}{\partial p_c}\right]_{Pp} \tag{2.7}$$

$$C_{pp} = -\frac{1}{V_p}\left[\frac{\partial V_p}{\partial p_p}\right]_{Pc} \tag{2.8}$$

The two compressibilities defined by Eqns. (2.5) and (2.6), namely C_{bc} and $C_{bp,}$ are referred to as bulk compressibilities, since they involve changes in the bulk volume of the rock. The bulk compressibility C_{bc} is analogs to the compressibility of a non-porous material as defined by Eqn. (2.1). As far as fluid-saturated sandstone can be treated as a homogeneous material, C_{bc} will be its effective bulk compressibility. The other bulk compressibility, C_{bp} that was called the "pseudo-bulk compressibility" by Fatt [1958a],

reflects the influence of pore pressure on the bulk volume. This compressibility is useful in subsidence calculations, for instance [Geertsma, 1973].

The compressibilities defined by Eqns. (2.5) and (2.6) involve changes in the bulk volume of the rock and not pressure variations on the volume of void space contained in the rock. I could point out these compressibilities are mainly applied to common engineering material such as steel or ceramics, and commonly used in civil engineering to prevent cause extensive damage to the building and other surface subsidence. Well-known examples of oilfield subsidence include the Wilmington-Long Beach field in Southern California [Gilluly and Grant, 1949], and the Ekofisk field in the North Sea [Johnson et al., 1989]. In the oil and gas sector, C_{bc} and C_{bp} are very useful for geophysical applications in large-scale tectonic as well as in wave propagation problems.

The other two compressibilities, C_{pc} and C_{pp}, are pore compressibilities, and express the effect of pressure variations on the volume of void space contained in the rock. Hall [1953] referred to C_{pc} as the "formation compaction" coefficient, and to C_{pp} as the "effective pore compressibility". The pore compressibility C_{pp} is used in reservoir analysis, since it reflects the volume of excess pore fluid that can be stored in the pore space with an increase in the pore pressure. This compressibility is added to that of the reservoir fluid C_f in order to represent the "reservoir compressibility", a term that is used in the basic equation of reservoir analysis.

These compressibilities express the effect of pressure variations on the volume of void space contained in the rock and truly reflect in-situ conditions. The CorLab's compressibility apparatus available in Miskolc University, which was used to carry this work out is designed to measure directly the value of C_{pc} values, not C_{pp} values.

The bulk and pore strain increments can be expressed in terms of the porous rock compressibilities as follows:

$$d_{\varepsilon b} = -C_{bc}dP_c + C_{bp}dP_p \tag{2.9}$$

$$d_{\varepsilon p} = -C_{pc}dP_c + C_{pp}dP_p \tag{2.10}$$

For single-phase liquid flow, the governing equation of pressure transient analysis for reservoirs is [Matthews and Russell, 1967],

$$\nabla^2 P_p = \frac{\phi \mu C_f}{k} \frac{\partial P_p}{\partial t} \tag{2.11}$$

where V^2 is the Laplacian operator, μ. is the viscosity of the pore fluid, k is the formation permeability and Ct = Cf + Cpp is the total "compressibility" of the rock/fluid system.

To measure the pore compressibility that truly reflects in-situ conditions, one should generally use C_{pp}, as defined in [Ruddy et al., 1989]. In order to correctly determine the in-situ pore volume, the core is placed in a pressure vessel, and the confining stress is increased to its in-situ value, P_c. Such experiments therefore involve the pore compressibility C_{pc} that relates the change in pore volume to the confining pressure.

Since positive confining pressures will decrease the volumes V_p and V_b while positive pore pressures will increase V_p and V_b, the definitions of the two compressibilities that involve changes in the confining pressure both contain minus signs, to ensure that the numerical values of all four compressibilities will be positive.

Typical behavior of a porous rock compressibility as a function of stress is shown in Fig. 2.3 for a Frio sandstone from East Texas [Carpenter and Spencer, 1940]. This core was taken from a depth of 5460 feet, and had an initial porosity of 30%. Fig. 2.3a shows the pore strain as a function of confining pressure, with the pore pressure held constant at 0 psi. At low pressures, the curve is very nonlinear, but above about 6000 psi the curve resembles that of a conventional elastic solid. The derived compressibility C_{pc} is shown in Fig. 2.3b. The behavior of the other porous rock compressibilities is qualitatively similar to that shown for C_{pc} in Fig. 2.3.
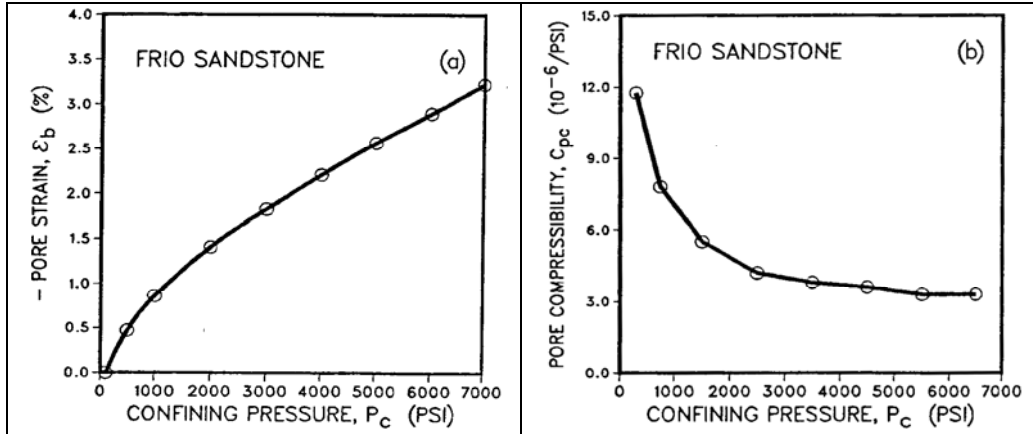
Figure 2.3: Pore strain ε_b (a) and pore compressibility C_{pc} (b) in a Frio sandstone from East Texas, as a function of confining pressure, at zero pore pressure [after Carpenter and Spencer, 1940].

I also observed similar behavior of porous rock compressibility as a function of pore volume change and pore volume compressibility with confining pressure held constant at 7 psi as illustrated through Algyo sandstones from Hungary. Figure 2.4 demonstrates that as

the pressures are low, the curve is very nonlinear, but above about 6000 psi, the curve resembles that of a conventional elastic solid material.
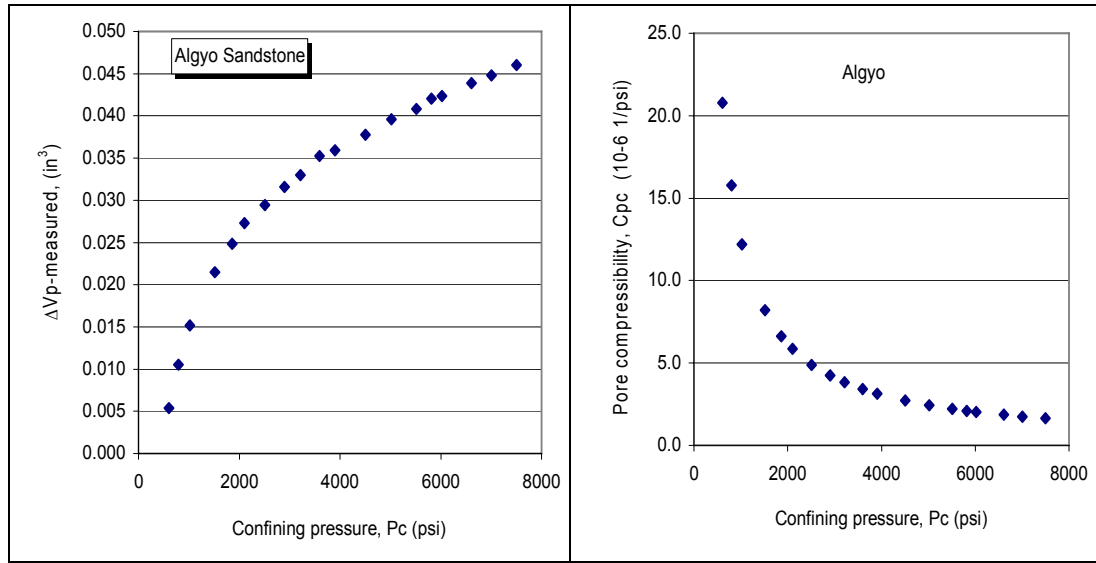
Figure 2.4: ΔV_p measured (Pore volume change) (left) and Pore volume compressibility C_{pc} (right) as a function of confining pressure P_c, at very low (7-psi) pore pressure in an Algyo sandstone from Hungary

The numerical values of the porous rock compressibilities, as well as the variation of the compressibilities with stress, are to a large degree determined by the geometry of the void spaces in the rock. The values are also, of course, influenced by the compressibilities of the various mineral components of the sandstone. Much research has been done to relate the numerical values of the compressibilities to mineralogy and pore-structure. Nevertheless, it is still generally true that compressibilities must be measured in the laboratory in order to arrive at values accurate enough for engineering calculations. As it is often not practical to measure all four compressibilities for each type of rock at all pressures of interest, it is desirable to have some method of correlating the different compressibility values to each other. This can be done using the theory of elasticity, along with a suitable idealized model for consolidated sandstones [Zimmerman et al., 1986]. Hamilton and Shafer [1991] provide an excellent discussion of pore volume compressibility and compaction measurements.

Consolidated sandstones behave elastically for confining stresses that are less than some critical yield stress [Zhang et al., 1990], beyond which irreversible plastic deformation will occur. This plastic deformation is usually associated with crushing of the grains that comprise the sandstone, or with cleavage along the boundaries between grains. Another type of inelastic deformation is fracture, which can be caused by sufficiently high tensile stresses. A common situation in which this occurs is the process of hydraulic

fracturing, in which fractures emanating from the borehole are induced by the injection of fluid into the borehole under high pressure [Economides and Nolte, 1989]. Such modes of irreversible deformation lie outside of the scope of my work. Most of the deformation that occurs in petroleum or groundwater reservoirs as a result of fluid withdrawal is elastic, as is much of the deformation in crustal rocks due to tectonic forces.

2.3 RELATIONSHIPS BETWEEN COMPRESSIBILITIES

In order to develop a mathematical theory of the compressibility of porous rocks, it is first necessary to choose a conceptual model for rock-like materials. One of the earliest such models used for sedimentary rocks was that of a packing of spherical grains [Gassmann, 1951b; Brandt, 1955; Digby, 1981], as seen in Fig. 2. 5a. Models based on this idealization are particularly useful for unconsolidated sediments. The usefulness of these models does not entirely carry over to consolidated sediments, however. For example, while sphere-pack models account for the effect of confining pressure with some accuracy, it is difficult to treat pore pressure effects within this context. Another drawback to applying these models to consolidated rocks is that they typically predict compressibilities that decrease with pressure according to a power law, while the compressibilities of consolidated sandstones actually level off to constant, non-zero values at high pressures.

A general theory of porous rock compressibility is more easily derived by starting with what is, in effect, the opposite model (see Fig. 2.5b). Instead of focusing on the grains, it is more convenient to consider a porous rock to be solid and yet containing discrete voids. More specifically, we will consider sandstone to be composed of an isotropic, homogeneous elastic matrix, permeated with pores of various shapes and sizes. The matrix is assumed to form a completely connected network, while the void space may consist either of a connected network of pores, isolated pores, or some combination of both pore types. The connected portion of the pore space is often referred to as the effective porosity, while the isolated voids are said to form the isolated or "non-effective" porosity [Dark, 1969]. Although this distinction is crucial when studying transport properties such as permeability or electrical conductivity, it is not a necessary distinction to make when developing a general theory of the mechanical behavior of porous rocks. In the development that will be presented here by Zimmerman et al. [1986], the voids need not be homogeneously distributed throughout the material, nor be random in their spatial orientation. Grain shape or size need not enter into consideration, as no explicit distinction

will be made between the grain-forming minerals and any intergranular clays or cementing material. In this regard, it should be noted that the word "matrix "is used here to refer to the totality of the mineral components, and should not be confused with the use of that word by petroleum geologists [Pettijohn, 1957] to refer to certain types of intergranular material. Application of the laws of continuum mechanics to this model leads to a theory of porous rock compressibility that is quite general, in that it applies to both sedimentary and igneous rocks. In many respects it is useful for unconsolidated sediments, also. The extent to which any of the assumptions mentioned above are necessary for a particular theoretical result, and the effect that different assumptions might have, will be discussed as the results are derived.
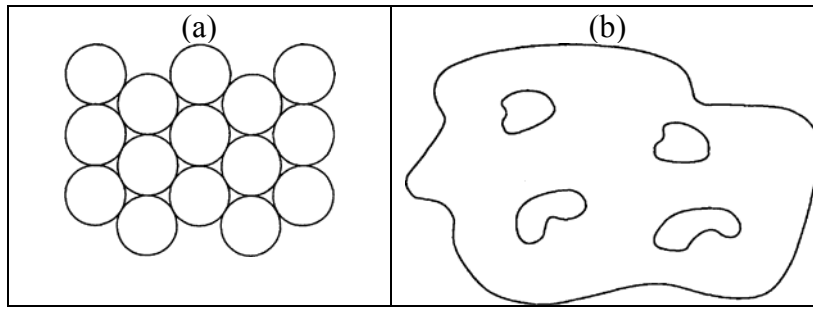
Figure 2.5: Sandstone modeled as (a) an assemblage of discrete grains in contact, and (b) a solid matrix containing voids.

For the idealized porous solid described above, the four porous rock compressibilities are not independent, and three relations can be found between them by using various concepts from elasticity theory. In the following derivation of these relations, applied pressures and the resulting strains will be incremental changes superimposed on a pre-existing state of stress and strain. While the stress-strain relations that result from this analysis will be nonlinear, representing the integration of incremental relations, the total strains will still be "infinitesimal" in the sense of classical linear elasticity [Sokolnikoff, 1956]. Higher order (i.e. nonlinear) terms in the relationships between the strains and the deformation gradient [Mumaghan, 1951; Knopoff, 1963] will thus be neglected.

Biot [1941] introduced four compressibility coefficients known as Biot's coefficients. Zimmerman [1986] proposed further compressibility coefficient [Laurent, et al., 1993]. Physical arguments put forward by Zimmerman et al. [1986], suggest that only three out of four compressibilities (i.e. C_{bc}, C_{pp}, C_{pc}, C_{bp}) have relations with initial porosity (ϕ^i) and rock matrix compressibility (C_r) .

$$C_{bp} = C_{bc} - C_r \tag{2.12}$$

$$C_{pc} = (C_{bc} - C_r)/\phi^i \tag{2.13}$$

$$C_{pp} = \left(\frac{1}{\phi^i}\right)\left[C_{bc} - (1 + \phi^i)C_r\right] \tag{2.14}$$

$$C_{bp} = \phi^i C_{pc} \tag{2.15}$$

Any three of the four porous rock compressibilities can therefore be expressed in terms of ϕ^i, C_r, and the other compressibility, although it is often convenient to consider C_{bc} to be the "fundamental" porous rock compressibility, since it is analogous to the compressibility of a non-porous material. In terms of C_{bc}, C_r and ϕ^i, the other three compressibilities are:

$$C_{bp} = C_{bc} - C_r \tag{2.16}$$

$$C_{pc} = (C_{bc} - C_r)/\phi^i \tag{2.17}$$

$$C_{pp} = (C_{bc} - (1 + \phi^i)C_r)/\phi^i \tag{2.18}$$

On the length scale of distances between pores, the matrix material is usually a single grain of a relatively anisotropic crystal such as quartz, whose elastic moduli differ by as much as 40% along the different crystallographic axes [Clark, 1966]. In addition, sandstones usually consist of more than one type of mineral. Common grain-forming minerals are quartz, feldspar, and calcite, while the intergranular spaces often contain clay minerals such as illite, kaolinite, or montmorillonite [Pettijohn, 1957]. Biot [1941] did not assume microscopic isotropy or homogeneity, and his analysis reproduces Eqns. (2.12) and (2.15), but not Eqn. (2.17). In Biot's theory, the difference between C_{pc} and C_{pp} is not necessarily equal to C_r, and the resulting equations contain an additional, independent parameter, which can be identified with the change in pore volume caused by equal increments of both the pore and confining pressures [Brown and Korringa, 1975].

Often the volume change of the matrix material is neglected [Domenico, 1977], leading to equations that can be derived from Eqns. (2.16)-(2.18) by setting C_r equal to zero. The two pore compressibilities are then equal to each other, as are the two bulk compressibilities. This assumption is acceptable for unconsolidated sands, for which C_{bc}/C_r may be as high as 10^2 [Newman, 1973]. For such materials, volumetric reduction occurs mainly in the vicinity of the grain contacts, as a result of the high contact stresses, as opposed to the hydrostatic compression of entire grains that occurs in consolidated rocks.

An extensive treatment of the compressibility of unconsolidated sands is contained in the treatise edited by Chilingarian and Wolf [1975].

The assumption that the mineral phase effectively behaves like an isotropic elastic medium can easily be tested experimentally through so-called "unjacketed tests". In these tests, which are discussed in more detail for compressibility measurements in Chapter 4, the rock is pressurized by a fluid (saltwater) which is allowed to seep into its pores, so that the pore and confining pressures are equal. Since changing in pore pressure $(dP_p) = dP_c$ (changing in confining pressure Eqn. (2.12) can be used to relate C_{bp}, and C_{bc}, and so on.

If the mineralogical composition of the rock is known, it is fairly easy to estimate a value for C_r by using the Voigt–Reuss-Hill method. Consider the problem of determining an effective C_r for a heterogeneous but non-porous body consisting of "n" different minerals, each with compressibility C_i and present in a volume fraction of χ_i, arranged in any geometry. If such a body is subjected to uniform hydrostatic stress dP over its outer boundary, the state of stress in the various mineral grains will not be homogeneous, due to the necessity of maintaining continuity of both traction and displacement at the grain boundaries. Reuss's method [Hill, 1952; Zimmerman et al., 1986b] for predicting the effective compressibility of such a body rests on assuming that the stresses are uniform throughout the body, and then ignoring the resulting discontinuity of displacements. If the stresses were uniform, the strain in each component would be $d\varepsilon_i = -C_i dP$. Since the total strain is the weighted average of the strains in each component,

$$\varepsilon = \sum X_i \varepsilon_i$$

$$d\varepsilon = \sum X_i d\varepsilon = -\sum X_i C_i dP$$

so,

$$\overline{C}[Reuss] = -\frac{d\varepsilon}{dP} = -\sum X_i C_i \qquad (2.19)$$

Voigt made the opposite assumption [Hill, 1952; Zimmerman et al., 1986b], which is that the strains are uniform throughout the body, so that in each grain $d\varepsilon = -C_i dP_i$. Since the average stress in the body is the volumetrically-weighted average of the stresses in each component,

$$p = \sum (\chi_i p_i)$$

$$dp = \Sigma(\chi_i p_i) = -\Sigma(\chi_i/C_i)d\varepsilon$$

thus

$$\overline{C}[Voigt\,] = -\frac{d\varepsilon}{dP} = [\Sigma(\chi_i\,/\,C_i)]^{-1} \qquad\qquad (2.20)$$

The Voigt method therefore consists of taking a volumetrically-weighted average of the bulk moduli. Hill [1952] proved that the Voigt and Reuss estimates are actually upper and lower bounds of the true effective moduli and proposed averaging these two estimates in order to find a best estimate of effective compressibility of homogeneous solid ($\overline{C}$) Experimental data that justifies use of the Voigt-Reuss-Hill average for non-porous crystalline rocks have been compiled by Brace [1965]. The experimentally measured elastic moduli always lie between the Voigt and Reuss bounds. While there are cases in which the measured values are much closer to one of the bounds than they arc to the Voigt-Reuss–Hill average, for most applications this average yields acceptable accuracy.

Verification of the compressibility relationship (2.16 – 2.18) is hampered by the fact that there are few published data sets in which more than one porous rock compressibility was measured on the same sandstone. Zimmerman [1986] measured C_{bp} and C_{pc} for the same Bandera sandstone core. Bandera is quartos sandstone consisting of 70% quartzite, 21% calcite, and 9% feldspar [Greenwald, 1980]. The average grain diameter is about 80 µm, and the initial porosity of the sample was 16.5%. According to Eqn. (2.15), C_{bp} should equal $\phi^i C_{pc}$. This relation follows from the reciprocal theorem of elasticity, and does not depend on the assumption that the mineral phase is isotropic or homogeneous.
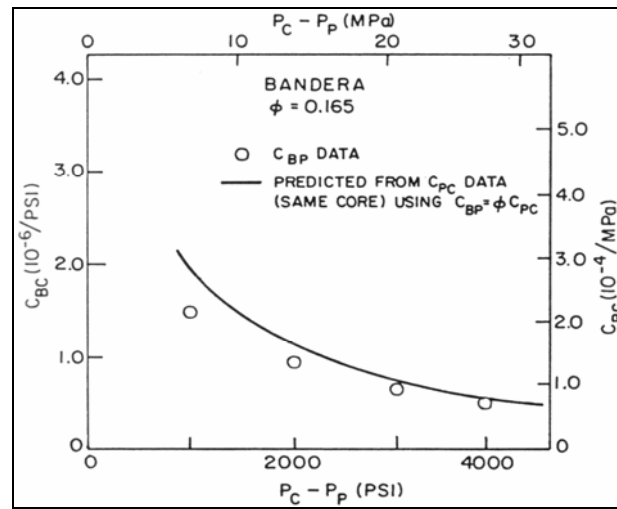
Figure 2.6: Measured values [Zimmerman, 1986] of C_{bp} for Bandera sandstone, compared with the values predicted from C_{pc} measurement on the same core, using $C_{bp} = \phi^i C_{pc}$.

Fig. 2.6 shows the measured C_{bp} and C_{pc} values over the range of pressures from 0 to 30 MPa (0-4500 psi). Note that the compressibilities are plotted against the differential pressure Pc-Pp, which is the "effective stress" that governs the variation of the porous rock compressibilities. The agreement between C_{bp} and $\phi^i C_{pc}$ is fairly close, particularly in light of the relative inaccuracy of the "extruded volume" method that was used to measure C_{bp}.
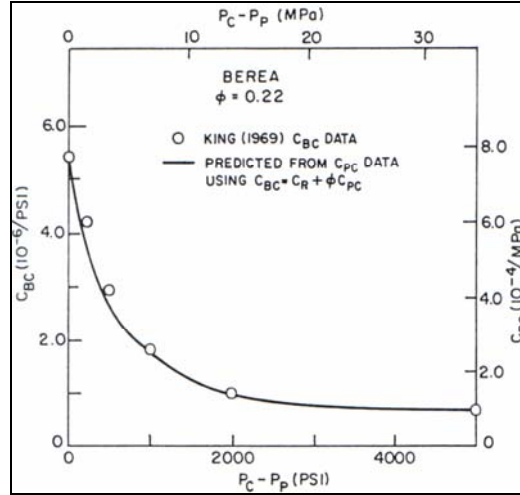
Figure 2.7: Dynamically measured values [King, 1969] of C_{bc} for a Berea sandstone, compared with the predictions based on Zimmerman's [1996] C_{bc} measurement, using $C_{bc} = C_r + \phi^i C_{pc}$.

Another test of the compressibility relations (2.16-2.18) was described by Zimmerman [1986]. C_{pc} pore compressibility measurements on Berea sandstone of 22% porosity were converted into C_{bc} values using Eqn. (2.17). The resulting C_{bc} (P) curve was then compared to the values determined dynamically by King [1969] on a dry sample. The dynamic compressibility values were found by measuring the wave-speed of the longitudinal "P-wave", V_L, and the velocity of the transverse "S-wave", V_T. The relation $K = \rho \left(V_L^2 - 4 V_T^2 / 3 \right)$, where ρ is the bulk density of the rock, was then used to find the bulk modulus K, which equals $1/C_{bc}$. Although the tests were not conducted on the same specimens, each of the two Berea cores had an initial porosity of 22%. The excellent agreement (Fig. 2.6) not only verifies Eqn. (2.18), but also illustrates that the dynamic compressibility of dry sandstone is equivalent to the static value. This issue has often led to confusion, mostly caused by the fact that when acoustic waves travel through a fluid-saturated rock, the proper dynamic compressibility is not equal simply to C_{bc}.

15
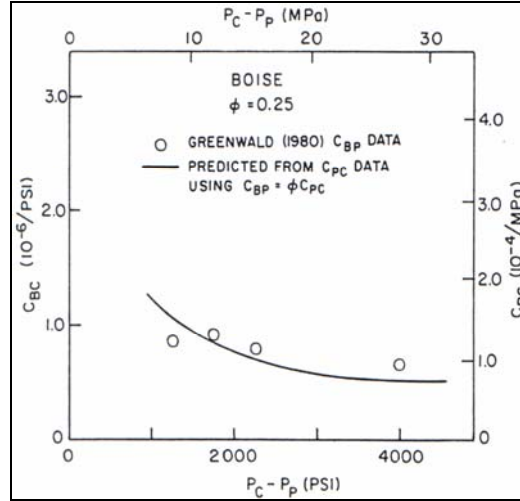
Figure 2.8: Measured values [Greenwald, 1980] of C_{bp} for a Boise sandstone, compared with the predicted values based on [Zimmerman, 1986] C_{pc} measurement, using $C_{bp} = \phi^i C_{pc}$.

A similar verification of the compressibility relation between C_{bp} and C_{pc} is shown in Fig. 2.8 for Boise sandstone of 25% initial porosity. Greenwald [1980] measured C_{bp} by varying the pore pressure and monitoring the resulting bulk volume change with strain gauges mounted on the outside of the rock. Zimmerman [1986] determined C_{pc} by increasing the confining pressure on the rock, and measuring the volume of the expelled pore fluid. The measurements were made on different cores that were cut from the same slab. According to Eqn. (2.15), these two compressibilities should be related through $C_{bp} = \phi^i C_{pc}$. Figure 2.8 shows the four discrete C_{bp} values measured by Greenwald, along with the C_{pc} values measured by Zimmerman, represented by a fitted curve. The agreement is fairly good, despite the inaccuracy inherent in compressibility data, which are found from "numerically differentiating" the stress-strain data. In particular, note that the average values of C_{bp} and $\phi^i C_{pc}$ over the range of 1000 - 4000 psi are extremely close.

2.4 EFFECTIVE STRESS COEFFICIENTS

The concept of effective stress has long been used in rock mechanics. The motivation for this concept is that since the pore pressure (P_p) and confining pressure (P_c) tend to have opposite effects on the volumes (as well as on most petrophysical properties, such as permeability, electrical resistivity, etc.), it would be convenient to subtract some fraction of the pore pressure from the confining pressure and then treat the pressure as a single variable. In other words, instead of considering a property such as the pore volume to depend on the two variables (P_c, P_p); it would be treated as a function of the single variable $P_c - nP_p$. This idea dates back to at least as far as the work of Terzaghi [1936], who

16

proposed based on a simple force-balance argument that effective pressure $P_e = P_c - \Phi P_p$ would be the variable that governed the mechanical behavior of porous rocks. His experiments, however, revealed that the differential pressure (P_d) governed the failure of geological materials $P_d = P_c - P_p$.

Following the introduction of the concept of effective stress, this concept has often been used in an overly simplified and imprecise way, by assuming that all properties of a porous rock could be expressed as functions of $P_d = P_c$ - nP_p, where n is the "effective stress coefficient".

The most general form for expressing the effective stress concept for elastic porous rocks deformation is the following expressions for the bulk and pore-strains:

$$\varepsilon_b\left(P_c, P_p\right) = -C_{bc}\left(P_c - m_b P_p\right)\left(dP_c - n_b dP_p\right) \tag{2.21}$$

$$\varepsilon_p\left(P_c, P_p\right) = -C_{pbc}\left(P_c - m_p P_p\right)\left(dP_c - n_p dP_p\right) \tag{2.22}$$

In Eqns. (2.21) and (2.22), the compressibilities C_{bc} and C_{pc} depend on the variable $P_c - mP_p$ and the strains are computed by multiplying the compressibilities by the bracketed stress increments. The effective stress coefficients "m" governs the manner in which the compressibilities vary with pressure, while the "n" coefficients reflect the relative amounts of additional strain caused by increments in the pore and confining pressures. Since the bracketed terms can always be written in that form by merely factoring out the appropriate compressibilities, the n coefficients can always be defined. However, there is no a priori reason to expect that the compressibilities will vary with stress as they do in Eqns. (2.21) and (2.22), since in general a function of the two variables [P_c, P_p] cannot be written as a function of some linear combination of the those two variables.

Comparison of Eqns. (2.21) and (2.22) with Eqns. (2.9) and (2.10) shows that the effective stress coefficients n are simply equal to the ratios of the appropriate compressibilities. The relationships (2.16)-(2.18) show that the effective stress coefficients n can be expressed as [Robin, 1973]:

$$n_b = \frac{C_{bp}}{C_{bc}} = \frac{C_{bc} - C_r}{C_{bc}} = 1 - \frac{C_r}{C_{bc}} \tag{2.23}$$

$$n_p = \frac{C_{pp}}{C_{pc}} = \frac{C_{bc} - C_r\left(1 + \phi\right)}{C_{bc} - C_r} = 1 - \frac{\phi C_r}{C_{bc} - C_r} \tag{2.24}$$

The effective stress coefficients are expressed in terms of C_{bc} in Eqns. (2.23) and (2.24), although this is not necessary. The form of these equations shows that n_b (effective stress of bulk strain) and n_p (effective stress of pore strain) will in general not be equal to each other.

Since the n coefficients depend on the compressibility C_{bc}, they will therefore vary with stress, as well as be dependent on pore structure and mineral composition. Various bounds and relationships can be found for these effective stress coefficients, however, thus greatly constraining their possible range of values. C_{bc} and C_r, are both positive, as is $C_{bc} - C_r$ so Eqns. (2.23) and (2.24) imply that neither effective stress coefficient will exceed 1.0. This indicates that the pore and bulk volumes are each more sensitive to changes in confining pressure than to changes in pore pressure. Since n_b is a decreasing function of C_{bc}, the Hashin-Shtrikman bounds on C_{bc}/C_r lead immediately to the following bounds for n (Fig. 2.9), which are again independent of the pore geometry:

$$\frac{3(1 - V_r)\phi}{2(1 - 2V_r) + (1 + V_r)\phi} \leq n_b \leq 1 \tag{2.25}$$

The most general bounds, which are independent of rock volume (V_r), are [Norris, 1989]:

$$\frac{3\phi}{2 + \phi} \leq n_b \leq 1 \tag{2.26}$$

Since $3\phi/(2 + \phi)$ always exceeds (ϕ) by a finite amount, n_b, must be greater than (ϕ) As there is no upper bound on C_{bc}, either of the two n coefficients can approach arbitrarily close to unity.

Bounds on n_p can also be established, starting with the following expressions that result from comparing Eqns. (2.10) and (2.22):

$$n_p = \frac{C_{pp}}{C_{pc}} = \frac{C_{pc} - C_r}{C_{pc}} = 1 - \frac{C_r}{C_{pc}} \tag{2.27}$$

In this form, it is clear that the bounds for C_{pc} given in Eqn. (2.35) lead to bounds for n_p (Fig. 2.10):

$$\frac{(1 + V_r) + 2(1 - 2V_r)\phi}{3(1 - V_r)} \leq n_p \leq 1 \tag{2.28}$$
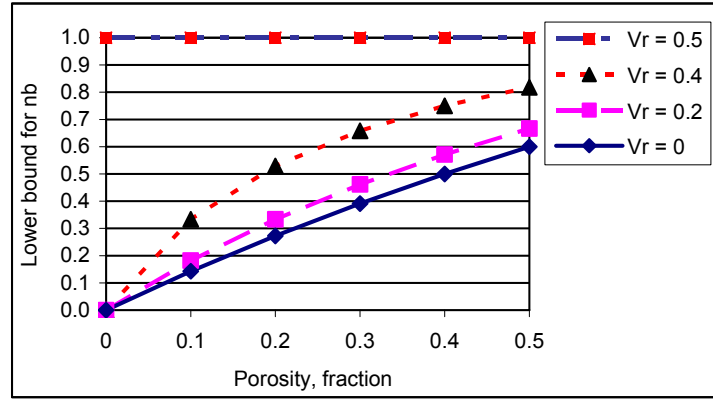
Figure 2.9: Lower bounds in effective stress coefficient from n_b. The upper bound is equal to 1.0
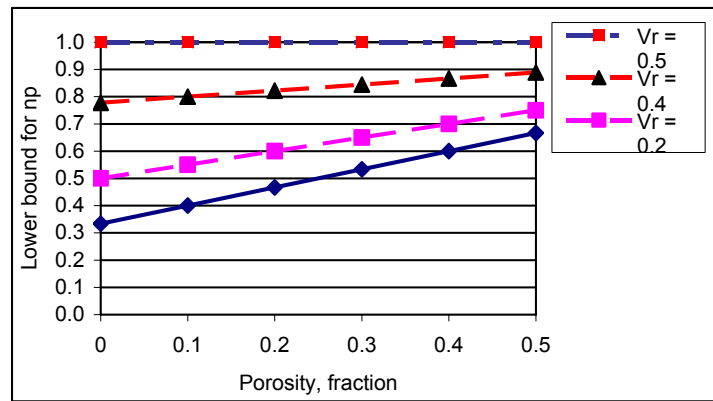
Figure 2.10: Lower bounds in effective stress coefficient from n_p. The upper bound is equal to 1.0

The most general lower bound, which again occurs for v_r (Poisson's ratio for the rock matrix material) = 0, is

$$\frac{(1+2\phi)}{3} \le n_p \le 1 \tag{2.29}$$

In the limit as V_r approaches its maximum possible value of 0.50, which corresponds to an incompressible mineral phase, both n_b and n_p approach 1.0. Hence, if the matrix compressibility can truly be neglected, the pore and confining pressures will each have the same effect on the volumetric strains, except for sign.

The two coefficients n_p and n_b, are not only in general different, but in fact n_p is always greater than n_b. This is proven by forming the difference ($n_p - n_b$,), and examining the sign of the resulting expression. In terms of C_{bc}, C_r, and ϕ,

$$n_p - n_b = \frac{C_r\left[C_{bc}(1-\phi) - C_r\right]}{C_{bc}(C_{bc} - C_r)} \tag{2.30}$$

Since (1-ϕ) is the Voigt upper bound on C_r/C_{bc}, it follows that both the numerator and the denominator in Eqn. (2.30) are non-negative. In fact, since a real porous material

never attains the Voigt bound, because the Hashin-Shtrikman bound is more restrictive, the numerator must always be positive, proving that n_p will always be greater than n_b.

The most extensive investigations of the effective stress coefficients were those carried out by Fatt [1958a, 1958b, 1959]. Fatt measured both C_{bc} and C_{bp} for a Boise sandstone with an initial porosity of 26%. The Boise was a feldspathic graywacke consisting of 35% quartz, 29% feldspar, 6% rock fragments, 23% chert and clayey material, and 7% biotite [Fatt, 1958a]. The C_{bp} values were measured at a confining pressure of 12,000 psi, while the C_{bc} values were measured at zero pore pressure. Using a mineral phase compressibility of 2.0 x 10^{-7} psi, which is roughly that of quartz or feldspar, Fatt compared the exact value of n_b, as given by C_{bp}/C_{bc}, with the theoretical value of $(C_{bc} - C_r)/C_{bc}$. C_{bp}, measured at a confining pressure of 12,000 psi, while C_{bc} was measured at a pore pressure of 0 psi. The results are shown in Fig. 2.11 as functions of the differential pressure $P_d = P_c - P_p$. The measured values of n_b were very close to unity for low values of the differential pressure, and decreased down to a high-stress asymptotic value of 0.77. The measured values agreed fairly well with the "theoretical" value, and each lay above the lower bound, which, for a Poisson ratio of 0.20, would be about 0.42.
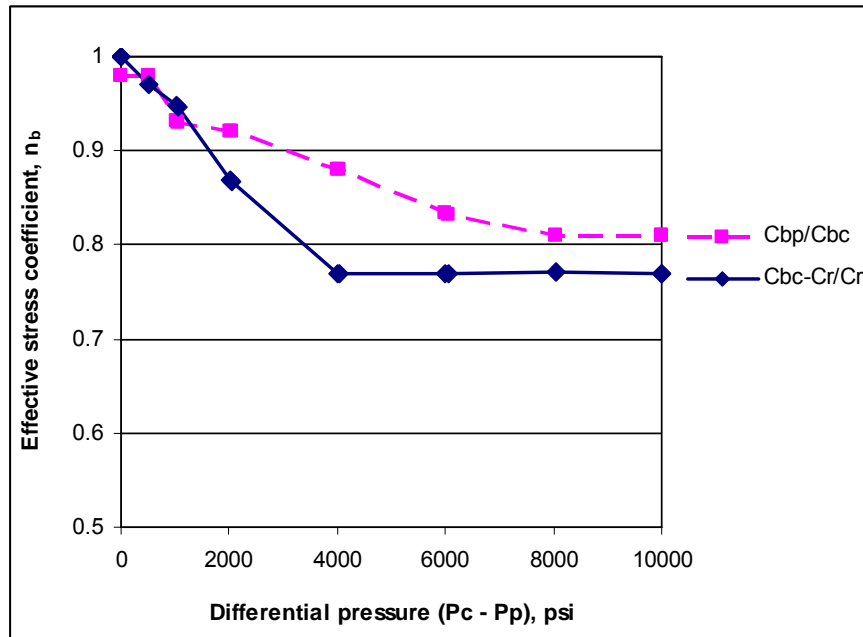
Figure 2.11: Comparison of direct and indirect measurements [Fatt, 1958a] of n_b for a Boise sandstone.

Starting with the definition $\phi = V_p/V_b$ and using the rules for differentiating quotients, Zimmerman [1986] obtained the following equation:

$$d\phi = -\left[C_{bc}(1-\phi) - C_r\right]d(P_c - P_p) \qquad (2.31)$$

The effective stress coefficient $d\phi$ is therefore always equal to 1.0, and the incremental porosity change depends only on the change in the difference between P_c and P_p. The term $[C_{bc}(1-\phi)-C_r]$ is necessarily positive, so the porosity is a decreasing function of the differential pressure $P_d = P_c - P_p$. This is a non-trivial conclusion since, for example, as an increase in confining pressure will decrease both the pore and bulk volume, there is no *a priori* reason for the ratio V_p/V_b to also decrease in response to an increase in the confining pressure.

An equation for the strain of rock matrix material can be similarly found by starting with the fact that $V_r = V_b - V_p$:

$$d\varepsilon_r = \frac{dV_r}{V_r} = \frac{-C_r d(P_c - \varphi P_p)}{1-\phi} \qquad (2.32)$$

where the compressibility relations of Chapter 2 have been freely used. Hence, the effective stress coefficient that governs changes in the volume of the mineral phase is simply equal to the porosity ϕ. Another interpretation of Eqn. (2.41) is that the average pressure $\overline{P}$ in the mineral phase of the rock is given by

$$\overline{P} = \frac{P_c - \phi P_p}{1-\phi} \qquad (2.33)$$

in the sense that $d\varepsilon_r = -C_r d\overline{P}$. This result can easily be motivated [Greenwald, 1980, p. 40] by considering the two-dimensional force-balance argument shown in Fig. 2.12.
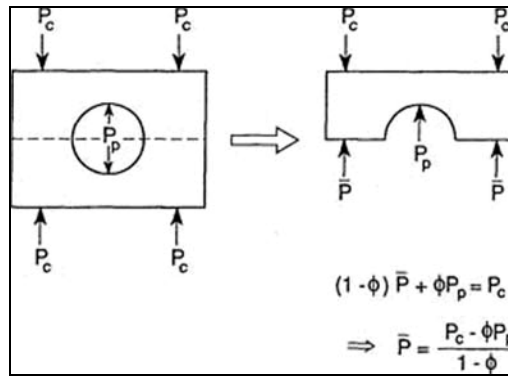
Figure 2.12: Force-balance arguments [after Greenwald, 1980] for the derivation of the mean-stress relationship. If the idealized rock on the left is cut by the dotted line (plane), the fractional amount of areal porosity that is exposed will be ϕ. The average stress acting over the exposed internal rock surfaces is denoted by $\overline{P}$. Equating the upward and downward forces then leads to Eqn. (2.44).

If we assume that an "average" stress $\overline{P}$ acts over the interior rock material, equating the upward forces to the downward forces leads to the relationship $P_c = (1-\phi)\overline{P} + \phi P_p$, from which Eqn. (2.33) follows. Hence, since ϕ usually will not vary by more than a few percent for elastically deformed sandstone, these effective stress coefficients are essentially constant. Furthermore, since the rock volume compressibility C_r is also essentially constant, the nonlinearity of sandstone compression manifests itself only in the C_{bc} coefficient, in the Carroll-Katsube approach [1983].

2.5. LITERATURE REVIEW

The earliest attempt for measuring the compressibility of reservoir rocks was reported by Carpenter and Spencer [1940]. The use of pore-volume compressibility-porosity correlations in engineering calculations is well known. The correlations developed by Hall [1953] for both sandstones and limestones have been widely distributed. Hall reported that rock compressibility ranges from 3x10-5 to 10-7 (pore volume/pore volume). Fatt [1958] did a more detailed investigation on sandstone reservoirs. B. C. Craft and M. F. Hawkins [1959] summarize Hall's results and those of Fatt. In 1959, Van der Knaap published a similar correlation using limestone samples from a single well and also correlated the data with net pressure. Van der Knaap [1959] and Dobrynin [1962] have studied the effect of overburden and pore-space pressure upon rock compressibility. A more comprehensive discussion of this can be found in Geertsma [1957]. In the 44th Annual SPE Fall Meeting in 1969, Von Gonten and Choudhary presented a useful paper studying the effect of pressure and temperature on pore-volume compressibility. In the same meeting Kohlhaas and Miller [1969] submitted their work on rock-compaction and pressure-transit analysis. Newman [1973] summarizes most of the above experimental observations. He concluded that the pore-volume compressibility-porosity values obtained in his study are in poor agreement with published compressibility-porosity correlations. This is also supported by values in the literature. In 1986, Zimmerman conducted extensive work and published his laboratory experiments mainly on sandstone. Later on, Lurent et al. [1993] performed research work on six samples of limestone. They concluded that the compressibilities and Biot coefficient appear to increase with porosity according to a Hashin-Shtrikman type law. He also stated that for the same porosity the Biot coefficient is apparently larger in a limestone than in sandstone.

Toth et al [1988] published two papers in Hungarian dealing with porous rock deformation of Hungarian reservoir rocks. The first paper reviews the mathematical formulation of the deformation of porous rock structures and derives the theoretical equations by which the physical changes in the structure of porous rocks as function of effective stress can be calculated. The second paper summarizes the results of measured deformation of fourteen samples of Algyo field sandstone rock under hydrostatic condition.

Z. Harai et al. [1995] made measurements and from these determined the pore-compressibility characteristics of some limestone samples obtained from a Saudi Arabian petroleum reservoir. They present the experimental data in the form of relative porosity and hydrostatic pore-compressibility values as functions of differential pressure

.

CHAPTER 3
3. POROELASTICITY MEASUREMENTS

3.1 INTRODUCTION TO POROELASTICITY THEORY

Poroelasticity theory, first introduced by Biot (1941), provides a means for analyzing the interaction between fluid flow and skeletal-matrix deformation. Although the general theory considers both compressible fluid and grains, applications to ground-water investigations can often invoke the assumption of incompressible grains. This assumption is adopted in the following discussion. When grains are incompressible, the derivation of poroelasticity equations is remarkably simple.

The only stresses that were considered in the earlier chapter were pore pressures or hydrostatic confining pressures. Poroelasticity is a more general theory of the mechanics of porous rocks, which allows for completely arbitrary states of stress. Although the theory, in its basic form, was developed chiefly by Biot [1941, 1973] and has existed for several decades, only recently has it been used to solve basic rock mechanics problems such as the state of stress around a borehole [Detoumay and Cheng, 1988], and to study phenomena such as the stress-dependence of permeability [Walder and Nur, 1986]. Biot [1956a, b] and others who dealt with dynamic processes such as seismic wave propagation have extended poroelasticity theory. Recently, for instance, Coussy [1989] extended the theory to thermo-poroelasticity. The theory of poroelasticity is fundamentally a higher-order theory than that of classical elasticity, in that it involves concepts such as "pore pressure" and "pore strain" that have no analogue in classical mechanics [Nunziato and Cowin, 1979]. In this sense, the theory in the previous chapters can be viewed as a special case of poroelasticity for rocks under hydrostatic loading. Poroelasticity not only utilizes concepts and variables that do not exist in classical mechanics, it also predicts certain phenomena that have no counterpart in the classical theory. For example, the equations of dynamic poroelasticity predict the existence of "slow" compressional waves that travel at a speed much less than that of classical compressional waves. These slow compressional waves attenuate very rapidly as they travel through rock, since they are characterized by motions in which the pore fluid oscillates out of phase with the rock matrix. This solid/fluid counter-flow produces large viscous forces at the pore walls, which lends to dissipate energy. Although

such waves have been observed in laboratory tests [Plona, 1980], they have yet to be observed in the field.

Another distinction between the theory of poroelasticity and the more "primitive" approach developed in the preceding chapters is that in contrast to the theory of hydrostatic compression, which can be developed in a fully nonlinear form, a usable theory of poroelasticity that accounts for the stress-dependence of the elastic moduli is still in the process of development. Hence, the term "poroelasticity" usually refers to the linearized theory of poroelasticity, in which the compressibilities and the other constitutive coefficients are independent of stress. The stress increments are small enough that this restriction is of no consequence, since the governing equations can be always linearized for small stress increments in many physical processes. An example of such a process is wave propagation. Both the naturally occurring waves that result from seismic activity, as well as the artificially created "acoustic" waves used in well logging, typically involve stress increments of only a few mega-Pascal, which are very small in relation to the existing in-situ stresses. Another process that has been treated successfully by linearized poroelasticity is the oscillation of the water level in wells due to fluctuations in barometric pressure at the surface or due to solid-earth tidal forces [van der Kamp and Gale, 1983]. In these problems, the bulk strain increments are approximately 10^{-4}, and so the linearized theory is appropriate. Such water-level fluctuations can be used in the inverse problem of estimating the formation compressibility and other poroelastic constitutive parameters. For other problems, such as determining the state of stress around a borehole, linearized poroelasticity may be only a rough first approximation, since the induced stresses will be of the same order of magnitude as the initial stresses, and hence large enough for the nonlinearity of the stress-strain relationship to become an important factor. Some progress has been made in treating the borehole stress problem for a rock with a nonlinear stress-strain relationship [Biot, 1974; Santarelli et al., 1986], but these treatments have not included the effects of pore pressure.

A full discussion of aspects of the theory of stress can be found in elasticity texts such as that by Sokolnikoff [1956]. Here, our discussion will be restricted to the bare minimum that is necessary in order to be able to present the basic equations of poroelasticity.

In the previous chapter, the only measure of deformation that used was volumetric strain. This measure of deformation does not fully describe the possible types of deformation that may occur in a rock. For example, since a rock may be compressed by

different amounts in the three different directions of a rectangular coordinate system (Fig. 3.1), it is obvious that more than one quantity will be needed to specify the deformation. In the full generality of finite deformation, the strain matrix is related to the displacement vector in a nonlinear manner, and it is consequently difficult to interpret the physical meaning of its components. For some geological problems, the use of nonlinear strain measures is unavoidable, since the deformations that occur over geological time may be quite large [Jaeger and Cook, 1979]. For most engineering and geophysical problems, however, it is acceptable, and very convenient, to use the linearized strain matrix that corresponds to infinitesimal strain.
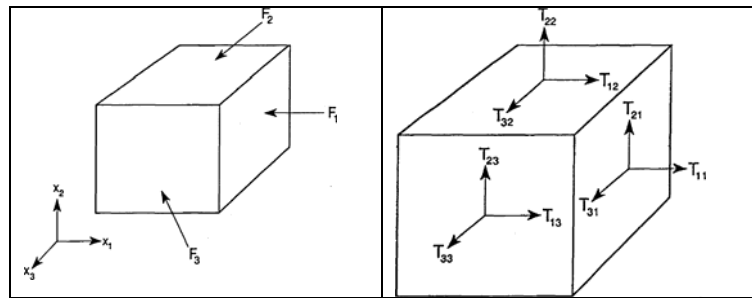
Figure 3.1: Infinitesimally small cube of rock material, "cut out" of a larger piece of rock that is subjected to various forces. The net force transmitted to the cube by the adjacent material can be represented by vectors F acting at the center of each face [after Zimmerman, 1986]

When a rock is stressed, there are two qualitatively different modes of deformation that may result. One mode of deformation is pure dilatation, in which the volume changes, but the rock is otherwise undistorted (Fig. 3.2). For example, if three points in die rock are aligned such that they form a right angle before deformation, they will continue to form a right angle after undergoing a pure dilatation. The other type of deformation is one in which the volume remains the same, but the rock distorts (Fig. 3.3). Somewhat more lengthy analysis shows that the shear strains are a measure of angular distortion [Jaeger and Cook, 1979]. In this sort of deformation, angles will be changed, but the overall volume will be preserved. These two modes correspond to die isotropic and deviatoric parts of a die strain matrix:
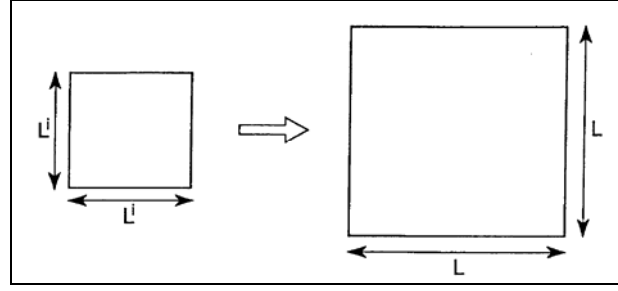
Figure 3.2: Schematic diagram of a purely dilatational deformation. The square on the left is stretched by equal amounts in all directions; its area changes, but its shape remains the same.
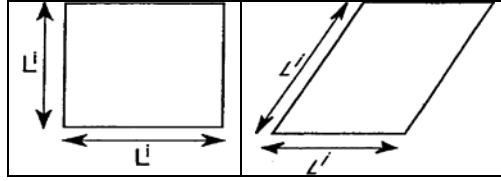
Figure 3.3: Schematic diagram of a purely deviatoric deformation. The square on the left is distorted into a rhombus, but its area remains unchanged.

If the stress increments are sufficiently small, it is reasonable to assume that the resulting strains will be linear functions of the stresses. It is at this point that the decomposition of the stresses and strains reveals its usefulness. Within the theory of poroelasticity, the constitutive variables will include the stress matrix and the bulk strain matrix, as well as the pore pressure and the pore strain. These stresses and strains are coupled in the sense that the pore pressure affects the bulk strain and effective stress. However, a partial decoupling is brought about through the isotropic/deviatoric decomposition. First, note that in classical elasticity, the isotropic part of the strain is related only to the isotropic part of the stress, while the deviatoric part of the strain is related only to the deviatoric part of the stress [Billington and Tate, 1981]. This is equivalent to saying that shear stresses do not alter the volume, and hydrostatic stresses do not lead to distortion. (This assertion applies only to macroscopically isotropic materials, of course. If the material is anisotropic, equal stresses in different directions will give rise to unequal strains, and so an isotropic stress state may lead to distortion.) When extending these concepts to poroelasticity, it is usually further assumed [Biot, 1941] that pore pressures cause no distortion, and that shear stresses do not alter the pore volume. If the pores are isotropically oriented, which they must be for a macroscopically isotropic rock, this first assumption is obvious. The second assumption follows from the fact that since it is not reasonable for a positive shear stress to increase the pore volume, say, and a negative shear stress to decrease the pore volume, the linear coefficient that relates each shear stress to the pore strain must be zero. Since there is only one independent component of an

isotropic matrix, it is convenient to use ε_b and ε_b as variables. Hence, ε_b will be a linear function of P_c and P_p, and ε_p will be a linear function of P_c and P_p [Zimmerman, 1986]. Seen from this point of view, the constitutive equations of linear poroelasticity should be an obvious combination of the porous rock compressibility relations (1.9) and (1.10) and the stress-strain equations of classical elasticity:

$$\varepsilon_b = -C_{bc} P_c + (C_{bc} - C_r) P_p \tag{3.1}$$

$$\varepsilon_p = \frac{(C_{bc} - C_r)}{\phi} P_c + \frac{[C_{bc} - (1 + \phi) C_r]}{\phi} P_p \tag{3.2}$$

$$\varepsilon^D = \frac{1}{2G} T^D \tag{3.3}$$

In Eqns. (3.1) and (3.2), the relationships between the various porous rock compressibilities that were derived in Chapter 2 have been used. The only additional relationship that appears in the more general poroelasticity equations is the usual relationship between shear stresses from classical elasticity, Eqn. (3.3), which involves the shear modulus G. The hybrid notation of Eqns. (3.1-3.3), involving both compliances (i.e., the compressibilities) and stiffness (i.e., the shear modulus), is used here in order to preserve as much continuity as possible with the notation used in the previous equations. There are numerous other notations used in poroelasticity, as well as many slight differences in the formulations of the equations that are more than merely notational. Commonly used formulations are presented by Rice and Cleary [1976], and Green and Wang [1986].

For purely static problems, or steady-state conditions, the only additional equation that is needed is one for the pore pressure field. The pore pressure is often found from the equations of fluid static,

$$\frac{dP_p}{dz} = -\rho f g \tag{3.4}$$

where ρf is the fluid density and z is the vertical coordinate, along with boundary

conditions (such as atmospheric fluid pressure at the surface $z = 0$).

In the next regime of behavior, which can be called quasi-static, the deformations are slow enough that inertial effects can be ignored, but the changes in pore pressure that result from pore fluid diffusion must be accounted for. The diffusion of pore pressure can be treated by the usual equation of reservoir engineering,

$$\frac{\partial P_p}{\partial t} = \frac{k}{\phi \mu C_t} \nabla^2 P_p \qquad\qquad (3.5)$$

in which k is the formation permeability, μ is the pore fluid viscosity, and C_t is the total compressibility of the pore space plus the pore fluid [Matthews and Russell, 1967].

This coupling between the rock stresses and the pore pressure leads to interesting phenomena, whose importance to petroleum engineering has only recently begun to be examined. Detournay and Cheng [1988], for instance, showed that because of transient changes in pore pressure, the borehole stresses in the first few hours after drilling may be appreciably, and qualitatively, different than those predicted by the Kirsch solution of classical elasticity [Sokolnikoff, 1956]. Rice and Cleary [1976] solved some basic problems in the quasi-static theory, such as finding the stresses arising from fault-like motions along planar discontinuities. Palciauskas and Domenico [1989] used quasi-static poroelasticity to study the long-term compaction of sedimentary basins. Walder and Nur [1986] used poroelasticity theory to infer the existence of sample-size dependence during measurements of permeability by the pulse-decay method.

3.2 LABORATORY MEASUREMENTS OF COMPRESSIBILITIES

In order to measure the various porous rock compressibilities in a laboratory, it is necessary to be able to subject a sandstone specimen to controllable levels of confining and pore pressures, and to measure the resulting pore and bulk volume changes. A typical system for carrying out these measurements is the one used by Greenwald [1980], which was later modified by Zimmerman [1984a]. This system is illustrated schematically in Fig. 3.4. Roughly speaking, it consists of four subsystems: a pressure vessel, a cylindrical specimen and its various fittings, a confining pressure system (left side of Fig. 3.4), and a pore pressure system (right side of Fig. 3.4).

The pressure vessel used by Greenwald [1980] and Zimmerman [1984a] was a hollow chrome steel alloy cylinder with walls with a thickness of at least 2.5 cm. The top of the vessel screwed into the bottom piece, with an 0-ring providing the pressure seal. The standard working pressure of this cell was 69 MPa (10,000 psi), although it would be advantageous to be able to pressurize the system to higher pressures. The internal length of the sealed vessel was about 23 cm. The bottom of the vessel had fittings to allow strain-gauge leads, thermocouple wires, etc., to enter the vessel. This simple vessel allowed

hydrostatic confining pressure only to be applied to the cores; triaxial loading requires modifications (see below) such as that of Andersen [1988]. The cylindrical vessel is surrounded by two semi-cylindrical heaters, which are in turn surrounded by layers of insulation. The heaters are controlled by a temperature controller, which allows operation of the system at elevated temperatures. Insulation is used to provide a longer thermal time-constant for the system, which allows easier temperature control. An alternative is to have smaller heaters inside the vessel, surrounding the core, thus eliminating the need to heat up the entire system. Contreras et al. [1982] and Somerton [1982] have made measurements of compressibilities under elevated temperature using the same equipment.
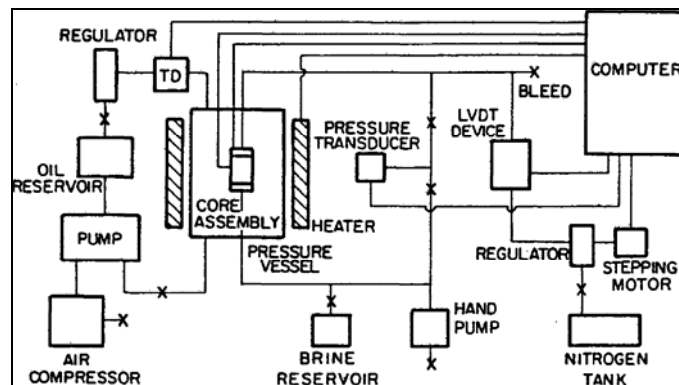
Figure 3.4: Schematic diagram of system used to measure compressibilities of porous rocks [after Zimmerman, 1984a].

The vessel is filled with a fluid that provides the confining pressure. In order for this fluid not to corrode the vessel, or to create short circuits for the electrical leads in the vessel, an insert of a nonconductive fluid such as silicone oil is usually used. The fluid is pressurized by an air-actuated positive-displacement pump, which is connected to an air-compressor (lower left of Fig. 3.4). The exit line from the cell passes through a pressure transducer, which measures the confining pressure Pc and then a pressure regulator, after which it passes back into the oil reservoir, which supplies the pump. The reading from the pressure transducer is transmitted to a computer for data collection (upper right of Fig. 3.4); alternatively, the pressure could be read manually from a pressure gauge. The system used by Zimmerman [1984a] contained a strain-gauge type pressure transducer with a range of 0-20,000 psi (0-138 MPa), which measured the confining pressure to an accuracy of ± 5 psi.

The pore pressure system is indicated on the right side of Fig. 3.4. A strain-gauge type pressure transducer, with a range of 0-10,000 psi (0-69 MPa) and an accuracy of ±5 psi, is used to measure the pore pressure. The device depicted in Fig. 3.5 is used both to measure changes in the pore volume, and to control the pore pressure. The device,

consisting of a precision-bore cylinder containing a movable piston, is shunt-connected to the pore fluid system. Attached to this piston is a linear variable differential transformer (LVDT), whose motion allows volume changes to be measured to within $\pm 1.3 \times 10^{-4}$ cm^3. This piston is rigidly connected to a larger piston, with an area ratio of 20:1, upon which pressurized nitrogen acts to control the pore fluid pressure. A regulator that is operated by a stepping-motor, which in turn is controlled by the microcomputer, controls the pressure of the nitrogen.
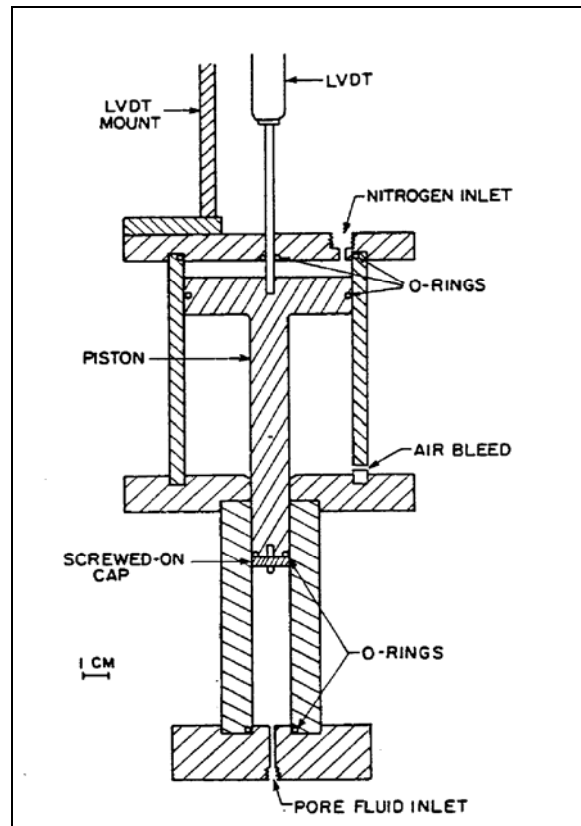
Figure 3.5: Device used by [Zimmerman, 1986a] to measure changes in the pore volume, and to control the pore pressure. The area ratio of the two pistons is 20:1, so that the pore fluid pressure is twenty times the nitrogen pressure, which is controlled by the computer. The pore volume change is measured by the LVDT attached to the piston.

The specimens used in most compressibility measurements are right circular cylinders, with diameters and length in the range of 1 -2 in (2.5-5.0 cm). It is of the utmost importance that the core be sheathed so as to keep the confining fluid and pore fluids from mixing. One such method for accomplishing this is the system used by Greenwald [1980] and Zimmerman et al. [1985a]. Cylindrical cores, 5.08 cm in length and 5.08 cm in diameter, were fitted with stainless-steel end-caps of the same diameter as the cores, which have holes drilled through them to allow for the passage of the pore fluid. A thin sheet of copper foil is then wrapped around the core, overhanging slightly onto the end-cap. Rubber

0-rings are fitted into grooves, which are cut around the circumference of each end-cap, after which the entire core and end-cap assembly is sheathed in trifluorethylene heat-shrink tubing. A heat gun is used to shrink the tubing onto the core assembly. As a final precaution against leaks, a bead of silicone rubber is placed along the interface between the end-cap and the tubing [Greenwald, 1980].

The first part of the testing procedure is the fitting and saturation of the cores; Greenwald [1980] describes this procedure in detail. After cutting the cores from a slab of sandstone, the faces are then milled square and flat. The specimen is then dried for twenty-four hours at 66°C in a vacuum oven to remove any moisture from the pores, after which it is carefully saturated with brine composed of 5 gms Kcl per 1000 cm^3 of de-aerated, distilled water. Saturation is accomplished with an apparatus such as that shown in Fig. 3.6.

With valves A and C closed, a vacuum of about 100 urn Hg (13.3 Pa) is maintained on the core for about twelve hours, in order to avoid trapping any air in the pores. Valve B is then closed, and valve C is opened, allowing the brine to saturate the core. The saturation process is complete when the liquid level in the burette stabilizes. The pore volume of the core is then determined from the difference between the dry and saturated weight, while the bulk volume is determined by measuring the specimen's dimensions with Vernier calipers.
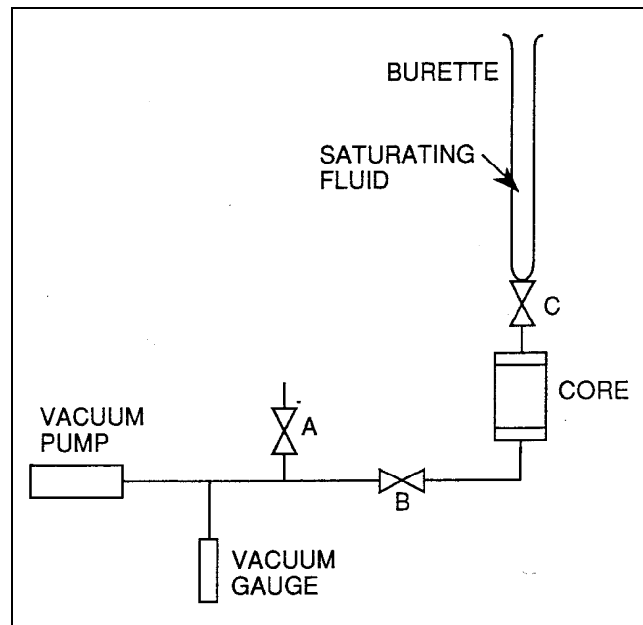
Figure 3.6: Apparatus used to saturate the cores with the pore fluid [after Greenwald, 1980].

Of the various porous rock compressibilities, by far the easiest to measure is C_{pc}, which is the derivative of the pore strain with respect to the confining pressure, with the pore pressure held constant. The earliest measurements of C_{pc} were made by Carpenter and Spencer [1940], using a method which is accurate and simple, but which is restricted to measurements in which the pore pressure is atmospheric. In their system, the pore pressure-measuring device shown in Fig. 3.6 was in effect replaced by a graduated burette whose upper end is open to the atmosphere; a schematic version of this type of system is shown in Fig. 3.7.
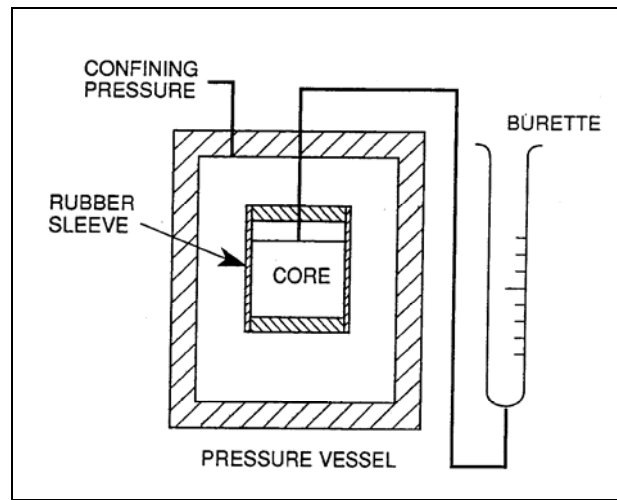
Figure 3.7: Schematic diagram of system used to measure C_{pc} [after Lachance and Andersen, 1983]. As the confining pressure is increased, the pore fluid is expelled from the core into the burette.

As the confining pressure is increased, the pore volume of the core will decrease, and some of the pore fluid will be expelled into the burette. Since the pore fluid is at constant pressure (and temperature), the total volume of the pore fluid will remain unchanged. Hence any fluid expelled from the core will be reflected as an increase in the height of the fluid in the burette. Hughes and Cooke [1953], using a similar apparatus, placed a slug of mercury above the water column in the burette, to facilitate the location of the water level, and to prevent evaporation of the pore fluid.

Zimmerman [l984a] measured C_{pc} by a semi-automated method, with the device shown in Fig. 3.5 used in place of the burette. The measurement process commenced with the computer instructing the stepping motor to alter the setting of the regulator, so as to provide a particular level of nitrogen pressure. This in turn provides a particular pore fluid pressure by means of the previously discussed piston device. The confining pressure is then increased by injecting more silicone oil into the pressure vessel with the air-actuated pressure intensifier. Following a specified increment in the confining pressure, a period of

several minutes is needed for the pore fluid system to equilibrate (which may be due to either frictional effects in the piston device or viscoelastic effects in the specimen), after which the computer records the pore volume change from the output of the LVDT.
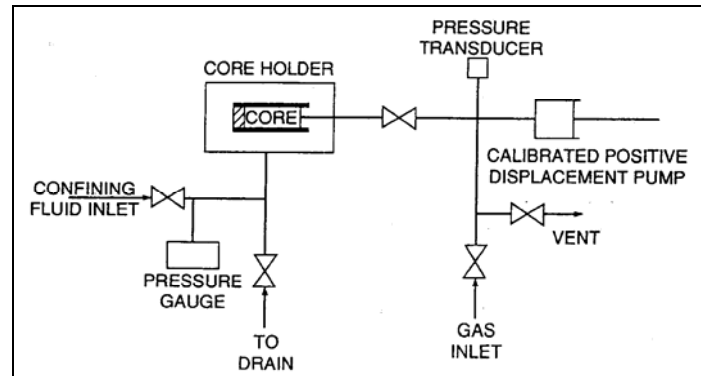
Figure 3.8: Schematic diagram of the apparatus used by Sampath [1982] to measure C_{pc} using nitrogen as the pore fluid.

This is continued through a cycle of increasing and decreasing confining pressure; the procedure is then repeated at several different pore pressures. The confining pressure increments could also be automated, by utilizing a stepping motor and a screw-type piston pump.

In the method used by Sampath [1982], the pore fluid (nitrogen) is connected to a hand-operated positive displacement pump (see Fig. 3.8). After each increment in the confining pressure, the position of the piston in the pump is altered until the pore pressure returns to its (fixed) value; the pore volume change is read from the dial of the pump. Note that use of a gas as the pore fluid necessitates strict temperature control, or else the thermal expansion of the gas overwhelms the volume change due to the pore compressibility. The advantage of this method is that by using nitrogen as a pore fluid, the difficulties associated with saturating the core with a liquid are avoided.

In order to measure C_{pp}, one must account for the fact that as the pore fluid pressure changes, the volume of the pore fluid will also change. For example, if the pore pressure is increased, the volume change measured by the pore pressure/pore volume device (Fig. 3.5) would partially reflect the fluid injected into the pore space of the core, but would also reflect the decrease of the pore fluid volume due to the fluid compressibility. Since the compressibility of the pore fluid is often of the same order as C_{pp}, this correction cannot be ignored. Another factor that must be taken into account is the "compressibility" of the measurement system itself. As the pore pressure increases, say, the volume available to the pore fluid outside of the vessel, in the tubes, pressure gauges, etc., will increase, due to the compliance of the apparatus. Fatt [1958] accounted for the compressibility of the pore fluid

35

(kerosene, in his case) by estimating the amount of pore fluid in the entire system, and using published pressure-volume-temperature data. Greenwald [1980] attempted to account for both the compressibility of the pore fluid and the compliance of the system by using a published equation of state for the pore fluid (brine), and by running calibration tests without a core. The procedure needed to account for these extraneous effects is described in detail by Sawabini et al. [1971]. Another way to correct for these effects would be to place a hollow steel core in the vessel, and vary the pore pressure while holding the confining pressure constant, using a device such as that shown in Fig. 3.5. Since the steel core is less compressible than sandstone by a few orders of magnitude, it could be considered incompressible. The piston device would then be measuring the pressure-volume relationship of the experimental apparatus system itself. If the same test is then carried out with a real sandstone core, the discrepancy in the measurements of the pore fluid volume could be ascribed solely to changes in the pore volume of the core.

The two bulk compressibilities, C_{pc} and C_{bp}, can be measured in an apparatus of the type depicted in Fig. 3.4, if the cores are fitted with strain gauges. The process of fitting the cores with strain gauges is described by Greenwald [1980]; see Fig. 7.6. Since the surface of the core is in general too rough and irregular for strain gauges to be directly attached, high-temperature epoxy resin is first applied to a small region of the core. The epoxy is dried in an oven for twelve hours at 66 °C, after which it is sanded down to be flush with the core. The epoxy serves the purpose of filling in the surface pores, so as to provide a smooth surface for the application of the strain gauge. The epoxy also prevents the pore fluid from reaching the strain gauge, and causing a short circuit. In order for the strain gauge wires not to be short-circuited or damaged by abrasion, a small patch of silicone rubber is applied at one end of the epoxy, for the gauges to be seated. The gauges are glued onto the epoxy with strain-gauge cement, and are then covered with a sheet of Teflon. The cores are then further prepared in the manner described above. Typically, strain gauges are applied in both the longitudinal and transverse directions, so as to detect any anisotropy of the core. Since strain gauges often fail in the high-pressure environment of the pressure vessel, it is prudent to use redundant gauges, in the event of one failing during a test. Greenwald [1980] also used a dummy gauge inside the vessel, not attached to a core, in order to compensate for the effects of pressure (or temperature).

Zimmerman [1986] made measurements of C_{pp} on a Bandera sandstone core, using a method analogous to that used by Sampath [1982] to measure C_{pc}. This was done with a modified version of the experimental apparatus shown in Fig. 3.4, with a manually

controlled screw-type pump replacing the air-actuated pressure intensifier. This pump functions as the bulk volume analogue of the device depicted in Fig. 3.5, with the volumetric displacement read manually from a vernier-type scale instead of as the output of an LVDT. As the pore pressure is increased, say, the bulk volume of the core will increase. The confining fluid then has less space to occupy, and its pressure increases slightly.
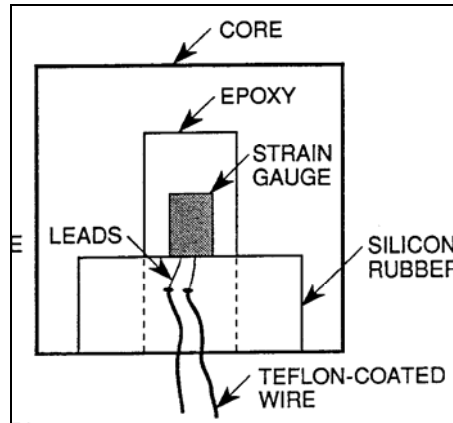
Figure 3.9: Schematic diagram of method used by Greenwald [1980] to attach strain gauges to cores.

The screw pump is then released, until the confining pressure returns to its nominal value. Since C_{bp} is measured at constant confining pressure, the volume of the confining fluid is constant, and so the bulk volume change of the core is measured directly by the Vernier scale of the pump. These measurements proved to be very sensitive to temperature fluctuations of the system, due mainly to the large ratio of confining fluid volume to rock volume. This problem was partially mitigated by using a less compressible confining fluid (glycerin) for the C_{bp} measurements; an optimal system would have as small a ratio of confining fluid volume to rock sample volume as possible.

The measurements discussed above were all made under conditions of hydrostatic confining pressure. Chierici et al. [1967] made triaxial stress measurements of sandstone compressibility. Wilhelmi and Somerton [1967], Teeuw [1971], and Andersen [1988] used devices similar to that shown in Fig. 3.10. This apparatus allows a uniaxial stress to be applied by a piston, superimposed on top of the biaxial stress applied to the sides of the core by the "annulus pressure" (see Fig. 3.10). Andersen [1988] used strain gauges to measure the bulk strain along the longitudinal and transverse directions of the core, and used an external burette to measure the volume of pore fluid expelled from the core. If the core was linearly elastic, relating triaxial compressibilities to hydrostatic compressibilities

would be trivial [Teeuw, 1971]; for typical nonlinear sandstone, this relationship is not yet entirely understood [Andersen, 1988].
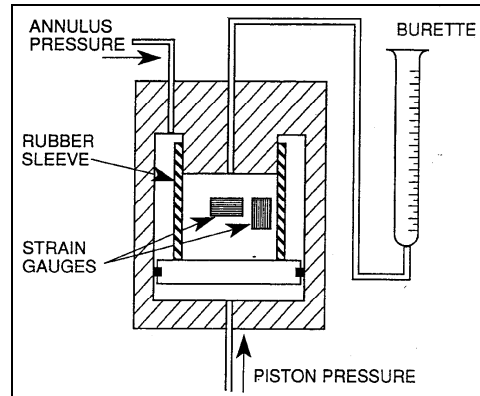
Figure 3.10: Schematic diagram of apparatus used to measure pore and bulk compressibilities under triaxial loading conditions [after Andersen, 1988]. The confining fluid in the annulus provides two equal horizontal principal stresses, while the fluid acting on the piston provides the third principal stress. An 0-ring is used to prevent pressure equilibration between these two fluids.

Undrained bulk compressibility can be measured by using the same procedure as used to measure C_{bc}, but with the pore fluid lines closed off. In order that the experimental set-up exactly reproduce "undrained" conditions, it is important that no pore fluid exist outside of the core. This is easily accomplished by plugging off the pore fluid lines at the end-caps. However, such an experimental configuration is not conducive to measuring the induced pore pressure, since these measurements require a pressure gauge of some sort to be in contact with the pore fluid. Excess volume in lines, gauges, etc., would provide a "sink" for the pore fluid; leading to an underestimation of the induced pore pressure coefficient (B). Wissa [1969] analyzed the "undrained" compression of a core connected to external pore fluid tubing, and concluded that the ratio of pore fluid volume exterior to the core to the actual pore volume should not exceed 0.003. Green and Wang [1986] devised a system to measure B that placed a pore pressure transducer flush against the core (Fig. 3.11). The only extraneous volume was in the transducer chamber itself, and it typically amounted to only about 5×10^{-4} of the pore volume of the core. This system was used to measure the induced pore pressure coefficient of Berea, Massillon, and Tunnel City sandstone cores. Measurements of induced pore pressures in porous rocks and sands have also been made by Mesri et al. [1976] and Dropek et al. [1978].

More recently, Laurent et al. [1993] conducted and performed experiments similar to those done by Zimmerman et al. [1986]. The used apparatus is shown in Fig. 3.12. In their experiments, the pore pressure remains constant (2MPa) during the whole experiment. The fluid used is composed of 90g/l NaCl and 10g/l $CaCl_2$. The Berea limestone sample

characteristics are diameter 4 cm, length 7.61 cm, porosity 19.5%. The obtained results for C_{pc} are quite similar to the values previously published by Zimmerman.
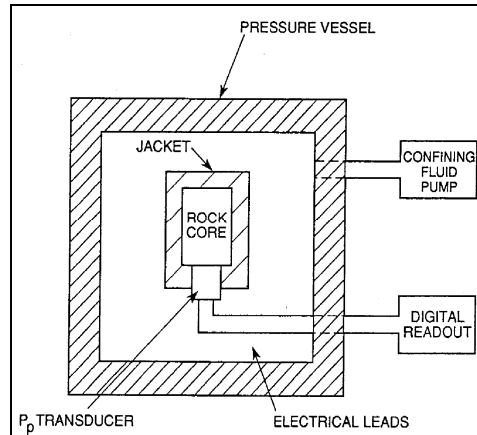
Figure 3.11: Schematic diagram of apparatus used by Green and Wang [1986] to measure induced pore pressures during undrained compression.
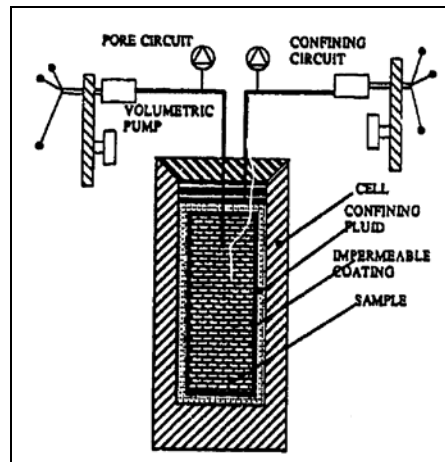
Figure 3.12: Schematic diagram of apparatus used by Laurent et al. [1993] to measure induced pore pressures during undrained compression and similar to those performed by Zimmerman et al. [1986].

The compressibility apparatus (see Fig. 3.12) used by Laurent et al. [1993] and Zimmerman et al. [1986] is one of the best available to measure and investigate the effect of the four compressibility relationships (i.e., Eqns. 2.5 - 2.8). My study is performed by a compressibility apparatus which has been developed by CoreLab. Co. Ltd. This apparatus has similar features to the one used by Laurent and Zimmerman. With this CoreLab compressibility instrument, I can measure only the pore volume compressibility effect with changing reservoir pressure. Pore volume compressibility is widely used in reservoir engineering practice.

CHAPTER 4
4. **DESCRIPTION OF EQUIPMENT AND SAMPLES TEST PROCESSES**

4.1 PRINCIPLE OF APPARATUS COMPONENTS

Figure 4.1 below illustrates the main component used to perform my research. In my context, I will describe the control panel in most detail, and the other main two principle components will be described only briefly.
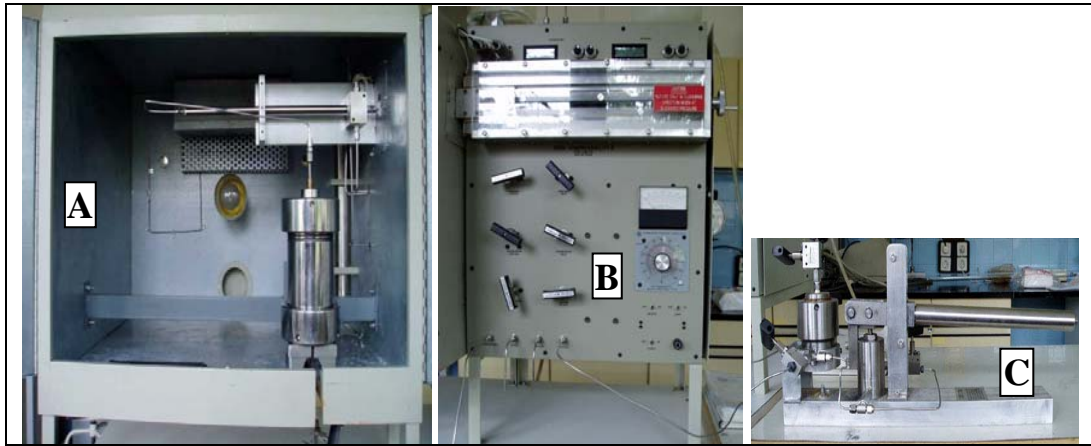
Figure 4.1: The main three components of the compressibility apparatus: A) the oven and the core holder assembly, B) the control panel, C) special water pump.

4.1.1 Oven

The outside dimension of the oven is 30 x 25 x 24 inches. It has a temperature range to 52^0C with a heater rated at 1000 watts. This industrial oven has been modified to suit Core Laboratory Inc. requirements by installing a viewing panel. One 200 cm^3, 10,000 psi rated reservoir is also installed on the back wall of the oven.

The oven is used to maintain a constant temperature (52^0C) environment around the core holder. The reservoirs hold the fluid and are used to provide the effective overburden pressure. The core holder is used to house the core for pressure application. The fan mounted on the back wall provides forced air circulation to maintain stable temperatures.

4.1.2 Control Panel

Figure 4.2 shows the controls and indicators on the rock compressibility's control panel used to carry out this research. The numbers serve to identify the components and a functional description of each function is presented in Table 4.1.
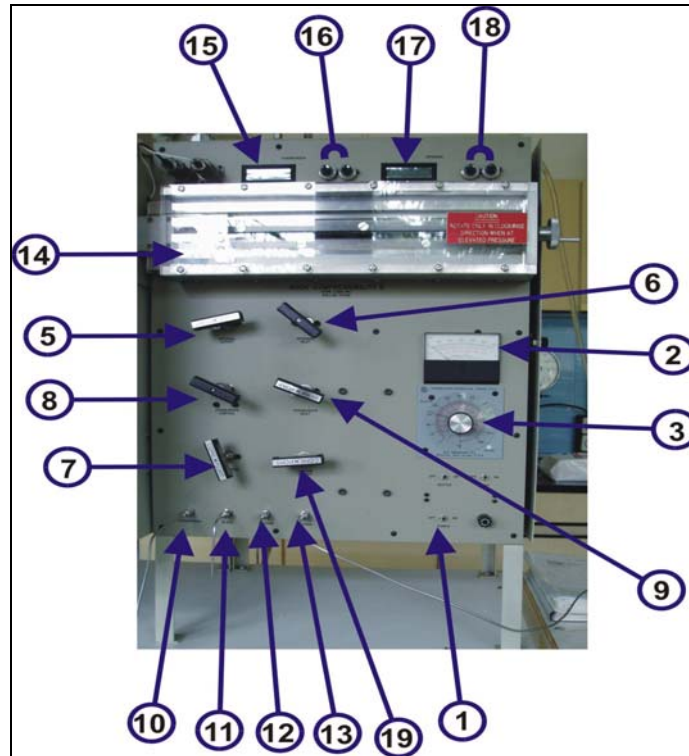
Figure 4.2: Control panel controls and indicators (see Table 4.1).

Table 4.1 Control and indicator function of the control panel

ITEM	CONTROL/INDICATOR	FUNCTION
1.	ON/OFF Power Switch	Toggle switch to control power to the chassis.
2.	Oven Temperature Indicator	Indicates oven temperature in degrees Centigrade or Fahrenheit. Accuracy of full scale is plus or minus 2%.
3.	Temperature Controller	Regulates oven temperature.
4.	Temperature On/Off switch	Switches on or off the heating system.
5.	Internal Cutoff Valve	Regulates internal pressure while system is being pressurized, and controls system volume during test. Valve is rated for 11500 psi and has non-rotating stem.
6.	Internal Inlet Valve	Controls the fluid and pressure entry into the internal system.
7.	Overburden Bleed Valve	Used for bleeding and isolating the system. Same type valve as item 5 above.
8.	Overburden Control Valve	Used for precise control of small flows, and to control overburden pressure during tests. A micro-metering valve rated at 11000 psi. This valve does not affect cutoff.
9.	Overburden Inlet Valve	Controls the high pressure fluid into [Core

41

		holder] the external system. The same type valve as described in item 5. NOTE: Valves described in items 9 and 10 serve the same purpose.
10.	Overburden Inlet Port	A quick-connect port used to provide connections for overburden network.
11.	Bleed Outlet Port	A quick-connect port used to bleed off the overburden pressure from the system
12.	Vacuum Port	A quick-connect port used to provide connections for the vacuum system when saturating core or drying the system.
13.	Internal Inlet Port	A quick-connect port used to provide connections for the internal system network.
14.	Internal Volume Control Assembly (Vernier Scale)	A linear displacement Vernier scale that works on the screw principle whereby one revolution of the rotary scale slides the pointer on the linear scale. The rod is used to change the internal volume of the system. During a test, the rod is always withdrawn. The rod is never to be increased against high pressure.
15.	Overburden Digital Display	Displays overburden pressure reading
16.	Overburden Potentiometers Controls	The "Zero" potentiometer controls the zero reading of the transducer and the "Span" potentiometer controls the span. Used to calibrate the overburden pressure transducer.
17.	INTERNAL Digital Display	Displays internal pressure reading.
18.	Internal Potentiometers Controls	The "Zero" potentiometer controls the zero reading of the transducer and the "Span" potentiometer controls the span. Used to calibrate the internal pressure transducer.
19	Vacuum control Valve	Controls the fluids from the vacuum pump when saturating core or drying the system.
The following two items are shown on the plumbing schematic in Fig. 4.3		
20.	Core Holder Cutoff Valve	Isolates the core holder from the external pressure system. It has a larger orifice for greater flow than valves used elsewhere in the system. The valve is rated for 11000 psi.
21.	Core Holder Outlet Valve	Regulates the outflow of saturating fluid and the closing of the internal system during a test.
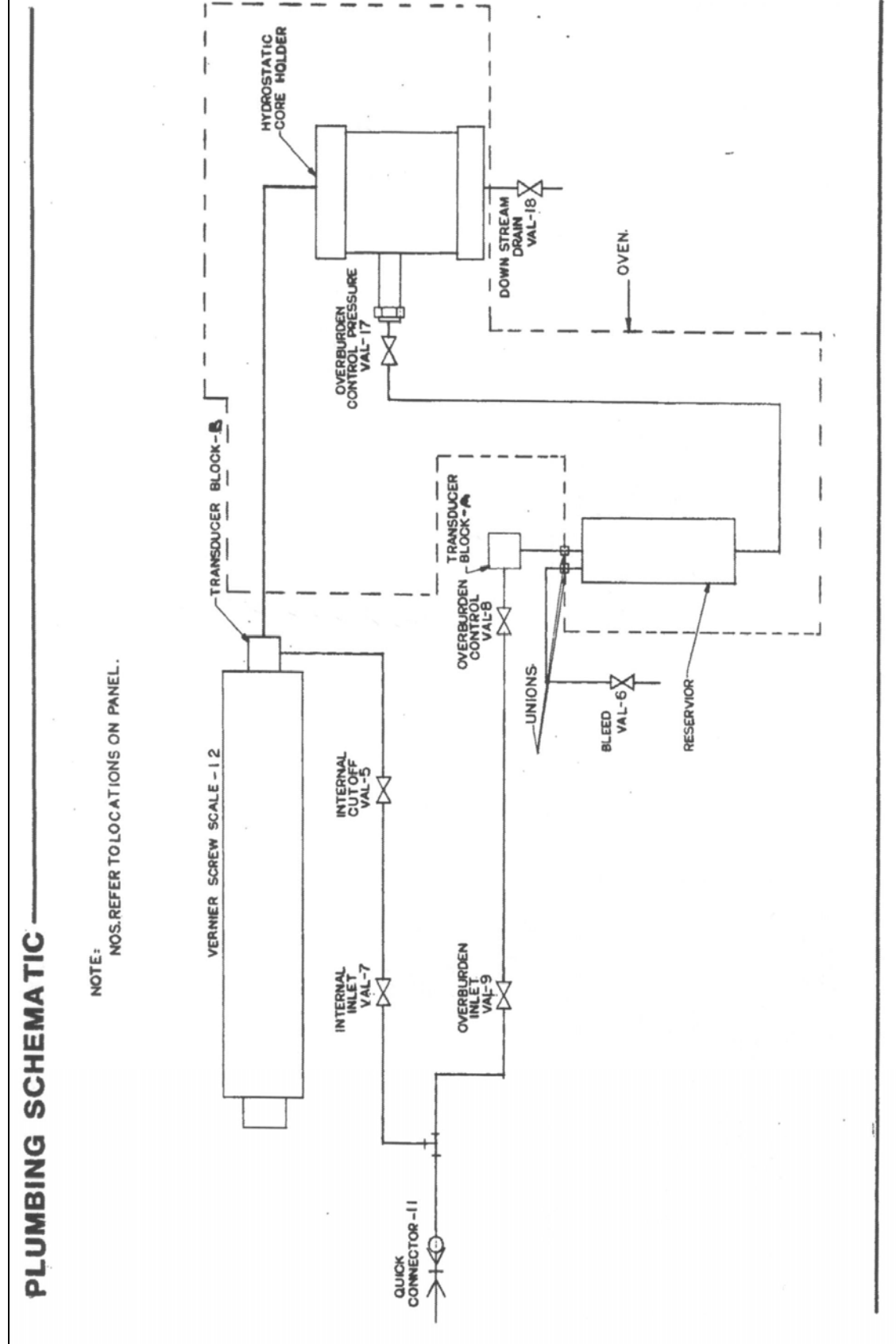
Figure 4.3: Compressibility apparatus II's plumbing schematic

4.2 EXPERIMENTAL TECHNIQUE

The four variables $P_{conf.}$, P_{por}, V_b and V_p must be independently measured and controlled. The use of small diameter tubing and low injection volumes reduces to a minimum the errors induced by the compressibility of the system. The compressibility apparatus used in this study was designed and manufactured by Core Laboratory Inc. It comes with a small manually operated pump to control the confining pressure on one side, as shown above in Fig.4.1C.

4.2.1 Preparation of Samples

All non-destructive tests that need to be performed on the sample should have been completed prior to the Compressibility test. The sample can be permanently damaged during the compressibility test if it is stressed beyond its elastic limit.

The samples should be cleaned and dried at about 180°F (82.2^0C). The permeability and porosity is then measured at the starting stress condition (usually 200 psi NCP). Before the compressibility test can be performed, the samples must be jacketed in the manner described later in this chapter, in order to suitability transmit effective overburden pressure and restrain the rubber core holder sleeve from intruding into the pore spaces.

4.2.2 Measuring Porosity

Initial porosities were determined by an API-approved method [API- RP40, 1960], which constituted of determining the pore volume by restoration and the bulk volume by displacement or caliber measurement. For accurate measurement, I estimate the porosity by using the two different techniques described below.

4.2.2.1 Helium Porosimeter

A porosimeter is an instrument used to measure the porosity of a sample by comparing the bulk volume of the sample with the aggregate volume of the pore spaces between the grains.

The Corex Helium Porosimeter (Fig. 4.4) used in this study is an analytical grade laboratory instrument used for measuring the pore volume, grain volume, porosity and grain density of rock samples. It is supplied with sample cups for 1 inch and 1½ inch diameter samples, but can also cater for a wide variety of other sample sizes using either custom size cups, or the remote cell connection. The remote connection also allows the

measurement of porosity at overburden pressure. The instrument designed to be quick and easy to use, and to give accurate, reliable and repeatable results. Optionally available is a built-in PC interface allowing automatic data acquisition via an IBM compatible PC's standard serial port.

Figure 4.4: Corex's helium porosimeter used for measuring porosity.

Steps for measuring porosity:

1. Determine the sample dimensional volume (Vgeo, cm^3).

2. Determine the volume of the cell V_{cell} and the volume of the expansion volume $V_{expansion}$ using the calibration sphere. You can do this by:

3. Determining the zero reading for your pressure sensor.

4. Introducing gas to the sample cell; measuring gas pressure.

5. Allowing the gas to expand into the expansion volume; measuring gas pressure.

6. Repeat the above steps with the calibration volume in the cell.

7. Calculate V_{cell} and $V_{expansion}$. Detailed steps are described in the instrument manual.

8. Determine the porosity of your samples by repeating steps (b) and (c) with your sample in the sample cell.

9. Read the on-screen and/or printout result for the average volume (V_{avg}, cm^3) as shown in table 4.2.

10. Calculate the helium porosity value,

$$Porosity\,(\phi) = \frac{Sample\,dimensional\,volume - Average\,volume}{Sample\,dimensional\,volume} = \frac{Vgeo - Vavg}{Vgeo}$$

Table 4.2: Output of Corex helium porosimeter results

Reference Volume	87.5717	cm^3
Number of runs	3	
Sample Weight	131.0153	g
Average Volume	50.8417	cm^3
Average density	2.5769	g/cm^3
Standard Deviation	0.0041	g/cm^3
$\Phi =$	**0.2344092**	

4.2.2.2 Porosity by Saturation Method

1. Measure the sample dimensions and calculate the volume (V_{geo}, cm^3).

2. Dry the sample in the oven (about 180^oC)

3. Determine the sample's dry weight (G_{dry}, g).

4. Completely emerge the samples in the prepared brine solution for one day. In this study 5 mg/l of CaCl salt was used

5. Place the samples in the vacuum till they are completely saturated under vacuum condition and no bubbles come out.

6. Re-determine the weight of the saturated sample "wet weight" (G_{wet}, g).

7. Using published tabulated data, estimate the fresh water density at the laboratory temperature (ρw) of the adjusted to the brine mixed solution (i.e. in our case 5g/ml). For these samples the result was about $\rho w = 1.0031 g/cm^3$

8. Arrange all the laboratory data in a table to simplify the calculation, see Table 4.3 as example.

9. Calculate the pore volume $V_p = \dfrac{\text{Wet weight - Dry weight}}{\text{Water density}} = \dfrac{G_{wet} - G_{dry}}{\rho_w}, cm^3$

10. Calculate the sample porosity $Porosity(\Phi) = \dfrac{\text{Pore volume}}{\text{Sample dimensional volume}} = \dfrac{V_p}{V_{geo}}$

Table 4.3: Collected input data for porosity estimation by saturation method

Sample wet weight = G_{wet} =	147.1100	g
V_{geo} =	66.3748	cm^3
Pore Volume = V_p =	16.045004	cm^3
Sample length = L =	69.980	mm
Sample radius = d =	34.760	mm
d/2 =	17.380	mm
Sample cross section area = A =	9.489633	cm^2
Sample dimensional volme =V_{geo} =	66.408452	cm^3
Φ =	0.24161087	

4.3 COMPRESSIBILITY APPARATUS OPERATION

4.3.1 Leak-off Test

It is necessary that the system be checked for leaks before starting to perform compressibility measurements. With the core holder in the system as shown in Figure 4.1B for the leak check, the leak test is performed as following:

Attach a pressure source (the special water pump) to the system by using the inlet port (quick connect, No. 13 on the control panel)). Open the internal inlet (No. 6 on control panel), overburden inlet (No. 9 on control panel) valves, and apply pressure to the system. Open the overburden valve (No. 7 on control panel) and raise the overburden pressure to 400 psi. It is necessary that a 200-psi differential be maintained between the overburden and internal pressures. The internal pressure will build up more slowly than the overburden pressure. Slowly open the internal cutoff valve (No. 5 on control panel), to increase the internal pressure, until the pressure begins to increase. When the pressure reaches 200 psi, close the internal cutoff valve (No. 5 on control panel). This process is repeated until the internal pressure reaches 10.000 psi. Hold these pressures from 1 hour to 2 hours and then check for leaks. Because the apparatus had been stored a long time, we noticed that pressure dropped during the leak test. The leak was located by looking for water drips, and all leaks were fixed before the equipment could be used for testing the compressibility of samples. Then the above process was repeated once again. Temperature changes can cause slight fluctuations in a degassed system, but they are not so apparent in the leaks check system.

4.3.2 Transducer Calibration

There are two transducers controlled by four potentiometers on the control panel. The zero controls are very fine. Crude controls are located inside the electronics package. These two transducers must be calibrated after the leak test has been performed. It is necessary that the calibration be checked after 150 hours of operation to correct any transducer characteristic change over the period of time, as recommended by the manufacture.

In order to perform the calibration, the following equipment is required:

⇒ A dead weight tester or 10,000 psi calibrated gauge such as a Heise Gauge (see Fig 4.5);and

⇒   A high-pressure source (see Fig 4.1C).

Figure 4.5: Heise gauge (Dead Weight Tester) used for potentiometer calibration.

Two potentiometers control each transducer. They are marked "Zero" and "Span". The "Zero" potentiometer controls the zero reading of the transducer and the "Span" potentiometer controls the span. Using a known pressure and the potentiometers, the transducer can be calibrated as follows:

1.   Select the transducer to be calibrated.

2.   Match the potentiometers with the related transducer.

3.   Adjust the "Zero" potentiometer until the meter reads zero.

4.   Connect the pressure source and dead weight tester/Heise gauge to the system via the inlet port.

5.   Isolate the transducer by capping the end of the appropriate tube.

6.   Cap the tube containing the metering rod for internal pressure.

7.   Cap the tube connecting the annulus of the core holder for confining (external) pressure.

8.   Open the inlet cutoff and control valves.

9.   Using the dead weight tester/gauge as a reference, apply 5000 psi. If the digital display does not indicate 5000, adjust the "Span" Potentiometer until it does.

10.   Repeat step 7 twice with 5000 psi.

11.   Release pressure until it reaches 0 psi.

12.   When all the pressure has been released, check the digital display. If the display is not zero, adjust the "Zero" Potentiometer until it displays 0.

13.   Repeat steps 2 through 10.

14.   Repeat steps 1 through 11 for the second transducer.

4.3.3 Equipment Composite Correction

The reduction in measured sample compressibility due to application of equipment corrections is small but significant. The instrument corrections are fairly constant for a given instrument, sample diameter, sample mounting method, and maximum effective confining conditions. However, it is recommended each operator must establish individual instrument corrections on their instrument using the same conditions used in testing the samples [CORELAB Operations manual, 1980].

I have developed the method and procedures for equipment composite correction, calibration and compressibility measurements, which presented in this chapter (i.e., Chapter 4). It is easier and simplified the recommended procedures by the manufactured company of compressibility apparatus.

Below are the steps, which I have been developed and followed to perform correction of the equipment

1. Prepare the equipment as is normally done for testing samples. The internal system must be clean and dry.

2. Place stainless steel plug (approximately the same length and diameter as samples tested, and mounted in the same manner as samples tested) in the core holder in the usual manner. The steel plug has a 1/16 inch diameter hole drilled through its vertical axis to allow saturation of the internal system in the same manner used for samples.

3. Seal the core holder by inserting the end plugs.

4. Screw the core holder caps down on the end plugs until seated.

5. Make sure the rod Vernier scale is set at zero.

6. Open the internal cutoff valve (No. 5 on control panel).

7. Pressurize the system as mentioned above, while the rod Vernier scale is at zero position. Record first readings (P_c. and P_i-1). See Table 4.4.

8. Increase (with constant value each time) the overburden (P_c). Close and allowed to stabilize and record readings. The internal pressure control rod is then withdrawn by rotating the knob at the end of the Vernier scale (No. 14 on control panel) until the internal pressure drops to the starting level (step no. 7). Record internal pressure value (Pi-2). This action increases the internal brine volume, which consists of the apparatus volume and the sample pore volume. The apparatus volume will remain constant, but the brine volume increases because of water expansion resulting from the decreased pore pressure. The sample pore volume decreases due to the increase in effective pressure ($P_{eff} = P_c - P_i$).

9. Take sufficient readings.

10. Open the core holder outlet valve (No. 18 on the plumping schematic) thereby bleeding the internal pressure to zero.

11. Open the overburden bleed valve (No. 7 on control panel) and vent the pressure to zero.

12. Unload the steel sample from the core holder.

13. Reset the rod Vernier to zero for the new sample.

Table 4.4 Display the collected readings used for equipment correction.

#	P_c (psi)	P_{i-1} (psi)	Rod Position (L, inch)	P_{i-2} (psi)	P_{eff} (psi)	ΔVp meas (inch^2)
1	608	304	0.0000	304	0.0	0.0
2	2035	1701	0.0625	334	1397	0.0007670
3	3038	2725	0.0750	313	2421	0.0009204
4	4045	3735	0.1000	310	3431	0.0012272
5	5074	4766	0.1025	308	4462	0.0012579
6	6985	6675	0.1125	310	6371	0.0013806
7	9063	8754	0.1250	309	8450	0.0015340

4.3.3.1 Equipment Correction Calculations

14. Determine the volume of the rod withdrawn at each pressure. (area of cross section for 1/8 inch diameter rod x length = ΔVp meas.), as shown in Table 4.4.

15. Calculate the pore volume (V_p) in the usual manner. The volume of the 1/16" hole diameter of steel plug (area of cross section for 1/16" diameter x length of the steel plug 3 inches) will not change during the test. Any amount of calculated pore volume at a particular effective pressure that is less than the steel plug hole volume should be added to pore volumes of similar sized samples tested under similar conditions of effective pressure at that particular P_{eff}.

16. By plotting the both results (ΔVp meas.) and (ΔVp calc.) versus the effective pressure (P_{eff}), it can be seen whether the measurement readings were reliable (Fig 4.6). If there is any mistrust in the results, you will need to repeat the measurements.

17. Use a statistical program such as Microsoft Excel and/or Sigma plot software for regression fitting, known as data points, by fitting a straight line using the least square method. The outcome of linear fitting approaches, the curve fit constant (n1* = 0.3906426 and a1* = 4.6163E-05) is used to produce Table 4.5. This is the composite equipment correction I of the system. Due to using two different rubber sleeves for some samples, a second equipment correction was made using the thin rubber sleeve (see Fig. 4.7). The same procedure was

carried for the system correction using thin rubber. The result of the composite equipment correction II was (n1** = 0.546769676, a1** = 1.48165E-05).

Table 4.5: Correction equipment calculation I results

#	P_{eff} (psi)	ΔVp-meas (inch^3)	ΔVp calc (inch^3)	LOG (P_{eff}) (psi)	LOG (ΔVp-actu) (inch^3)
1	1397	0.000767	0.000782	3.14520	-3.11521
2	2421	0.000920	0.000969	3.38399	-3.03603
3	3431	0.001227	0.001110	3.53542	-2.91109
4	4462	0.001258	0.001230	3.64953	-2.90037
5	6371	0.001381	0.001414	3.80421	-2.85994
6	8450	0.001534	0.001579	3.92686	-2.81418

Statistical fitting result	
b = slope =	0.39064
Intercept =	- 4.3357
a =	4.61632
R^2 =	0.98
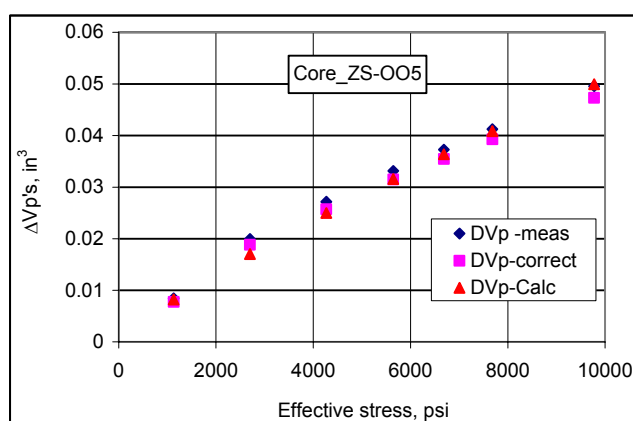
Figure 4.6: Cross plot illustrating measured and calculated pore volume changes versus effective pressure.
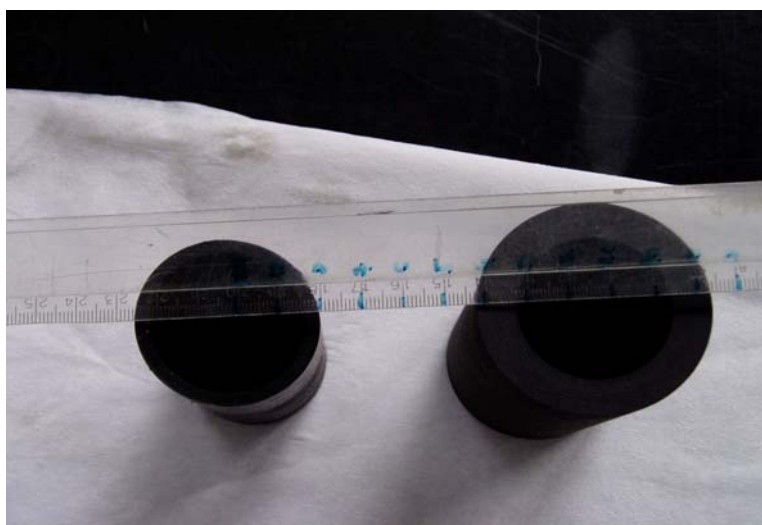
Figure 4.7: Thicknesses of core rubber sleeves used in this study

4.4 MEASUREMENTS OF PORE VOLUME COMPRESSIBILITY

This study is the first time measurement results have been published for such a wide range of porosity and rock types with rock obtained from Hungarian's hydrocarbon fields.. Three types of reservoir rocks have been studied in my experiments. These samples are collected from Hajduszoboszlo, Zsana, Algyő fields and two samples (F1 & F2) from Főldes gas field.

4.4.1 Pressurization of Samples

Connect the pressure source (water pump) to inlet port (No. 14 on the control panel). Open the overburden system valves (Nos. 9, 8, and 7 on control panel) and the internal valves (No. 6 on control panel), then apply pressure. Open the overburden valve (Nos. 9 and 7 on control panel) and raise the pressure. Maintain a 200 psi differential between the overburden pressure and internal pressure. Increase the internal pressure by slowly opening the internal cutoff valve (No. 5 on control panel) until an increase in the pressure is indicated on the digital display (No. 17 on control panel). Shut off the internal cutoff valve (No. 5 on control panel) when the desired internal pressure is reached. This process is repeated until the desired maximum overburden pressure is reached. Close all valves and let the pressures stabilize. If necessary during the test, build the pressure back to the desired level to maintain pressure at the desired levels.

The rock compressibility of the available rock sample has been obtained by applying the same procedure as described in the Equipment Composite Correction procedure (4.3.3) in this chapter.

1. Conduct and follow the steps from 1 to 13 as performed for equipment composite correction. Use core sample instead of the stainless steel sample.

2. Unload the rock sample from the core holder.

3. Reset the rod Vernier set to zero for the new sample.

4. Prepare for next test sample.

Table 4.6: Pore volume measurement data

#	Pc (psi)	Pi-1 (psi)	Rod Length (inch)	Pi-2 (psi)	P_{eff} (psi)	ΔVp –meas (inch^3)
1	660	358	0	660	0	0
2	1502	492	0.7125	1500	1141	0.008744
3	2990	536	1.5000	2981	2622	0.018408
4	4477	482	2.2000	4472	4114	0.026998
5	6099	468	2.7500	6094	5736	0.033749
6	7065	414	3.1000	7063	6705	0.038043
7	8048	412	3.5000	8047	7689	0.042951
8	10027	496	4.0000	10023	9665	0.049087

4.4.2 Laboratory Calculations of Pore Volume Compressibility

1. Determine the volume of the rod withdrawn at each pressure. (area of cross section for 1/8 inch Diameter rod x length = ΔVp meas), as shown in Table 4.7.

2. As a controlling step of our measurements we use statistical fitting of our measured data and the actual Peff as actual measurements (ΔVp actu.). This shows the amount of deviation from the measured data. See Table 4.8.

3. Calculate the equipment correction depending on the rubber type used for the sample. As example see Table 4.4 for composite equipment correction I of the system, (n1* = 0.3906426 and a1* = 4.6163E-05). See Table 4.5.

$$\Delta V_p = a1^* (P_{eff})^{n1^*}$$

(4.1)

$$\Delta V_p = a1^{**} (P_{eff})^{n1^{**}}$$

(4.2)

4. Use either Eqn. (4.1) or (4.2), depending on the rubber sleeve used, to calculate the fraction change in the pore volume. Calculate the corrected volume change (ΔVp correct). This is equal to step 1 minus step 3, (ΔVp meas. minus correction). See Tables 4.8 and 4.9.

5. Using a proper statistical program (e.g. Microsoft Excel and/or SigmaPlot software), get the fitting statistical results for the sample (i.e.,"b = slope" and "a = constant" values). see Table 4.7 as well as Table 4.9. Based on the statistical fitting type, the model should be differentiated at each point. Calculate the actual ΔVp.

6. Using the statistical program, find the best fit of the Peff and ΔVp corrected data points. For quality control of the data, Plot both points of (ΔVp meas), (ΔVp corrected) and the calculated (ΔVp actu) versus the effective pressure (P_{eff}). See Fig 4.7.

7. Find the pore volume (V_p) of the sample as calculated in Table 4.3, or from an alternative method.

8. Calculate the hydrostatic compressibility of the samples. For the limestone:

$$C_{pc}, 1/psi = \left(\frac{a \times b}{V_p}\right) \times \left(P_{eff}\right)^{b-1} \tag{4.3}$$

For the sandstone:

$$C_{pc}, 1/psi = \left(\frac{b}{V_p}\right)\left(\frac{1}{P_{eff}}\right) \tag{4.4}$$

The hydrostatic compressibility must be converted to uniaxial compressibility.

Uniaxial compressib ility = Hydrostati c compressib ility $\times$ 0.619 $\qquad$ (4.5)

Table 4.7: Statistical fitting results

LOG(Peff)	LOG(DVp -meas)		
3.057286	-2.094309		
3.418633	-1.761667		
3.614264	-1.591836	b = Slope =	0.827457
3.758609	-1.493962	Intercept =	-4.605445
3.826399	-1.441162	a =	0.000025
3.88587	-1.387458	R^2 =	0.998146

Table 4.8: Pore-volumecompressibility measurement correction calculations

#	P_{eff}	ΔVp -meas	ΔVp-Calc	ΔVp-correct	Correction
1	0	0	0		
2	1141	0.008744	0.008401	0.008048	0.000696
3	2622	0.018408	0.016723	0.017311	0.001096
4	4114	0.026998	0.024277	0.025596	0.001403
5	5736	0.033748	0.031963	0.032066	0.001682
6	6705	0.038043	0.036369	0.036211	0.001832
7	7689	0.042951	0.040733	0.040977	0.001974
8	9665	0.049087	0.04922	0.046850	0.002237

Table 4.9: Result of a linear statistical fitting approach estimation and results of uniaxial compressibility as a function of effective pressure

#	P_{eff}	ΔVp - meas	ΔVp - calc.	ΔVp - correct	Correction	C_{pc}-Zs-005 (2nd Run)
1	1141	0.008744	0.008401	0.008048	0.000695627	3.85E-06
2	2622	0.018408	0.016723	0.017311	0.001096351	3.34E-06
3	4114	0.026998	0.024277	0.025596	0.001402540	3.09E-06
4	5736	0.033748	0.031963	0.032066	0.001682049	2.91E-06
5	6705	0.038043	0.036369	0.036211	0.001831909	2.84E-06
6	7689	0.042952	0.040733	0.040977	0.001974335	2.77E-06
7	9665	0.049087	0.049220	0.046850	0.002237343	2.66E-06

LOG (P_{eff})	LOG ΔVp-actu
3.0572856	-2.0756729
3.4186327	-1.7766738
3.6142643	-1.6147970
3.7586091	-1.4953579
3.8263988	-1.4392649
3.8858699	-1.3900551
3.9852019	-1.3078622
b =Slope =	0.827456925
intercept =	-4.605445057
a =	2.48059E-05
R^2 =	1

V_p =	16.04500381	cm^3
	0.979126206	in^3
b - 1	- 0.17	
$a*b/V_b$	0.00002096	

CHAPTER 5
5. RESULTS AND DISCUSSION

5.1 ROCK IDENTITY CARDS

Twenty-two different cores were tested: five limestones, single friable and fourteen medium to hard sandstones as well as two very dense sandstones. Table 5.1 shows the characteristics of the various rock samples used in this study for pore volume compressibility measurements.
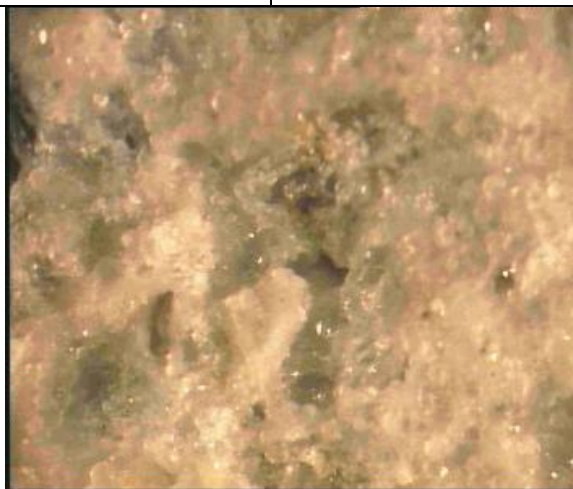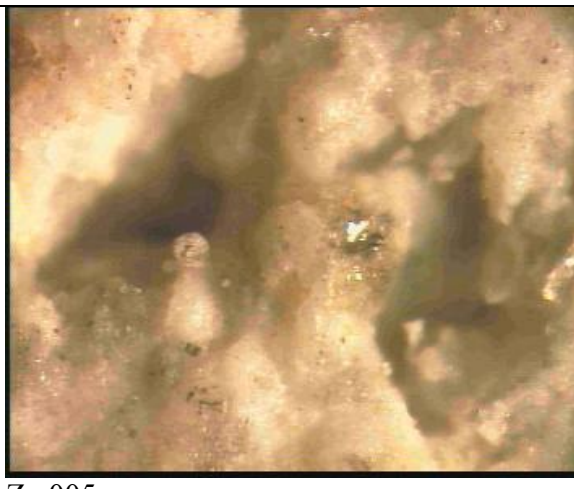
Table 5.1: Summary of the core samples used in the study

Field Name	Number of samples	Porosity range, %	Rock type	Hardness
Algyo	14	4 - 35	sandstone shales	medium to hard
Földes	2	less than 8	sandstone	very dense
Hajduszoboszlo	1	30	sandstone	friable
Zsana	8	22 - 25	limestone	medium hard

The eight limestone samples from the Zsana field are composed of more than 98% calcium carbonate. The only available friable sample from Hajduszoboszlo underground storage field is almost purely quartz sandstone. Algyo field samples are mostly medium to fine sandstone, and moderate to very hard. The samples 74.S, 76.S and 77.S have shale interbedded layers. The other samples F1 and F2 were obtained from the Földes Hungarian gas reservoir field.

Several high magnified power (200X) captured photographs of each texture of rock material have been studied and data from some other non-destructive measurements are presented in Tables 5.1 – 5.5.

Table 5.2: Magnified captured photograph of limestone textures from the Zsana field

Zs-001

Zs-002

Helium Porosity	0.23683	0.229384
Water Porosity	0.235376	0.235323
Rock type	Limestone	Limestone
Comments		

Zs-004

Zs-005

Helium Porosity	0.236425	0.234409
Water Porosity	0.23598434	0.241611
Rock type	Limestone	Limestone
Comments	Vuggy porosity	Vuggy porosity
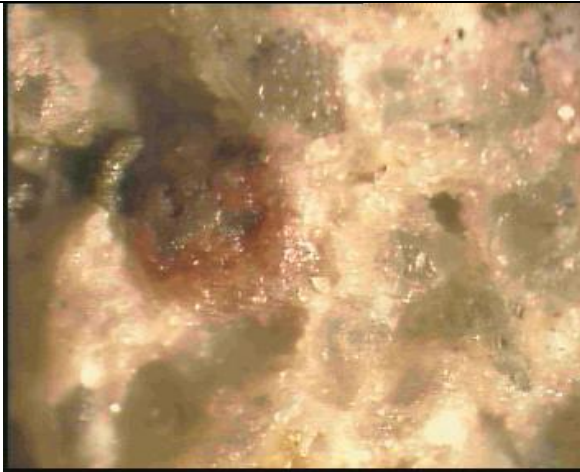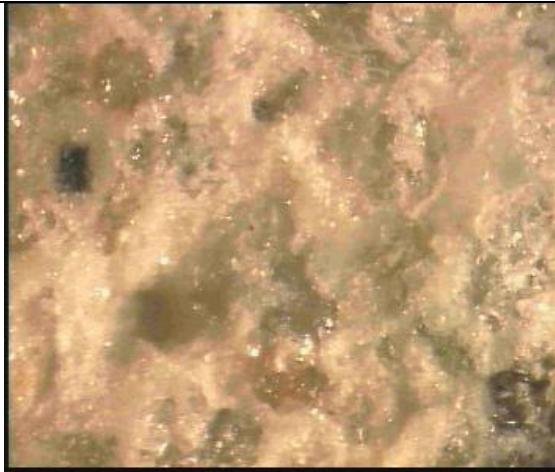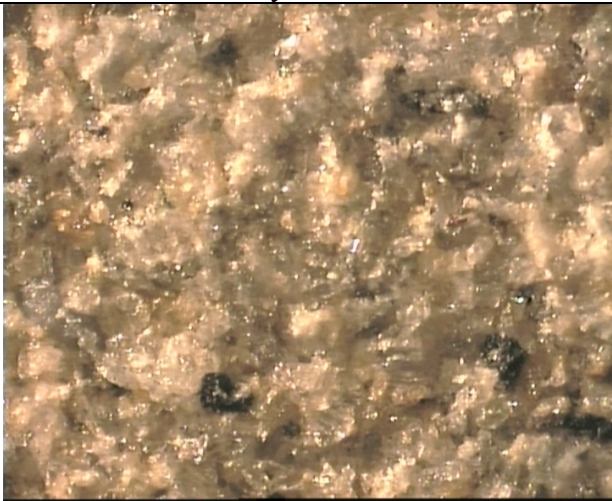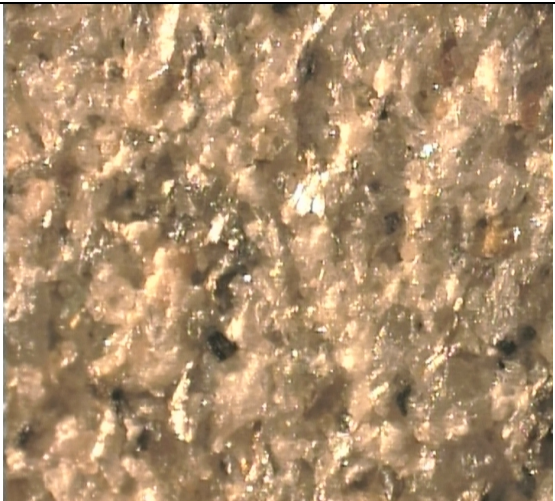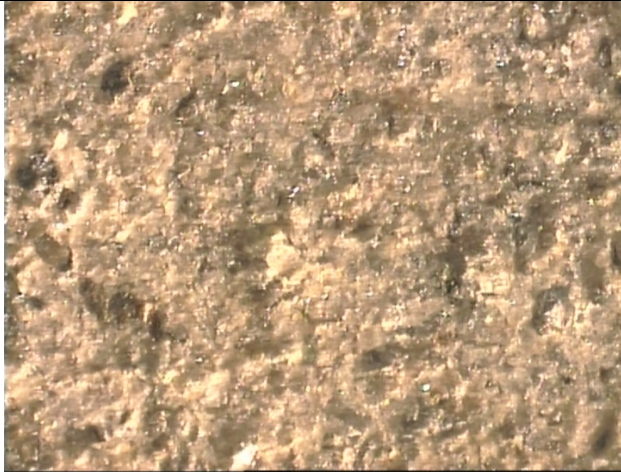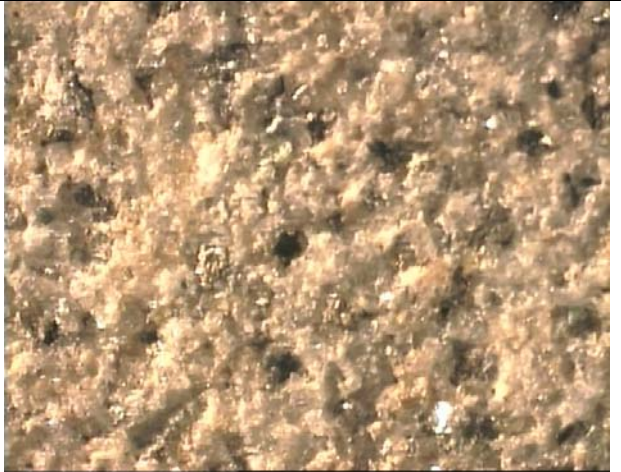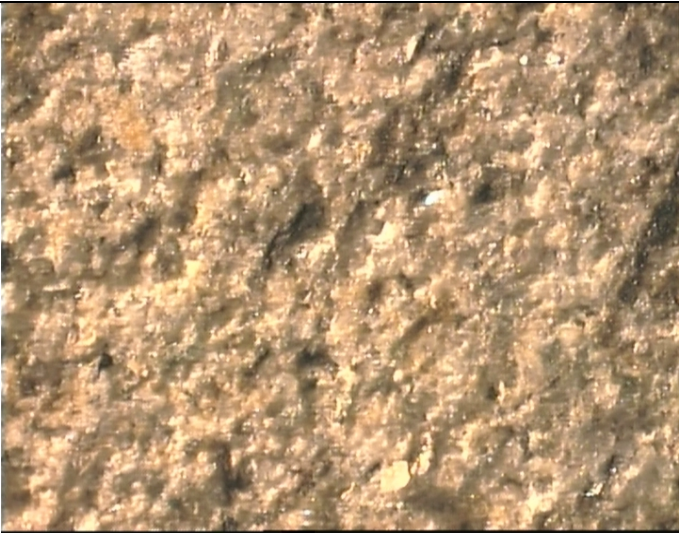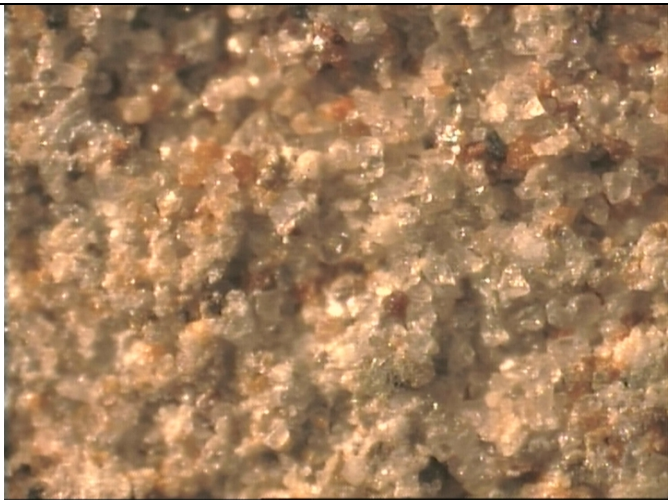
Zs-007		Zs-008
Helium Porosity	0.230799	0.282833
Water Porosity	0.248063	0.240416
Rock type	Limestone	Limestone
Comments	Vuggy/Intercrystalline	Vuggy/Intercrystalline

Table 5.3: Sandstone sample textures captured photograph magnified 200X and other laboratory measurements

30. S		43.S
Helium Porosity	0.1176	0.1721
Water Porosity	0.18940555	0.184454
Rock type	Sandstone	Sandstone
Comments		

69.S		74.S
Helium Porosity	0.1077	0.317
Water Porosity	0.100835	0.042092
Rock type	Sandstone	Sandstone
Comments		presence of shale interbedding

76.S		77.S
Helium Porosity	0.347	0.906
Water Porosity	0.044189	0.083878
Rock type	Sandstone	Sandstone
Comments	Presence of shale interbedding	presence of shale interbedding

82. S		83.S	
Helium Porosity	0.1499	0.1471	
Water Porosity	0.226856	0.148204	
Rock type	Sandstone	Sandstone	
Comments			

A. 1.1		A. .1. 2	
Helium Porosity	0.394506	0.305598	
Water Porosity	0.311308	0.31315	
Rock type	Sandstone	Sandstone	
Comments			
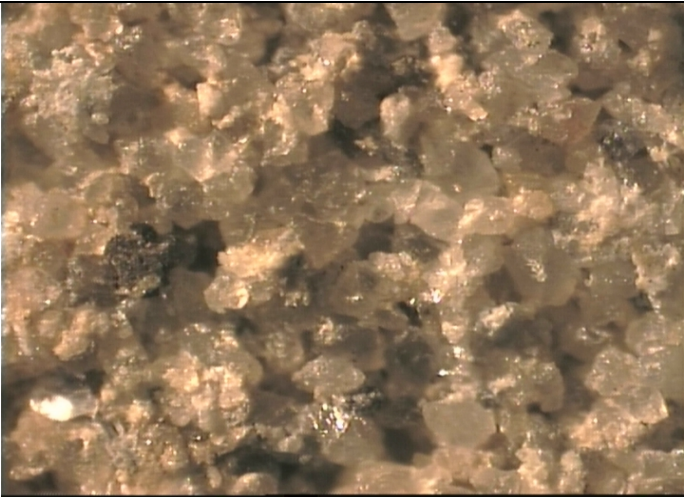
A 985.5..2

Helium Porosity	0.336857	0.342684
Water Porosity	0.322754	0.31419
Rock type	Sandstone	Sandstone
Comments		

SA-5

SA-7

Helium Porosity		0.13019
Water Porosity	0.088188	0.131103
Rock type	Sandstone	Sandstone
Comments		

Table 5.4: Magnified photographs of sample rock textures and other laboratory measurements
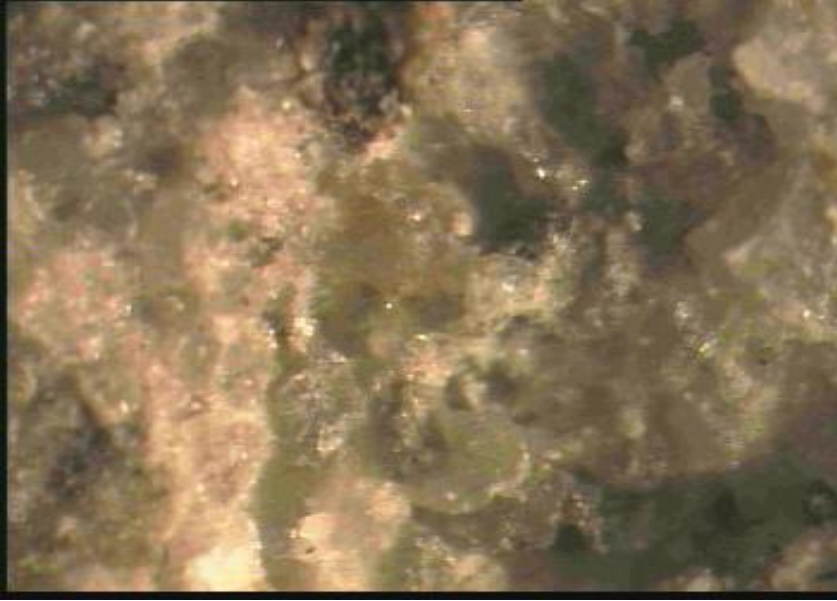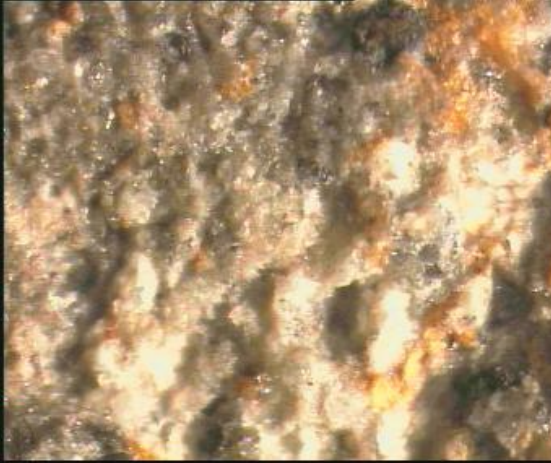
H	
Helium Porosity	0.394026
Water Porosity	0.292266
Rock type	Friable Sandstone
Comments	No Hcl. Acid reaction

Table 5.5: Magnified captured of sample's rock textures used in the study and other laboratory measurements

F1		F2
Helium Porosity	0.04717	0.019342
Water Porosity	0.055654	0.081079
Rock type		
Comments	No permeability	No Hcl reaction in either sample

5.2 EFFECTIVENESS OF CYCLING, TIME, AND TEMPERATURE

5.2.1 Cycling

Cycling is defined as a repeated application of the stress cycle. In other words, the sample is placed in the test cell and the effective pressure is increased to the same predetermined value (this value is sometimes higher than any stress the sample will ever be subjected to during reservoir depletion). The pressure is then released and a second, third, or even fourth cycle can be performed. Except for the case of exceedingly high-strength elastic rock, each cycle provides a lower compressibility value as a result of an irreversible change in the rock's internal structure (e.g. Fig. 5.1, Sample Zs-005). Cycling for any reason can result in lower compressibility volume on a rock that has failed internally, and the resulting condition is certainly not the condition of the sample as it is received in the laboratory. The effects of cycling can be more serious on friable samples because of their inelastic behavior (see Sample H). An exception to this would be in a compacting reservoir that had failed in situ during pressure depletion or a highly fractured reservoir that had failed because of tectonic forces during its history.

I have only one example (Sample F) where cycling may lead to a closer approximation of in situ compressibility and that was highly compacted rock samples.

5.2.2 Time

The pore volume compressibility values presented here were obtained from pore volume: effective-stress relationships by using pressure increments of about 10 to 30 minutes (about 20 min/300 psi). This time was generally sufficient to reach practical stress equilibrium for most samples. I am aware that true stress equilibrium for the samples cannot be obtained in the laboratory in any practical time. However, the most significant volume changes take place in the first few minutes of applied stress. It is not within the scope of my work to investigate these time effects; I only point out that they exist.

5.2.3 Temperature

The presented compressibility values in Fig. 5.1 were measured at room temperature (25°C). While I have not made a systematic study of the effect of temperature, a statistical analysis of pore volume compressibility at various temperatures between 54 and 135°C (130-275° F) by Newman [1973] showed no significant temperature effects. The results,

however, were not conclusive, since the scatter of the compressibility data at any one temperature was as great as any observable temperature effects, or greater. Von Gonten and Choudhary [1969], in discussing the effects of temperature on compressibility, show increases as high as 12 percent at 400° F (204°C). Therefore I recommend that all compressibility measurements be made at reservoir temperature. The apparatus used for this study is equipped with an industrial oven that has been designed to perform compressibility measurement at 52°C as maximum temperature. All the samples included in this study were measured at laboratory temperature 25°C.

As I mentioned, Sample Sz-005 showed no irreversible change in internal structure of the rock material. The only Sz-005 sample was measured at 25°C and 52°C to explore the effect of this temperature range (i.e. 25 – 52°C), where the internal structure material showed the same compressibility values on the second and third cycles. The effect of temperature was not that significant at high pressure, as represented in Fig. 5.1. However, as I mentioned before, all compressibility measurements should be made at reservoir temperature.
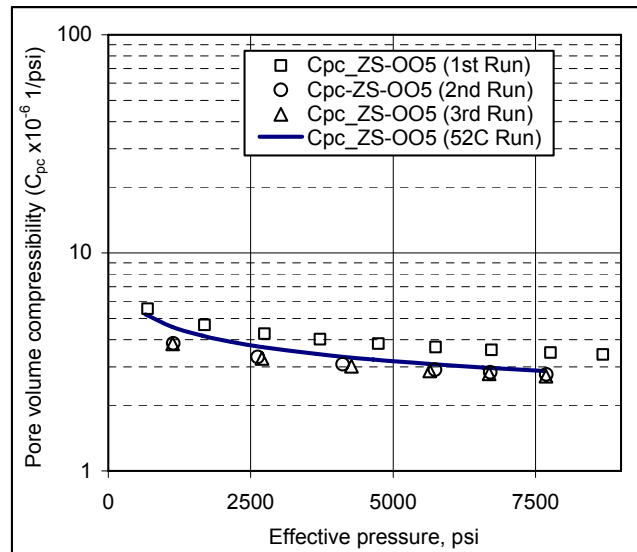
Figure 5.1: Compressibility plots for different cycle values at different temperatures, Sample Sz-005

5.3 COMPRESSIBILITY MEASUREMENT RESULTS

The results for evaluation of compressibility vs. pressure difference (i.e., effective stress) are presented in Figs. 5.2 and 5.8. The compressibilities are calculated over each corresponding pressure level, (C_{pc}) is estimated at each level.

64

5.3.1 Zsana Field Samples

Samples Zs-001, Zs-002, Zs-005, Zs-006 and Zs-007, represented by Fig. 5.2, show gentle slope compressibility curves and have closed compressibility values especially at high effective pressure. Although the five samples have closed porosity values, they has are not the same porosity type. This can be seen clearly in the captured sample pictures in Table 5.1 (e.g. Zs-006 and Zs-005 had vuggy type porosity). Heterogeneity is a well known characterization phenomenon for carbonate reservoir rocks. I should mention that Sample Zs-005 shows typical results for elastic rock (see Fig. 5.3) by displaying no irreversible change in its internal structure. This is supported by the same values of compressibility in the second and third cycle runs. Table 5.6 summarizes my results for measured compressibility carried out in this study.
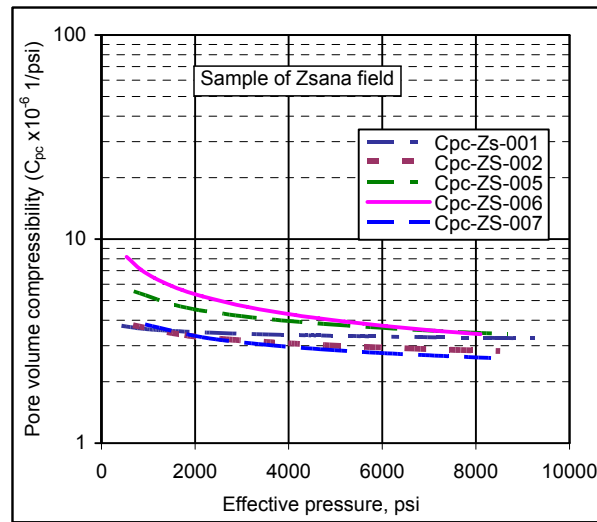
Figure 5.2: Group of compressibility values of all Zsana field samples versus effective pressure.
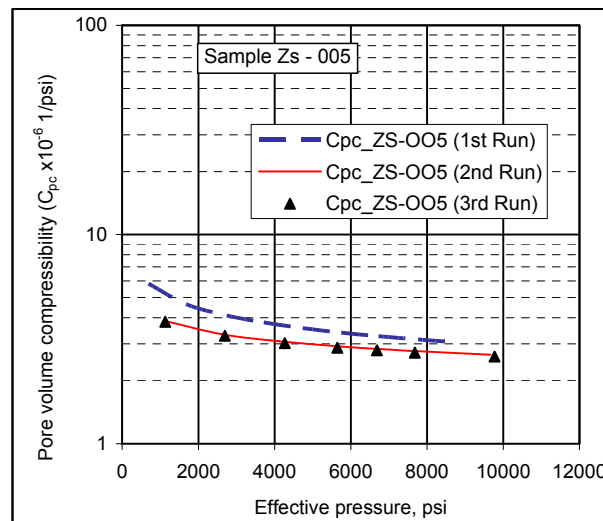
Figure 5.3: Pore volume compressibility of Sample Zs-005 from different cycle values at same laboratory temperature

65

Table 5.6: Summary of the obtained measured compressibility of Zsana field samples at average reservoir effective stress

Sample #	Porosity %	Effective stress psi	Compressibility 1/psi	Remarks
Zs-001	23.5	806.554	3.52287E-06	
Zs-002	23.5	806.554	3.38941E-06	
Zs-005	24.2	806.554	4.64884E-06	Run # 1
Zs-005	24.2	806.554	3.58065E-06	Run # 2
Zs-005	24.2	806.554	3.54481E-06	Run # 3
Zs-005	24.2	806.554	4.11771E-06	Run @ 52^0C
Zs-006	23.8	806.554	5.61481E-06	
Zs-007	24.8	806.554	3.42568E-06	

5.3.2 Hajduszoboszlo Field Sample

The quartzite friable sandstone was cut and cored from the Hajduszoboszlo reservoir. Cycling the sample twice led to higher compressibility values. This is an opposite result from the elastic limestone samples (e.g., Zs-005). Thus, the result confirms the inelastic behavior of the friable rocks. The compressibility results of various measured cycling runs of the friable sandstone (Sample H) are presented in Table 5.7.
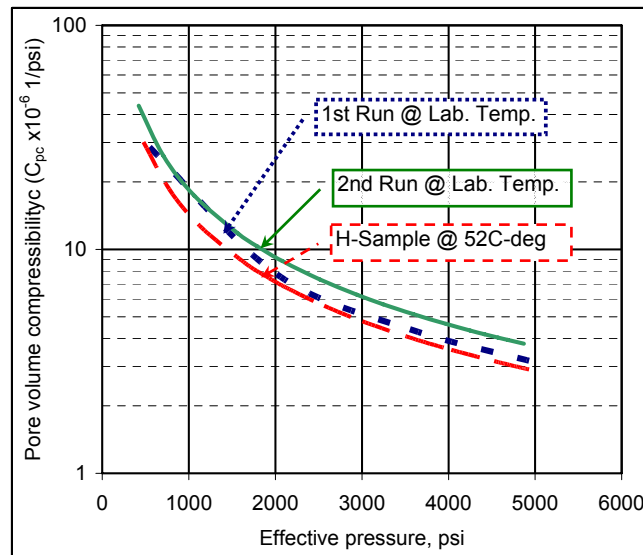
Figure 5.4: Pore volume compressibility plots of Sample H for different cycle run values at two different temperatures versus effective pressure

Table 5.7: Summary of measured compressibility of Hajduszoboszlo Field Sample at various measurement runs

Sample #	Porosity %	Effective pressure psi	Compressibility 1/psi	Remarks
H	28.8	508	1.44E-05	1st Run
H	28.8	508	1.73E-05	2nd Run
H	28.8	508	1.34E-05	@ 52^0C Run

5.3.3 Algyo Field Samples

The samples from the Algyo field used in this study are represented in Table 5.4. The porosity of the samples shows a wide range, from 4.21% to 32.28%. The samples are mainly composed of quartz sandstone with shale interbedding in some of the samples.

The compressibility results of the Algyo sandstone are presented in Figs. 5.5 - 5.8. Table 5.8 summarizes the measured results for compressibility and other data.

Table 5.8: Summary of measured compressibility of Algyo Field Samples

Sample #	Porosity %	Effective pressure psi	Compressibility 1/psi	Remarks
30.S	18.94	508	7.33E-06	
43.S	18.44	508	7.06E-06	
69.S	10.10	508	5.57E-06	
74.S	4.21	508	2.07E-05	
76.S	4.42	508	1.96E-05	
77.S	8.38	508	1.58E-05	
82.S	22.68	508	7.36E-06	
83.S	14.82	508	1.06E-05	
A985-1/2	32.28	508	6.77E-06	
A985-5/2	31.42	508	8.18E-06	
A.1.1	31.13	508	7.29E-06	
A.1.2	31.32	508	8.10E-06	
SA-5	8.82	508	3.16E-05	
SA-7	13.02	508	1.45E-05	
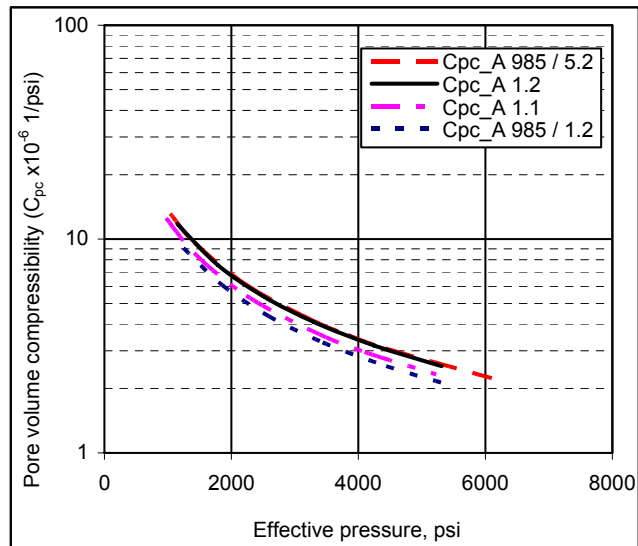
Figure 5.5: Pore volume compressibility of Samples A.1.1, A.1.2 and A 985 /5.2, A 985 /1.2 at same laboratory temperature
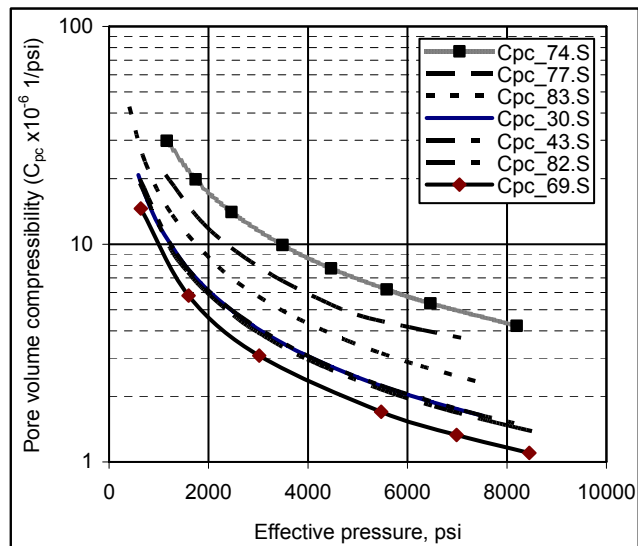
Figure 5.6: Measured pore volume compressibility of a group of sandstone sample readings at the same laboratory temperature.
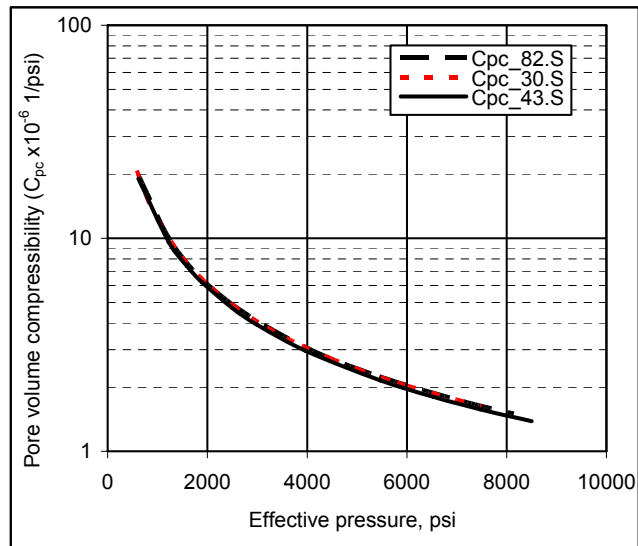
Figure 5.7: Measured pore volume compressibility readings of sandstone samples 30.S, 43.S and 82.S. Note: these samples have closed compressibility values and their porosity values are 18.94%, 18.44% and 22.68%, respectively.
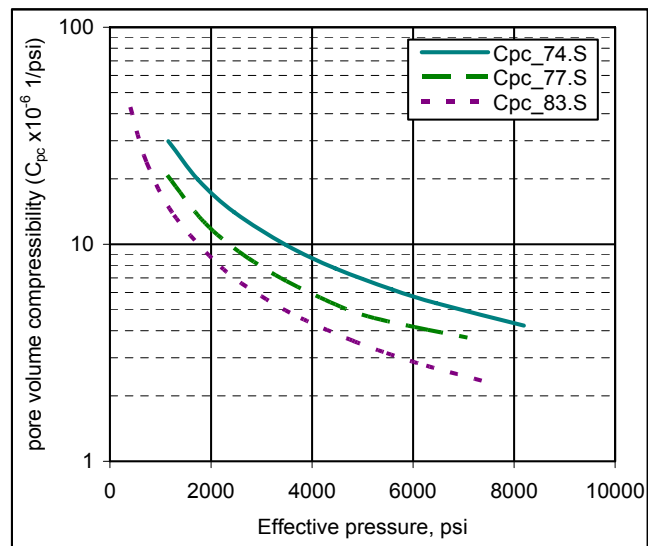
Figure 5.8: Display measured pore volume compressibility readings of shaly sandstone samples 74.S, 77.S and 83.S.
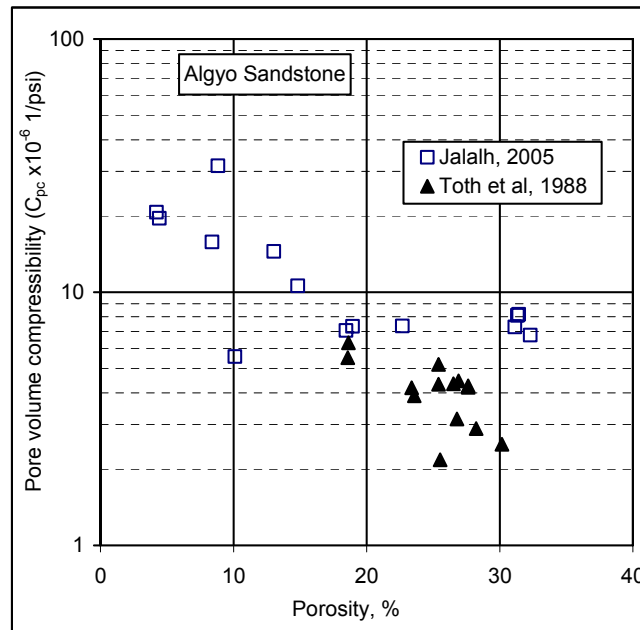
Figure 5.9: Comparison of data from Toth et al.[1988] and my recent results on the same Algyo sandstone

The pore volume compressibility data for Algyo sandstone from Toth and Bauer [1988] was plotted against my laboratory results for rock from the same field. My measurements show good agreement with the extracted data from Toth et al. on some Algyo sandstone samples from the same field. It should be noted that the samples studied by Toth and Bauer have a narrower range of porosity values, as shown in Fig. 5.9.

5.3.4 Földes Field Samples

Only two samples were available in this study. Both samples are very dense and well compacted, especially Sample F1. No sedimentary structures or features represent the rock identity. There was no reaction to Hcl acid (1:1 % concentration). Although both samples appear as if some metamorphic process took place, the mineralogy and lithology description is needed.

With no permeability in either sample, it is hard to consider the samples as part of a potential reservoir for water or hydrocarbon. Figure 5.10 and Table 5.6 summarize the physical and poroelastic parameter measurement results for Samples F1 and F2.
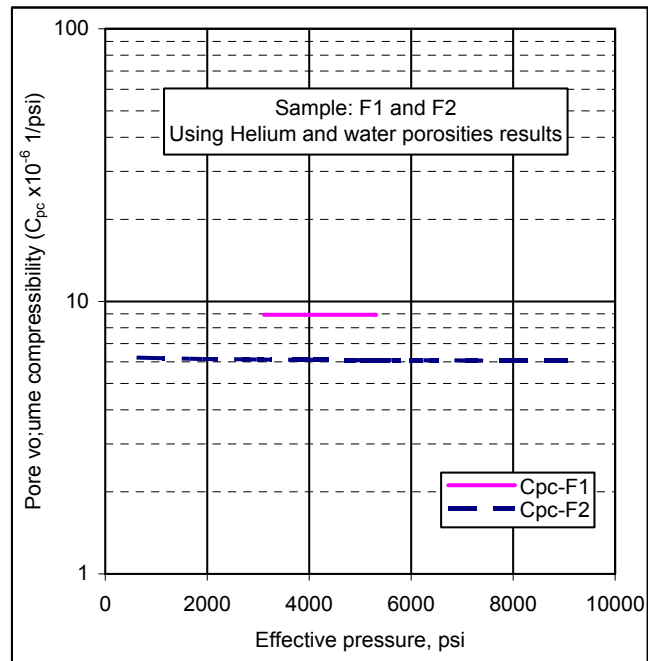
Figure 5.10: Compressibility readings of Földes field samples based on different porosity measurements

Table 5.9: Summary of measured compressibility of Földes field samples

Samples #	Porosity	Effective pressure psi	Compressibility 1/psi	Remarks
F1	0.0556	5299	8.93E-06	Impermeable
F2	0.0810	9071	6.05E-06	Impermeable
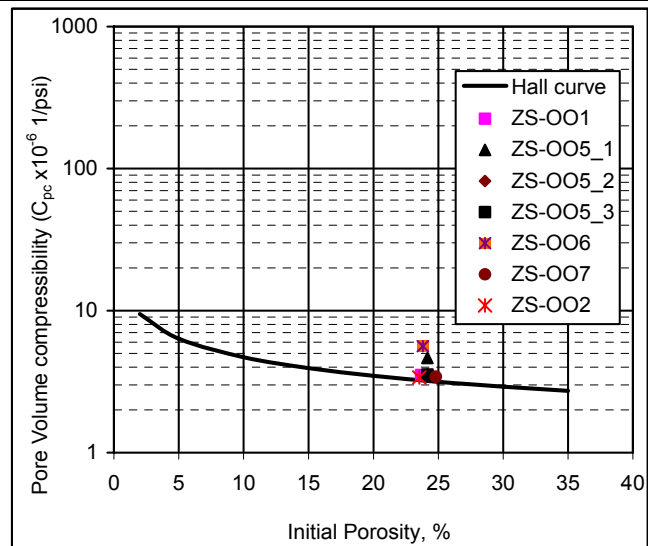
Figure 5.11a: Zsana limestone pore volume compressibility compared with Hall Correlation [1953]
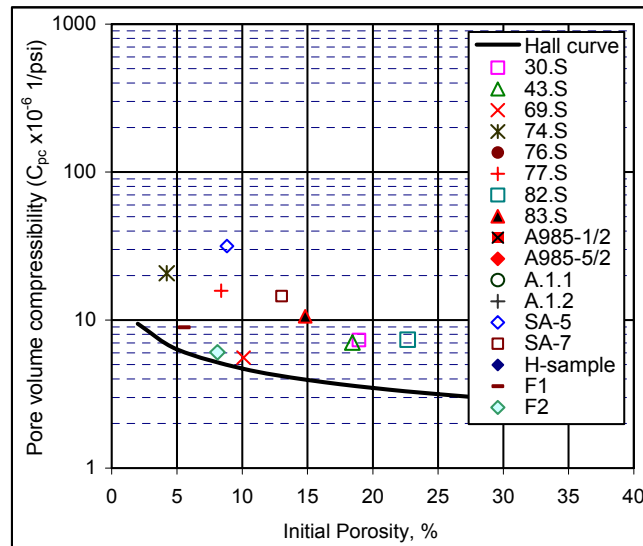
Figure 5.11b: Sandstone pore volume compressibility of Algyo, Hajduszoboszlo and Földes samples compared with Hall Correlation [1953]

The pore volume compressibility values shown in this work are in most cases pressure dependent. To compare samples that had been obtained from various depths, which means the samples were subjected to various effective stresses under reservoir conditions, a common effective pressure base of 100 percent or greater of the lithostatic pressure was used. This value was selected as the most probable average effective stress the sample would encounter during reservoir depletion. The lithostatic pressure is assumed to be 1 psi per foot of depth.
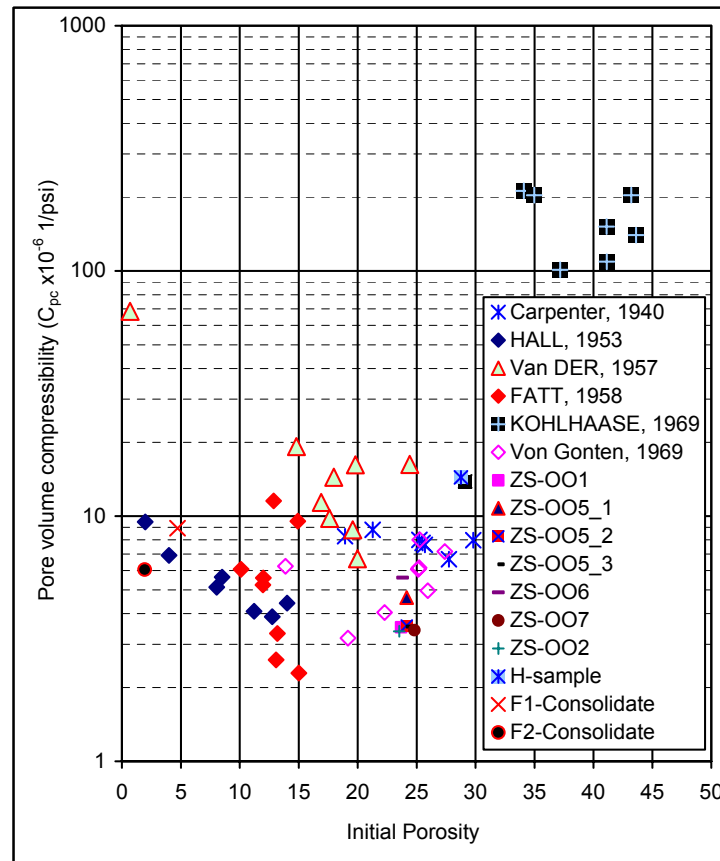
Figure 5.12: Pore volume compressibility vs. initial sample porosity obtained from this study and from literature as indicated

The values obtained at this pressure are plotted against the effective pressure and shown in Fig. 5.11 along with Hall's correlation. Compressibility-porosity values obtained from the literature, for both sandstone and limestone, are shown in Fig. 5.12. Data from Kohlhaase [1969] show different compressibility values in comparison to the rest of the published data.

The most extensive measurements are those of Newman [1973], who ran tests on 256 cores of limestone and sandstone from 40 reservoir rocks having porosities of between 1% and 35%. He also compared the results reported by other researchers. However, because Newman's compressibility values were computed at 75% lithostatic pressure (on the basis of the depth from which his samples were obtained), the comparison with the data from other researchers may not be accurate.

5.4 DISCUSSION

Figure 5.8 shows that our lower-porosity limestone and sandstone samples follow the general trend obtained by Hall [1953], i.e. the pore volume compressibility values increase with decreasing porosity. This is clear to see in Figs. 5.11(A)-5.15, where the consolidated sample data are compared with literature correlations and also, compared with Hall and Horne's correlation curves.
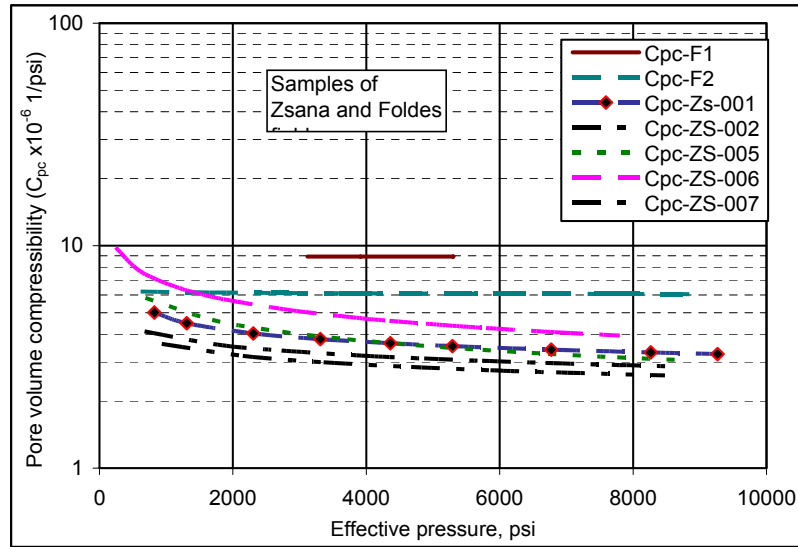
Figure 5.13: Compressibility of consolidated and very compacted samples vs. effective pressure stress (shows elastic behavior)

The individual compressibility curves for the consolidated samples in Fig. 5.13 (Zs-001, 002, 005, 006 and Zs-007) showed substantially elastic behavior. Applying more than one run on the same sample resulted in a lower compressibility value. This is due to rearrangement of the rock material.

The very compacted samples with low porosity (F1 and F2) in Fig. 5.13 tend to have very low compressibility. This is due to low initial porosity values that give no chance for the rock material to compress, and act as solid compressibility instead, which shows constant curves. The friable sample in Fig. 5.14 shows inelastic behavior.
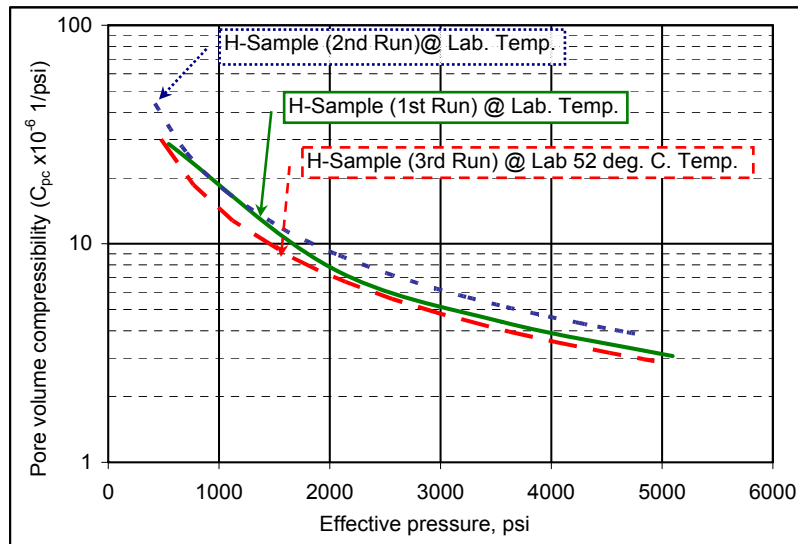
Figure 5.14: Repeated compressibility test of friable sandstone samples at different temperatures vs. effective pressure (shows inelastic behavior)

My results for friable and very compacted samples are in poor agreement with Hall's correlation. The literature of compressibility for more than 79 samples (including Hall's data), shown in Fig. 5.12, supports my results and has about the same scatter. Van der Knaap [1959] obtained a good correlation for 23 limestone samples taken from a single well; his values are also in poor agreement with Hall's but in same range as my data.

I believe that the poor agreement between my data and Hall's is in part because Hall's are based on only 12 samples – 7 limestone and 5 sandstone in the porosity range of 2 to 26 percent. My data are based on twenty-two samples having more or less the same porosity range as Hall's but with more variability in rock type ,such as friable sandstone and very compact sandstone.
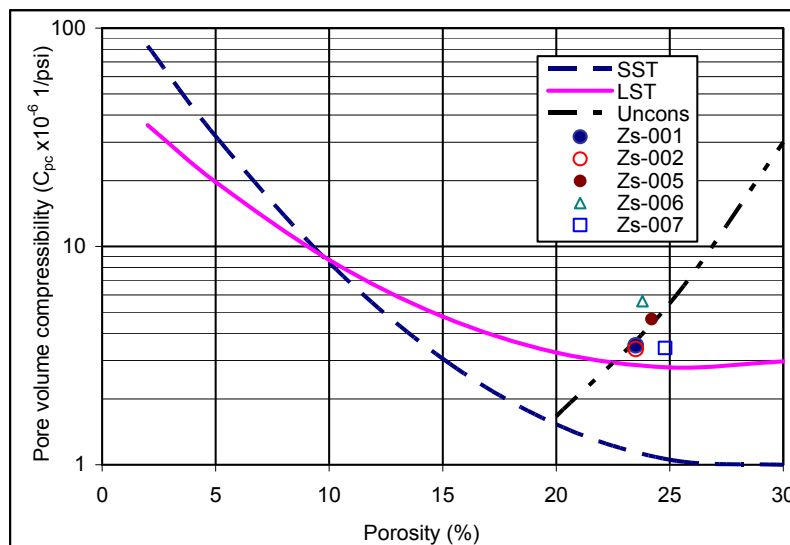
Figure 5.15: Measured compressibility of studied limestone (Zsana field) samples compared to widely used compressibility correlations [after Horne, 1990]

Both Figs. 5.15 and 5.16 illustrate the widely used Horne [1990] correlation, upon which my laboratory compressibility results are plotted for both limestone and sandstone. Figure 5.15 displays clearly poor agreement with Horne's correlation and shows that Zsana limestone lies along unconsolidated compressibility rock curve.

The situation is the same for Algyo sandstone, as presented in Fig. 5.16. My laboratory results for Algyo sandstone compressibility are very scattered and in poor agreement with Horne's correlation. Furthermore, Algyo data do not follow any rock type curve of Horne's correlation.

Figure 5.17 compares the measured laboratory data of Algyo sandstone with the available published data for sandstone compressibility. The comparison shows a good agreement between the data and fits in the same range of rock compressibility.

I should note that the extending Horne's curves to a larger porosity range by using his published equations for limestone and sandstone curves shows upward curvature [Jalalh, 2006a].

The above discussion supports the necessity for laboratory compressibility measurements in evaluating rock compressibility for a given reservoir. It is obvious that the pore volume compressibility for a given porosity could vary widely according to rock forming mineral and/or porosity structure type. Therefore, modifying and/or establishing the new rock compressibility correlation with more data would be a better alternative approach in case laboratory measurements are not available.
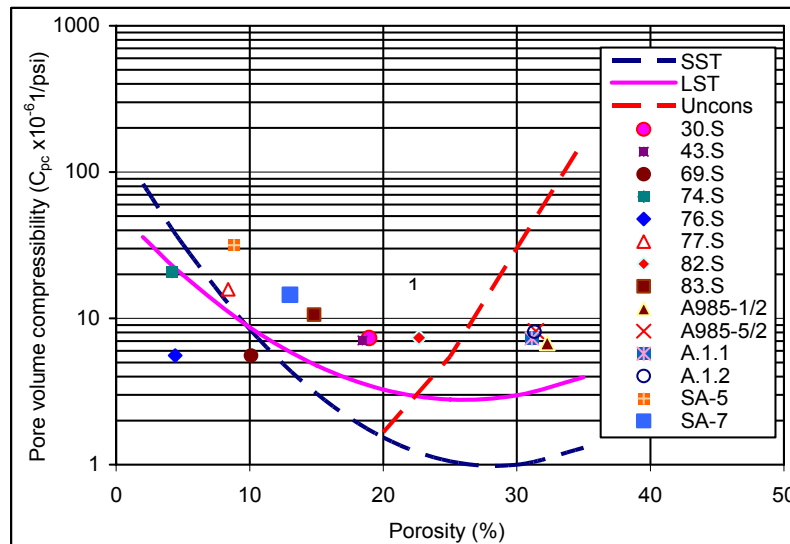
Figure 5.16: Measured compressibility of studied sandstone samples (Algyo field) compared to widely used compressibility correlations [after Horne, 1990]
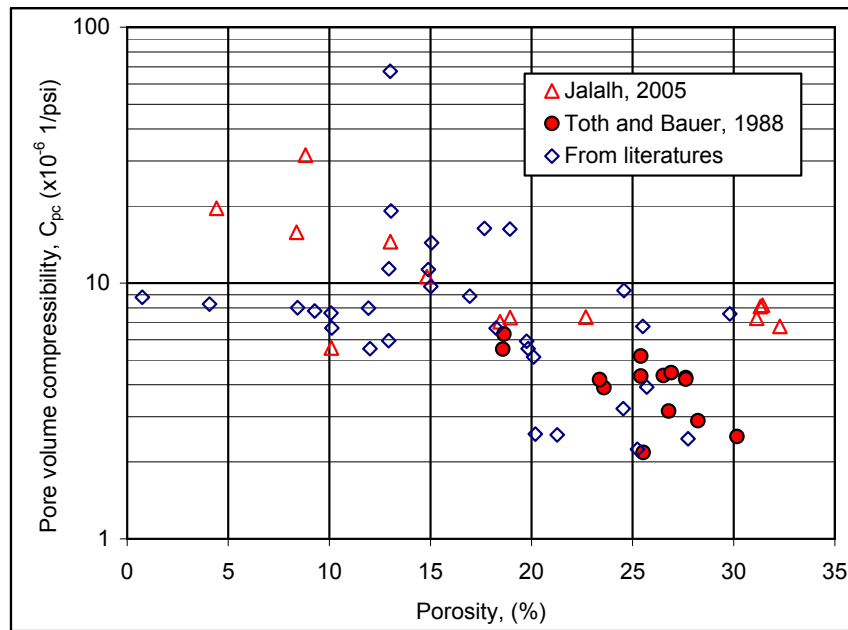
Figure 5.17: Compare the laboratory measured compressibility of studied Algyo sandstone samples and published compressibility sandstone rocks from literatures.

CHAPTER 6
6. NEW CORRELATIONS OF ROCK COMPRESSIBILITY

6.1 INTRODUCTION

Reservoir rock is compressible as pore pressure drops. Rock compressibility can provide a certain energy to drive oil out of reservoirs. In order to evaluate the drive energy that rock can provide in the process of oil production, the compressibility coefficient is defined and conventionally measured for most reservoirs. Many researchers such as Hall [1953], Van der Knaap [1959] and Horne [1990] conducted a series of theoretical and experimental studies on the compression phenomena of rocks (see Fig. 5.10).

In 1953, H. N. Hall produced a plot of rock compressibility versus porosity from the statistics of laboratory a measurement, which afterwards became called Hall's plot (see Fig.6.1) and which was simulated by an empirical formula (Eqn. 6.1). R. N. Horne [1990] obtained a similar trend of rock compressibility with porosity to Hall's plot (Fig. 6.2) for consolidated sandstones, unconsolidated sandstones, and limestones. Many reservoir managers assume the calculated compressibility of rock from Hall's plot or the corresponding empirical formula has the same value as laboratory measurement, so they do not do the core experiment anymore since they can get the compressibility quite easily from Hall's plot. Hall's plot and the corresponding empirical formula have served as the main method for calculating rock compressibility in most commercial software of well test interpretation and reservoir numerical simulation.

In the laboratory, the pore volume of the core can be measured at a given pore pressure with outer stress being constant, and the relationship of pore volume versus pressure can be plotted, from which the compressibility of rock can be calculated according to Eqns (2.7) and (2.8).

Based on the statistics of measurements of rock compressibility, Hall obtained a relationship of compressibility with porosity of rock (see Fig. 6.1), which can be simulated by the following empirical formulas (either Eqn. 6.1a or 6.1b):

$$C_{pc} = \frac{1.78 * 10^{-5}}{\varphi^{0.4358}} / psi \qquad (6.1a)$$

$$C_{pc} = \frac{2.587 * 10^{-4}}{\varphi^{0.4358}} /MPa \tag{6.1b}$$
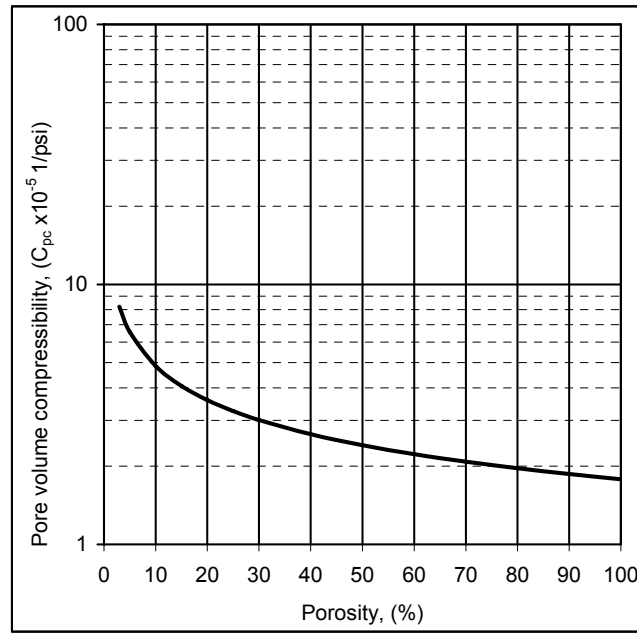
Figure 6.1: Earlier published rock compressibility versus porosity plot [after G. H. Hall, 1953]

R. N. Horne's [1990] empirical formulas for different rock type compressibility (C_{pc}) correlations are the following:

For consolidated limestone

$$C_{pc} = \exp\left[4.026 - 23.07\phi + 44.28\phi^2\right] \times 10^{-6} /psi \tag{6.2}$$

For consolidated sandstone

$$C_{pc} = \exp\left[5.118 - 36.26\phi + 63.98\phi^2\right] \times 10^{-6} /psi \tag{6.3}$$

For unconsolidated sandstone (where $\phi \geq 0.2$)

$$C_{pc} = \exp\left[534.01\left(\phi - 0.2\right)\right] \times 10^{-6} /psi \tag{6.4}$$
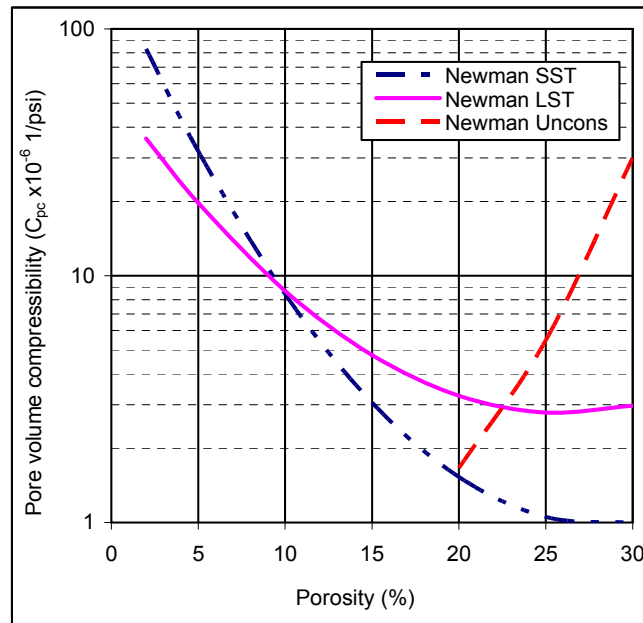
Figure 6.2: Recently published rock compressibility correlation [after Horne, 1990]

However, I would caution against the use of the Hall plot or the Horne compressibility plot unless core data is unavailable. The following are important points that support my suspicion and argue against direct use of these published compressibility plots and/or their corresponding empirical formula in reservoir analysis and well testing [Jalalh, 2004].

1. In the normal range of reservoir porosity, rock compressibility by Hall's plot is usually larger than that of reservoir liquid compressibility. For example, rock of 10% porosity has a compressibility of 4.8677×10^{-5} 1/psi, and Horne's correlation gives 8.43×10^{-6} 1/psi while the formation water has an approximate compressibility of $2.7579 – 3.4474 \times 10^{-5}$ 1/psi.

2. Hall's plot gives the same value of compressibility for rocks of different lithology if they only have the same porosity, regardless of their different rigidity.

3. For the same porosity value, Horne's correlation gives double value of Hall's correlation. For example, rock of 10% porosity has a compressibility of 4.8677×10^{-5} 1/psi from Hall's plot, and Horne's correlation gives 8.43×10^{-6} 1/psi.

4. The plots are represented in pore volume compressibility versus porosity, not versus effective stress (Pc-Pp). For accurate estimation of the reserve by using the newly developed material balance equation, the variable of formation compressibility with declining reservoir pressure (i.e., effective stress = P_c-P_p) data are needed.

80

5. Horne's curves are constructed for each rock type separately, while Hall's correlation represents pore volume compressibility for mixed types of reservoir rocks (i.e., sandstone. limestone and friable rocks).

6. Hall performed laboratory measurements and developed his correlation, while Horne summarized the published data for compressibility by Newman and then developed a correlation for each rock type. The original data of Newman's compressibility values were computed at 75% lithostatic pressure (on the basis of the depth from which his samples were obtained), and therefore comparison with the data computed at 100% lithostatic pressure may not be accurate.

The newly developed methods by Fetkovich et al. [1991] for Original Gas In Place (OGIP) calculation and Yale et al. [1993] for, Original Oil In Place (OOIP) calculation depart from earlier proposed methods in the use of a variable rather than a fixed or average value of formation volume factor and pore volume compressibility. This method of calculation properly integrates pore volume compressibility and formation volume factor effects over the full pressure range of investigation [Jalalh, 2006b]. Two examples of the use of variable compressibility for improving reservoir analysis are presented in the Chapter 7 as well as the derivation of both of the newly developed material balances.

Many researchers have conducted a series of theoretical and experimental studies on the compression phenomena of rock compressibility. I present in this chapter a better rock compressibility correlation as an alternative approach to laboratory measurements. It has been more than 30 years since R. N. Horne [1990] obtained a similar trend of rock compressibility with porosity similar to the earliest correlation of rock compressibility published by Hall in 1953. I collected the published rock compressibility and labeled it "Original data". After investigating the available compressibility correlation published after Horne (1990), it is clear that there is a necessity to find better fitting rock compressibility data. Using the same Horne empirical formula type and incorporating the latest rock compressibility data available in the literature for limestone and sandstone, I find better fitting correlation constants than Horne's original correlations for limestone and sandstone rock. This correlation will be referred as the modified Horne correlation, or "Mod-Horne".

6.2 MODIFIED HORNE'S CORRELATION APPROACH (Mod-Horne)

Figure 6.3 displays the collected published limestone's rock compressibility data, which is referred as "Original data", and Horne trend curves versus porosity. The two dashed lines represent 68% of the upper and lower confidence intervals from the standard deviation of the Horne correlation.

H. J. Motulsky and A. Christpoulos (2003) have extensive practical applications for linear and nonlinear regression. They conclude that using the sum-of-squares is a useful statistic calculation to compare models. The sum-of-squares (SS) is the sum of the squares of vertical distances of the points from the curve. It is expressed in the units used for the Y-values, squared. Standard (Least Squares) nonlinear regression works by varying the values of the model parameters to minimize the SS.

The equation below calculate s the value of root mean square ($S_{y,x}$) from the sum of squares and degrees of freedom:

$$S_{y,x} = \sqrt{\frac{SS}{N-P}}$$

(6.5)

$S_{y,x}$ is the standard deviation of the vertical distances of the points from the line, N is the number of data points, and P is the number of parameters used in the model. Tables 6.6 and 6.7 at the end of this chapter summarize the sum-of-squares (SS) and degree of freedom (DF) of all the models used in this study.

Figures 6.3 and 6.4 compare the Horne and Mod-Horne models with the upper and lower confidence interval (dashed lines). The confidence interval is calculated by using the standard deviation ($S_{y,x}$) of the sample mean obtained from Eqn. 6.5.

Data in Figs. 6.3 and 6.4 is very scattered and the points with less than 5% porosity (i.e., 8 points out of the dashed lines) lie out of the confidence interval of Horne. Table 6.1 shows a comparison of statistical correlation data.

Table 6.1 Descriptive statistical data of Horne and published rock compressibility of limestone

	C_{pc} Original	C_{pc} Horne
Summation of Data	5.31E-04	6.681E-04
Mean of Data (average)	1.29E-05	1.629E-05
Average of standard deviation (Sy,x average)	9.964E-06	

The descriptive statistical data in Table 6.1 show that the mean and summation from the Horne model are higher than the original rock compressibility data. This means that the

Horne trend does not fit the data used in this study. Therefore, the necessity to find a better rock compressibility trend with more accuracies fitting is raised. Using the same Horne model formula (i.e., Eqn. 6.2 Polynomial Quadratic Equation) and incorporating the latest rock compressibility data available in the literatures and my own laboratory data for limestone and sandstone, I find better fitting correlation constants than Horne's correlations for limestone rock. This correlation will be referred as the modified Horne correlation ("Mod-Horne"). Obviously, Fig. 6.4 shows mainly four points with very low porosity falling outside of the confidence interval of Mod-Horne. The modified Horne correlation can simulate the curve by an empirical formula for limestone and for sandstone. For limestone this is:

$$C_{pc\text{-Mod-limestone}} = \exp\left[3.9952 - 33.933\phi + 98.040\phi^2\right] \times 10^{-6} \text{ 1/psi} \tag{6.6}$$

and for sandstone:

$$C_{pc\text{-Mod-sandstone}} = \exp\left[3.4895 - 15.249\phi + 31.599\phi^2\right] \times 10^{-6} \text{ 1/psi} \tag{6.7}$$

Comparing the descriptive statistical data in Table 6.1 and 6.2 indicates an improvement in the fitting curve to the data with the Mod-Horne model. The mean and summation of data in Table 2 are much closed to the original data. This is clearly seen by the lower value of the standard deviation of the Mod-Horne. Graphically comparisons are represented in Figs. 6.3 and 6.4.
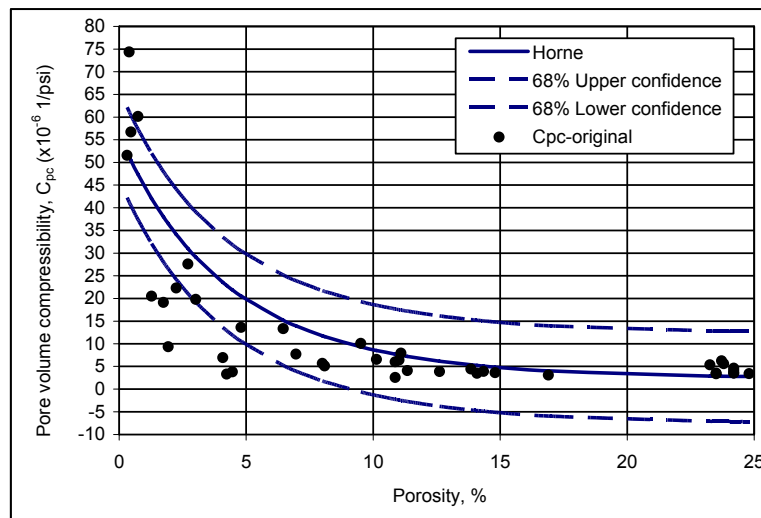
Figure 6.3: Published limestone compressibility data ("original data") and Horne trend curves versus porosity with upper and lower 68% confidence interval
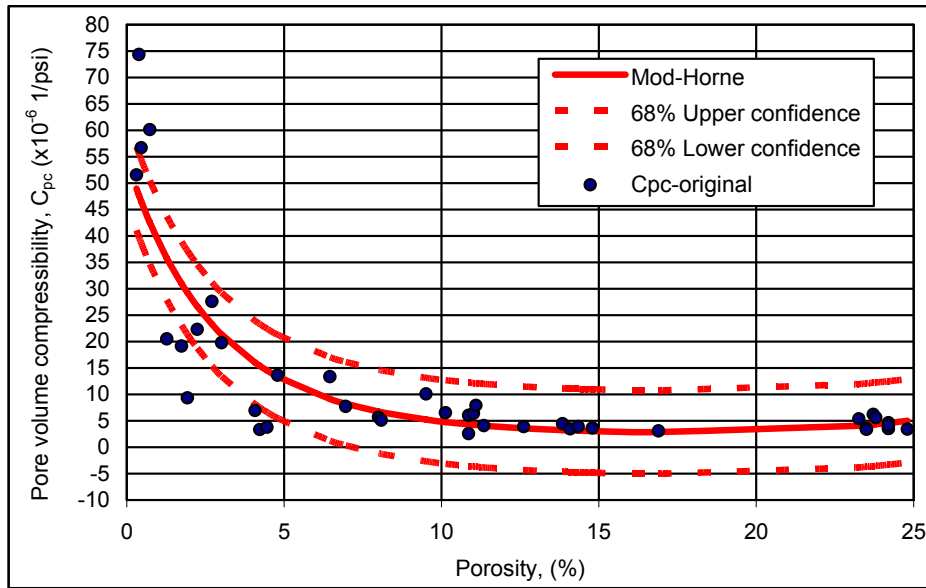
Figure 6.4: Published limestone compressibility data ("original data"), and Mod-Horne curves versus porosity with upper and lower 68% confidence interval

Table 6.2: Statistical correlation data of Mod-Horne and published rock compressibility of limestone

	C_{pc} Original	C_{pc} Mod-Horne
Summation of Data	5.31E-04	5.38E-04
Mean of Data (average)	1.29E-05	1.31E-05
Average of standard deviation (Sy,x average)	7.903E-06	
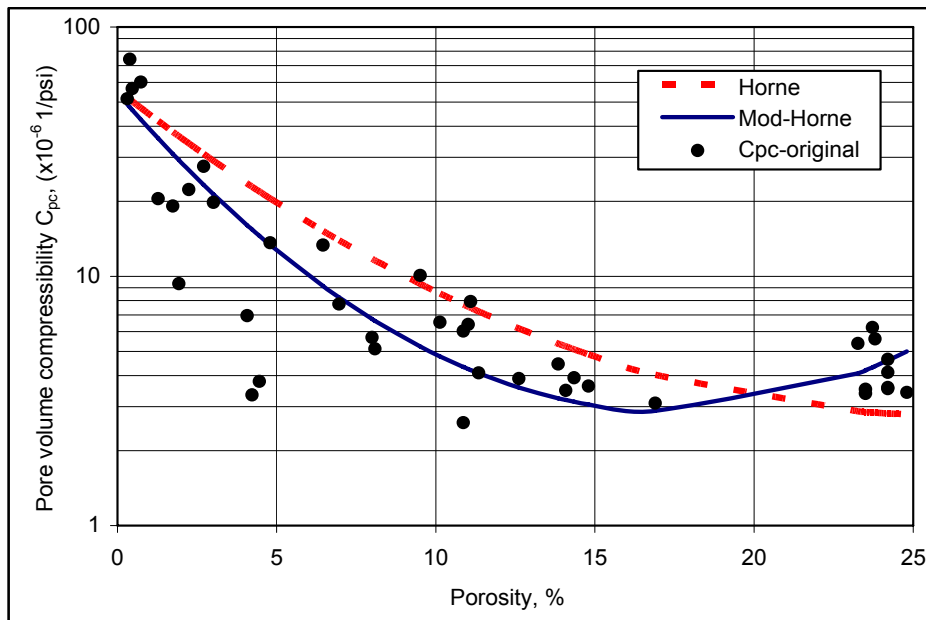
Figure 6.5: Comparison of Mod-Horne and Horne curves with the published limestone compressibility data ("original data"), versus porosity

Figure 6.6 represents the simulated curve by the formula given in Eqn. 6.5, for sandstone rocks. The Mod-Horne curve for sandstone gives a better correlation and its trend passes through most of the available published sandstone data. This is also seen in

the statistical data in Table 6.4. The model of Mod-Horne gives a lower standard deviation (6.958E-06) and better value for summation and average mean of the data.

Table 6.3: Statistical correlation data of Horne and published rock compressibility of sandstone

	C_{pc} Original	C_{pc} Horne
Summation of Data	5.575E-04	2.706E-04
Mean of Data (average)	8.577E-06	4.164E-06
Average of Root Mean Square (Sy,x average)		8.504E-06

Table 6.4: Statistical correlation data of Mod-Horne and published rock compressibility of sandstone

	C_{pc} Original	C_{pc} Mod-Horne
Summation of Data	5.575E-04	4.647E-04
Mean of Data (average)	8.577E-06	7.149E-05
Average of Root Mean Square (Sy,x average)		6.958E-06
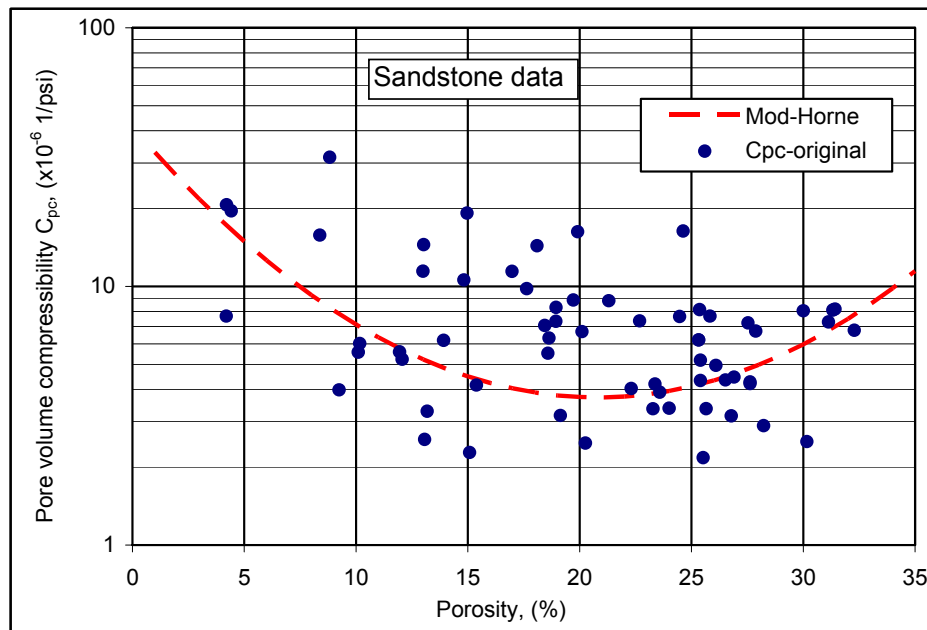
Figure 6.6: Mod-Horne curve and the published sandstone compressibility data "original data", versus porosity

6.3 NEW ROCK COMPRESSIBILITY CORRELATION

Using the modified formulas gives more accurate compressibility values for most reservoir rock compared to the original Horne formulas.

After the modification of the Horne equation, I attempted to find a simple and accurate formula, which gives more precise pore volume compressibility values, considering all of my measured compressibility data and the available published data. I used 12 different formulae with two parameters and used a spreadsheet of Microsoft Excel to find the best match for the sandstone and limestone compressibility data. The twelve different formulas are listed in Appendix B. Then I transferred the data into a simple and more comprehensive professional fitting regression program called CurveExpert version 1.38. CurveFinder examines every possible regression model for the input data set and returns the best one. As curve fits are applied, a ranking chart keeps track of the best to worst models.

For detailed information on the models used and related information, see Appendix B.

The last phase of my calculations was performed through a more sophisticated statistical program called Prism-4. With this program, I was able to enhance the fitting parameters obtained from CurveExpert.

6.3.1 NEW LIMESTONE ROCKS COMPRESSIBILITY CORRELATION

The best fitting result is the Harris Model (see Appendix C, Yield-Density Models, Eqn. B.33). This model gives the correlation coefficient (R) = 0.95. The new limestone compressibility relationship is:

$$C_{pc-new-\lim estone} = \left[\frac{1}{1.022^{-2} + 1.681^{-2}(\phi)^{1.05}}\right] \times 10^{-6} \; 1/\text{psi} \qquad (6.8)$$

Figure 6.7 presents my newly obtained pore volume compressibility trend for limestone rocks with porosity in X-axes. Most of the limestone data are within the lower and upper band of 68% confidence interval, as presented in Fig. 6.7b. The descriptive statistical values in Fig. 6.7a and in Table 6.4 support the new trend of my correlation for the pore volume compressibility of limestone rocks. In addition, Figs. 6.8 and 6.9 demonstrate graphical comparisons of the original Horne and Mod-Horne's correlation curves to my new correlation curve. Comparing the statistical data presented in Table 6.1

and 6.2; it can be seen that they are in support and good agreement with goodness fit data of my new fitting curve.
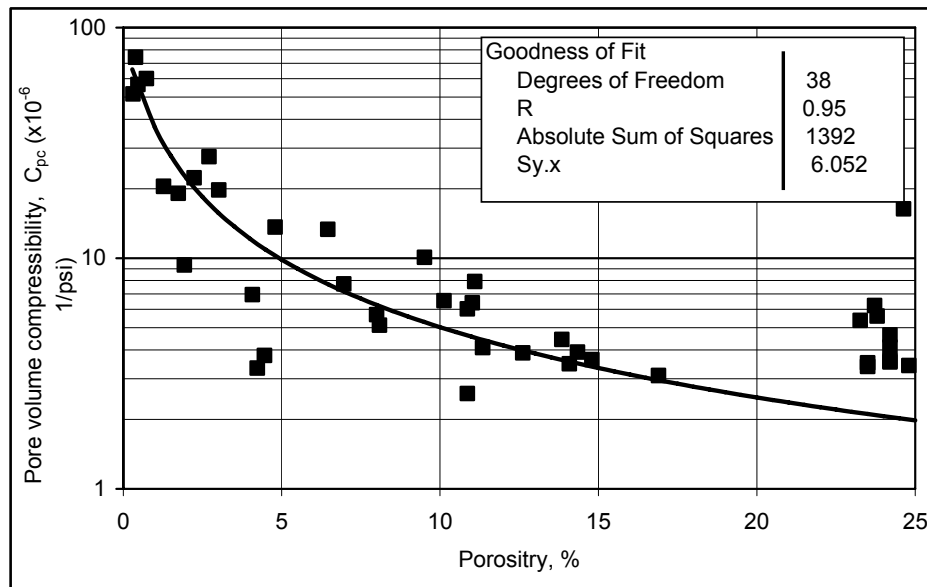
Figure 6.7a: New fitting curve of pore volume compressibility for limestone rock with porosity. The goodness of fit parameters are also presented.

Table 6.4a: Statistical data of the new fitting curve of published rock compressibility of limestone

Runs test	
Points above curve	28
Points below curve	13
Number of runs	14
P value (runs test)	0.06028
Deviation from Model	Not Significant

Table 6.4b: Statistical data of nonlinear regression of new fitting curve and published rock compressibility of limestone

	C_{pc} Original	C_{pc} New Fitting
Summation of Data	5.31E-04	5.072E-04
Mean of Data (average)	1.29E-05	1.237E-05
Average of standard deviation (Sy,x average)		6.052E-06
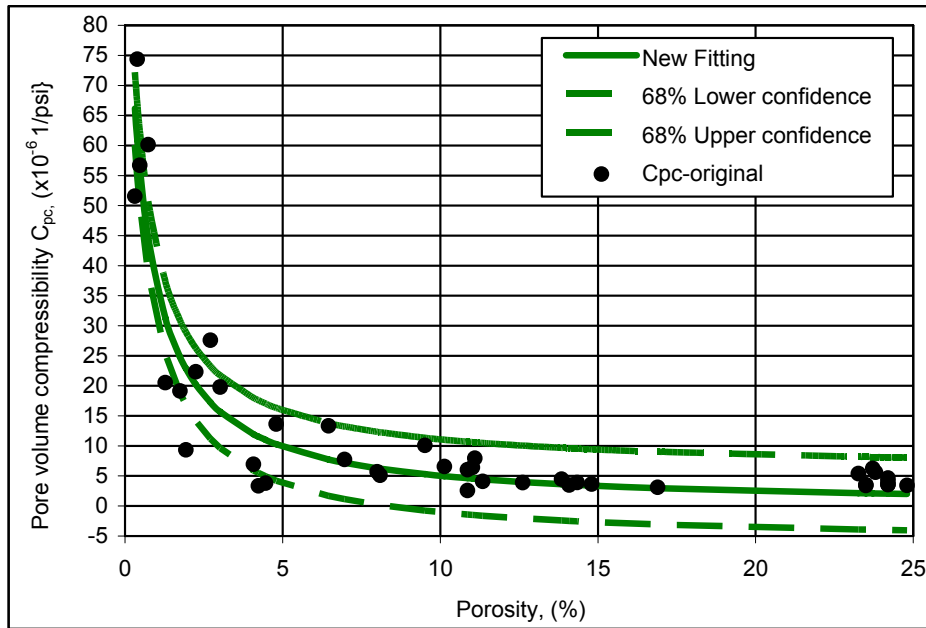
Figure 6.7b: The new fitting curve from limestone compressibility data "original data", versus porosity with upper and lower 68% confidence interval
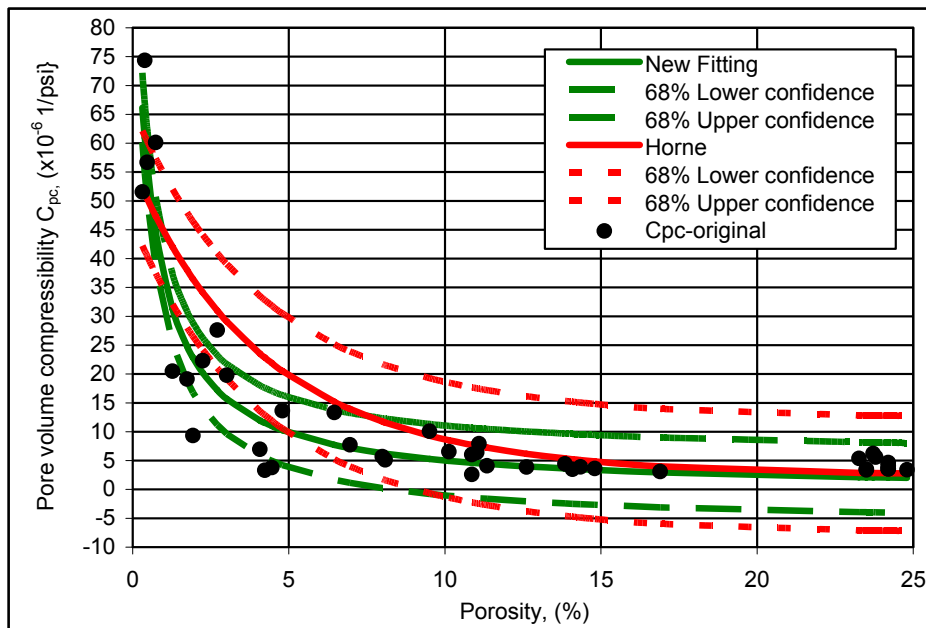
Figure 6.8: Standard deviation of New-fitting and Horne curves from the limestone compressibility data "original data" versus porosity with upper and lower 68% confidence interval
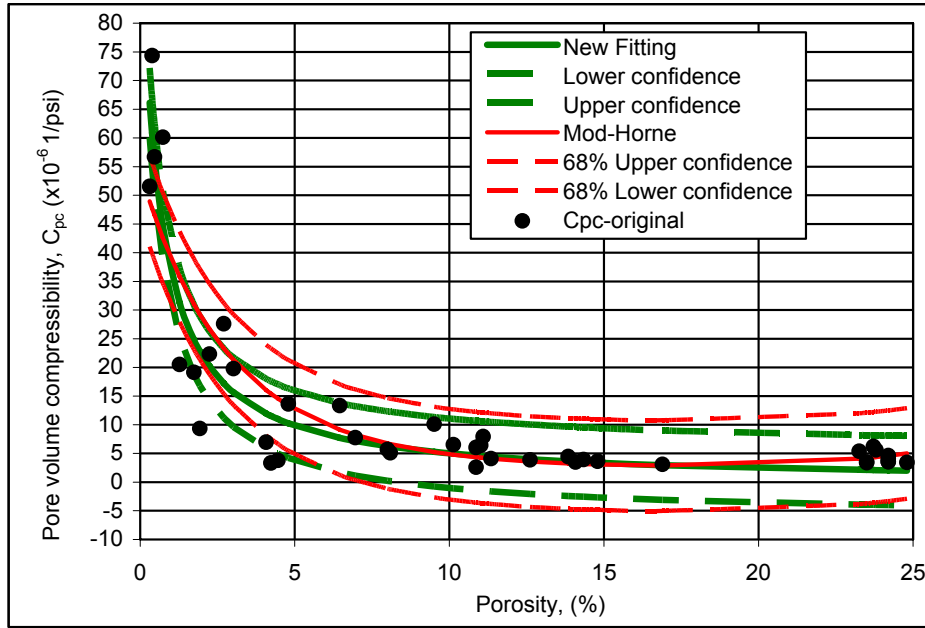
Figure 6.9: Comparison of statistical standard deviation fitting approaches New-fitting, Mod-Horne and Horne curves from limestone compressibility data "original data" versus porosity with upper and lower 68% confidence interval

6.3.2 NEW SANDSTONE COMPRESSIBILITY CORRELATION

For sandstone compressibility, I found the best fitting result by the same model type as for limestone rocks (see Appendix C, Yield-Density Models, Eq. B.33). This model gives the correlation coefficient (R) = 0.87.

$$C_{pc-new-\text{sandstone}} = \left[\frac{1}{-2.141^{-2} + 4.064^{-2}(\phi)^{0.4652}}\right] \times 10^{-6} \ 1/\text{psi} \qquad (6.9)$$

Bates and Watts [1988] stated that it is not appropriate to use the correlation coefficient R as the main criteria of whether a fit is reasonable. A high R tells normally tells us that the curve comes very close to the points, but does not tell us if the fit is sensible in other ways. The best-fit values of the parameters may have values that make no sense, (e.g. negative rate constants) or the confidence intervals may be very wide. Descriptive statistical data presented in Table 6.5and illustrated in Fig. 6.10 support the new correlation trend of the pore volume compressibility of sandstone data with porosity.

Table 6.5a: Descriptive statistical data of the new fitting curve of published rock compressibility of limestone

Runs test	
Points above curve	31
Points below curve	34
Number of runs	29
P value (runs test)	0.162
Deviation from Model	Not Significant
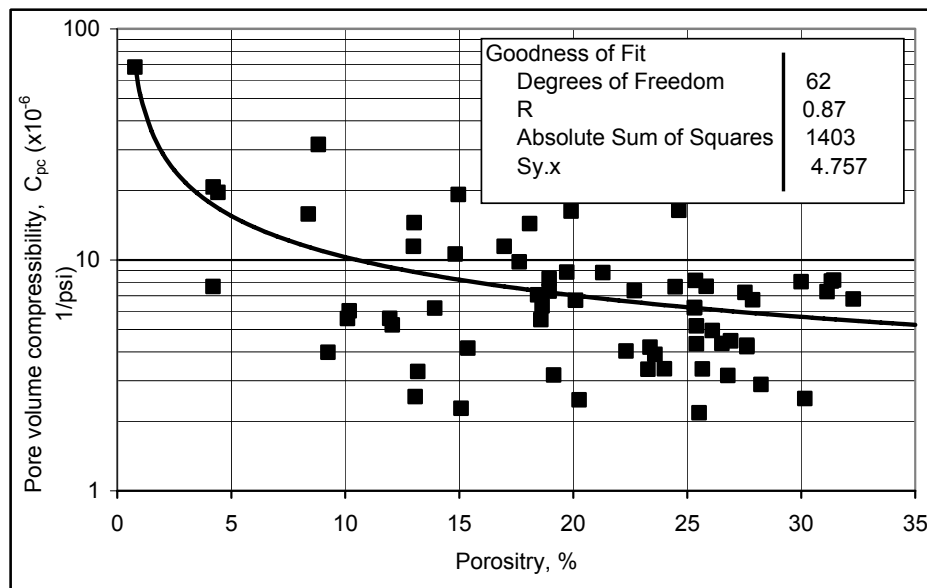
Figure 6.10a: New fitting curve of pore volume compressibility for sandstone rock with porosity. The goodness of fit parameters are also presented.

Table 6.5b: Statistical data of nonlinear regression of new fitting curve and published rock compressibility of sandstone

	C_{pc} Original	C_{pc} New Fitting
Summation of Data	5.57E-04	5.58E-04
Mean of Data (average)	8.58E-06	8.58E-06
Average of Root Mean Square (Sy,x average)		4.76E-06
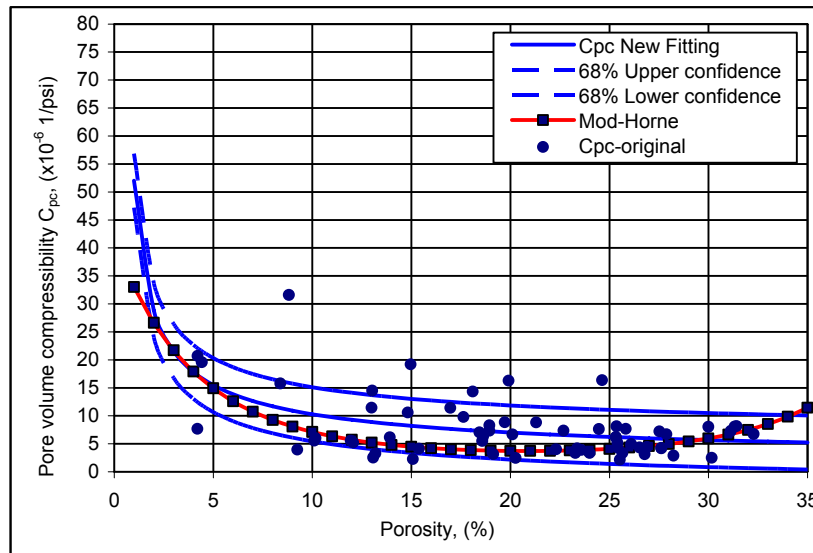
Figure 6.10b: New fitting and Mod-Horne curves and sandstone compressibility data "original data" versus porosity.
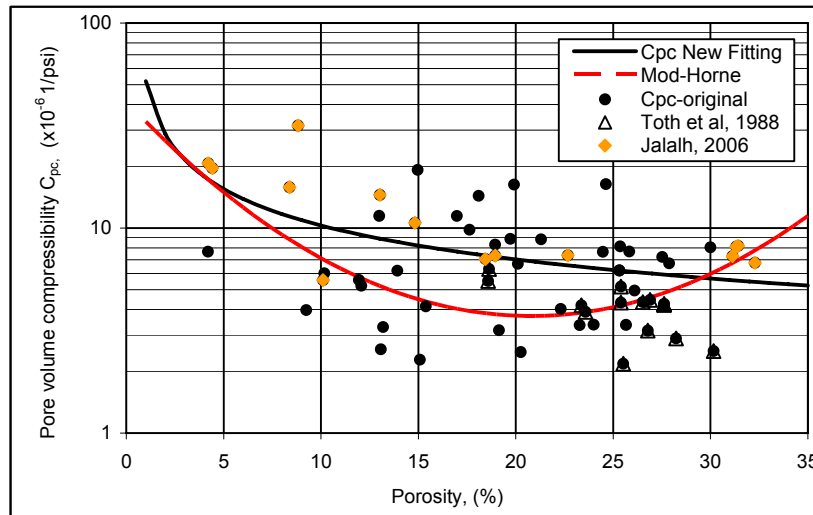
Figure 6.11: New fitting, Mod-Horne curves and sandstone compressibility data "original data and Algyo sandstone measured compressibility data versus porosity.

Table 6.6: Sum-of-squares (SS) and degree of freedom (DF) of the models used, for limestone samples

Model Name	SS	DF
Horne model	3.77E-09	38
Mod-Horne model	2.37E-09	38
The New model	1.39E-09	38

Table 6.7: Sum-of-squares (SS) and degree of freedom (DF) of the models used, for sandstone samples

Model Name	SS	DF
Horne model	7.88E-09	62
Mod-Horne model	3.00E-09	62
The New model	1.39E-09	62

91

CHAPTER 7
7. USE OF COMPRESSIBILITY DATA IN OIL AND GAS CALCULATIONS AND FOR IMPROVING RESERVOIR ANALYSIS

7.1 AN EXAMPLE OF A GAS RESERVOIR

7.1.1 Introduction

Rock compressibility has long been recognized as an important factor in material balance calculations of oil in place for closed reservoirs producing above bubble-point pressure.

Conventional calculation of the original hydrocarbon in place usually neglects the isothermal compressibility of the reservoir rock and fluids. In the petroleum industry, there are many cases where this neglect of compressibility results in an incorrect estimation of original oil or gas in place. Especially in high pressure or tight gas reservoirs, the error can be very high.

For example, if the pore volume compressibility of the reservoir rock is half of the compressibility of the under-saturated oil, neglect of the rock compressibility term results in an overestimation of oil in place of about 50 percent. In general, it may be stated that in material balance calculations on closed reservoirs, consideration of rock compressibility becomes increasingly important as the fluid compressibility decreases. For this reason, the effect of rock compressibility is commonly neglected in studies on gas reservoirs where gas compressibility is usually great.

Because gas compressibilities decrease with increasing pressures, the consideration of rock compressibility becomes increasingly important for deeper, high-pressure gas reservoirs. An example of the compressibility of the gas in the reservoir will be discussed. material balance calculations on a closed reservoir will verify the results of estimation of initial gas in place.

 Fetkovich et al. [1991] have presented a new derivation of a general material balance for high-pressure gas reservoirs. Using this derivation, I investigated the new reservoir calculations presenting different reservoir scenarios. Data from Zsana underground gas reservoir are used for the calculation.

7.1.2 Aspects of the new (Fetkovich) Material Balance Equation

An important aspect of the material balance for high-pressure gas reservoirs is that the gas in solution in the connate and associated water provides both pressure support and additional gas available for production. The level of pressure support provided by the evolved solution gas depends on the level of depletion, and it is shown that this support is significant below about 1,500 psi. The solution gas available for production also depends on the level of depletion, i.e., how much of the original solution gas has evolved $[R_{sw}(pi) - R_{sw}(p)]$ and the quantity of this gas that is mobile.

The term G is used for the initial free gas in place, and it is this quantity that will be determined from the material balance plot given by Eqn. C.2 ($VpR = VpRi - \Delta V_{pR}$) when extrapolated to $(p/z)[1 - \overline{C}_e(p)(p_i - p)] = 0$. This condition is reached at a pressure when $1 - \overline{C}_e(P_i - P) = 0$ and not when p = 0, i.e., additional gas may be produced after G_p reaches original free gas in place G. At pressures where G_p exceeds G, the corrected p/z term $(p/z)[1 - \overline{C}_e(p_i - p)]$ becomes negative. If reservoir pressure could be brought to standard conditions (p = p_{sc}) the total gas would be G plus the total solution gas in place G_s (G + G_s).

The effect of connate water saturation S_{wi}, and water volume ratio M are important to the magnitude of $\overline{C_e}$. In this investigation the author has applied the calculation when is with a typical M = 0.0 and actual estimation based on the reservoir data M = 0.4 and M = 5.7 as the upper limit of the M value. Below these main three categories, we have four scenario cases.

The reservoir data, which has been used in this study as an example to investigate the effect of the compressibility on OGIP calculations, is given in Table 7.1.

Table 7.1: Reservoir Data,

DATA	Conversion factor		Field unit	SI unit	
Permeability of the aquifer	50	mD	1	50.0	mD
Porosity of the aquifer	0.20		1	0.20	
Porosity of the reservoir	0.20		1	0.20	
Porosity of the nonproductive layers	0.05		1	0.05	
Connate water saturation	0.30		1	0.30	
Pay thickness	98.44	ft	0.3048	30.00	m
Pay thickness non productive zone	65.62	ft	0.3048	20.00	m
Pay thickness of aquifer	98.44	ft	0.3048	30.00	m

Productive area	1797.5361	acres	4046.86	7274370.37	m2
Formation compressibility (cf)	5.6.00E-06	1/psi	14.504	8.557E-05	1/bar
Water viscosity	0.4	cP	1.00E-03	4.000E-04	Pas
Reservoir temperature	224.6	oF		107.00	oC
Water formation volume factor	1.02	BBL/STB	1.00	1.02	m^3/m^3
Original gas in place	105944.0	MMscf	2.83E-02	3000.000	Mm^3
Effective reservoir radius	4791.63	ft	0.3048	1460.49	m
Aquifer radius	4791.63	ft	0.3048	1460.49	m
Time interval	1	year	365	365.00	day
ρgr				0.582	
Tpc		353.774	R	196.5414	K
Ppc		672.743	psi	46.384	bar
Tpr		3.474	R	1.93	k

Case #1 in our scenario is the ideal one. Using pressure dependence of $\overline{C_f}$ is the best we determined from core sample under appropriate reservoir condition pressure and 52°C temperature. The cumulative compressibility function $\overline{C_f}(p)$ is the most appropriate to use with the forms of the material balance that apply the cumulative pressure drop (pi − p), the same as the calculations done in this study.

Case #2: In this case, I only choose constant value for compressibility term $\overline{C_f}$ from our laboratory measurement at average reservoir pressure. The value of $\overline{C_f}$ used is 5.9×10^{-6} 1/psi (8.55×10^{-5} 1/bar).

Case #3: The compressibility term here neglected $\overline{C_f}$ = zero.

Case #4: The author considered pressure dependence in the calculation but neglected the total cumulative effective compressibility $\overline{C_e}(p)$ that represents all the available pressure support from rock and water.

I noticed that $\overline{C_f}(p)$ might have an impact on $\overline{C_e}(p)$, but in our reservoir example the term of cumulative total water compressibility $\overline{C_{tw}}(p)$ dominates the behavior of $\overline{C_e}(p)$ at our reservoir pressure. The impact of $\overline{C_f}(p)$ and $\overline{C_e}(p)$ is clearly greater than $\overline{C_{tw}}(p)$ in Case #4 when M value is at the upper limit (M = 5.7).

The following is a summary of the results of the calculations with a graphic plot of Case #1 from each scenario.
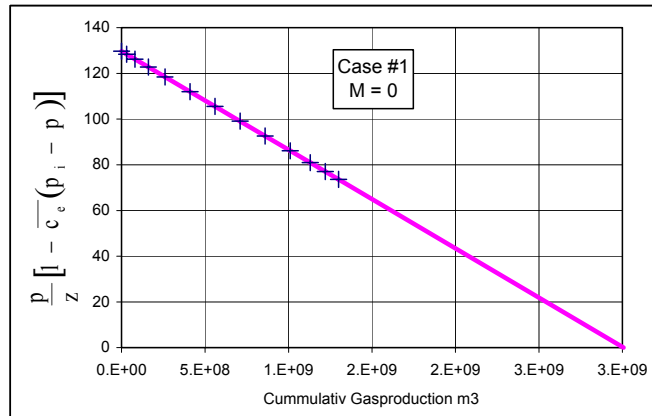
Case#	M = 0.0		
	OGIP	GIP	%
#1	2.981E+09		
#2	2.95803E+09	-23.151	-0.777
#3	2.98143E+09	0.251	0.7917
#4	3.00291E+09	21.734	0.721
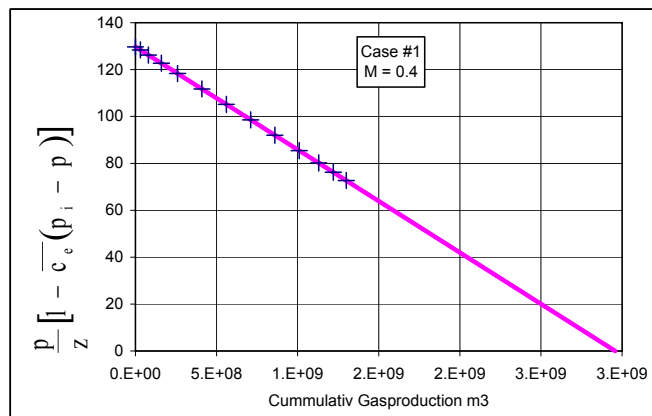
Case#	M = 0.4		
	OGIP	ΔGIP	%
#1	2.95175E+09		
#2	2.91798E+09	-33.769	-1.15
#3	2.95210E+09	0.349	1.17
#4	3.00291E+09	51.163	1.72
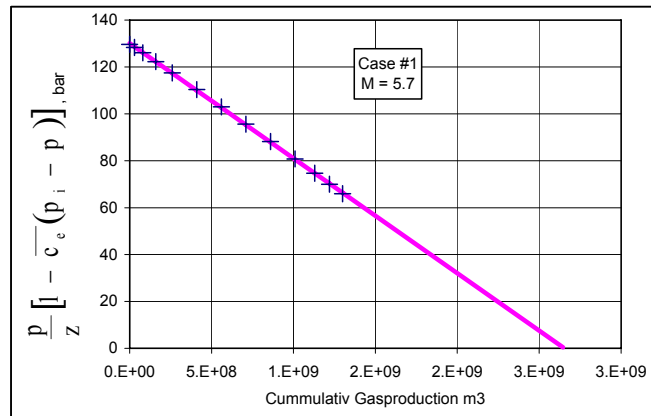
Case#	M = 5.7		
	OGIP	GIP	%
#1	2.646E+09		
#2	2.541E+09	-105.197	-3.976
#3	2.647E+09	1.323	4.193
#4	3.026E+09	380.693	14.332

7.1.4 Notes on sample calculations

Cumulative compressibilities ($\overline{C}_f(p)$ and $\overline{C}_{tw}(p)$) can be used in plot p/z vs. G_p, because they apply the cumulative pressure drop (p_i - p).

The equation is a forward calculation and more precise than the earlier material balance calculation in estimation of OGIP.

Investigation of the compressibility result of the new material balance in the range of water volume ratio from 0.0 to M = 5.7 shows the dominant drive mechanism is compressibility at high M values.

Using the correct rock compressibility gives the actual estimation of the gas reserve. Rock compressibility has a great impact on material balance calculation when M value is greater than 0.4.

Appendix C presents a detailed derivation of material balance equation for Fetkovich's Calculation.

7.2 OIL RESERVOIR EXAMPLES

7.2.1 Introduction

Primary depletion, EOR, and numerous hydrocarbon production operations induce important variations in pore pressure in the producing layers. These variations induce PV deformations, which are thought to contribute to oil and gas productions, are responsible for compaction phenomena, and may induce surface subsidence.

A petroleum engineer describes fluid flow in reservoirs, which is influenced by the permeability, porosity and compressibility of the rock. Formation compressibility (C_f) is a source of drive energy in addition to that provided by expansion of fluids. However, its effect, and also that of connate water, is often ignored in analyzing reservoir performance since its contribution is minor compared with the other drive mechanism such as cap gas, liquid expansion, gravity drainage or solution gas drive. The effects are usually considered, however, when undersaturated oil reservoir performance is analyzed and the contribution of rock and water expansion can easily exceed 10 percent of the total.

It has been recognized that decline in reservoir pressure accompanies a decrease in pore volume. The relative change in pore volume per unit of pressure change, i.e., the formation compressibility, depends on the rock type, mineral contents, its degree of hardness, and the tectonic setting. Laboratory measurements show a wide range of compressibility levels over the spectrum of rocks from competent carbonates to unconsolidated sands. Compressibility declines, sometimes drastically, as laboratory stress is increased to correspond to reservoir pressure changes from discovery to abandonment.

Hammerlindl [1972], who recognized the importance of compressibility in reservoir analysis, used a constant high formation compressibility value. This is one of the reasons why formation compressibility has been left out or underestimated in reservoir analysis, since it has been assumed that pore compressibility is fairly constant with stress and of the same order of magnitude as the compressibility of water. Pore compressibility measurements are not performed routinely for all reservoirs and data are especially sparse for those formations where it is most important (i.e. friable and unconsolidated formations).

Incorporation of accurate formation compressibility measurements in reservoir performance analysis can allow for the correct partitioning of drive energies and estimates of remaining reserves, which can aid in the most efficient development of the reservoir.

Use of variable formation compressibility in material balance analysis for initial reserves leads to accurate estimates of reserves. Applying accurate laboratory- measured pore compressibility data will allow accurate reserve estimates from early time data in overpressured systems.

7.2.2 A New Concept of Pore Volume

The conditions found in abnormally pressured reservoirs also lead to greater significance of formation compressibility as a source of expansion energy, particularly if the formation is poorly consolidated. Abnormal pressure at discovery means a lower effective reservoir stress condition, and higher formation compressibility. Since pressure level is often high, gas compressibility $[(1/P)-(1/Z) (dz/dp)]$ is relatively low, and formation compressibility may in fact be of the same order of magnitude; it will often exceed oil compressibility. Formation compressibility contributions may be further magnified if an aquifer even a small one—is present, since all of the water-bearing rock present will provide formation compressibility drive, energy [Yale et al., 1993].

Formation compressibility, however, is defined in most reservoir engineering handbooks as the relative change in pore volume divided by the change in reservoir pressure that caused the change in pore volume:

$$C_f = \frac{\Delta V_p / V_p}{\Delta p} \qquad (7.1)$$

The difference between pore compressibility and formation compressibility therefore is related to the difference between reservoir pressure and laboratory stress.

In order to easily incorporate variable formation compressibility into reservoir analysis, Yale et al. [1993] define a "pore volume FVF" (formation volume factor) as:

$$B_f = \frac{V_p}{V_{psc}} \qquad (7.2)$$

It is convenient, though not strictly necessary, to choose one atmosphere and reservoir temperature as the standard or reference condition, where $B_f = 1.0$. The pore volume is easily related to formation compressibility. In differential form, the formation compressibility equation (Eqn. 7.1) can be written as:

$$C_f \, dp = d V_p / V_p = d\left(\ln V_p\right) \qquad (7.3)$$

which can be integrated between limits p_{sc} and p to give

$$\ln\left(V_p / V_{psc}\right) = \int_{P_{sc}}^{p} C_f \, dp = f(p) \qquad (7.4)$$

The laboratory test from which C_f is determined in fact gives a nearly direct determination of B_f. The ratio of sample pore volume at any stress level to pore volume at a stress level corresponding to that reached in the reservoir when pressure declines to standard pressure gives the pore volume formation volume factor; the data needed are initial pore volume and fluid volume expelled as a function of stress applied to the sample. The laboratory measurement does not even have to be carried to the "standard condition" stress level; it need only cover a stress range that encompasses the expected range of reservoir pressure. This amounts to defining a reference condition tied to the highest stress level reached (i.e., reservoir pressure below the lowest expected operational pressure).

7.2.3 Modified Fluid Formation Volume Factors

Based on the above formulations, Yale et al. [1993] defined a modified gas/oil/water formation volume factor FVF as:

$$\tilde{B}_j = B_j / B_f \qquad (7.5)$$

where j refers to gas, oil, or water. With this definition, we have the advantage of simultaneously considering the changes, with pressure, of both fluid and the pore space associated with that fluid. In material balance work, use of these factors allows us to center attention on fluid volume changes, knowing that pore space changes are being carried along automatically. The result, as we shall see, is a compact form of equation that accurately considers all facets of the formation and fluid expansion processes while retaining an appearance similar to that with which reservoir engineers have long been familiar.

Appendix C presents a detailed derivation of the material balance equation for black oil.

7.2.5 Examples of Application

For elastic energy-drive reservoirs, the material balance equation is as follows

$$N_p B_o = N B_{oi} C_{eff} \Delta p \qquad (7.6)$$

where C_{eff} is the effective compressibility of reservoir oil, calculated by

$$C_{eff} = \frac{C_o S_o + C_w S_w + C_{pc}}{1 - S_w} \qquad (7.7)$$

Table 7.2: Main data of the reservoir

Rock type	Sandstone
Porosity	10%
Initial volume factor of oil	1.2
Saturation of connate water	0.3
Compressibilities of oil	4.14 10^{-5}/psi
Compressibilities of water	2.76 10^{-5}/psi
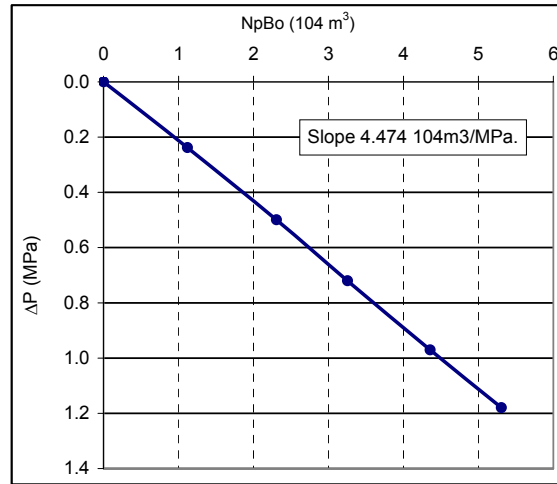
Figure 7.1: Production index curve of the reservoir.

If the compressibility of reservoir rock takes the value of Hall's plot, the oil's effective compressibility is 1.23×10^{-4} 1/Psi, by which the calculated reserve of the reservoir is **21.19 10^6m^3** using Eqn. 7.6. If the compressibility of reservoir rock takes the value of laboratory-measured data, the oil's effective compressibility is 5.45×10^{-5} 1/psi, by which the calculated reserve is **47.75x10^6m^3** using Eqn 7.6.

The investigation radius of wells is calculated by the following formula

$$r_{inv} = \sqrt[2]{\frac{kt}{\mu \phi C_t}} \qquad (7.8)$$

where C_t is defined as the total compressibility of reservoir, calculated by

$$C_t = C_o S_o + C_w S_w + C_{pc} \qquad (7.9)$$

The permeability of the reservoir is 10 mD and the viscosity of oil is 0.2 cP. If the compressibility of reservoir rock takes the value of Hall's plot, the total compressibility of

reservoir is 8.591x10^{-5}1/psi, by which the calculated investigation radius is **400.6 m** for t=100ks using Eqn. 7.8. If the compressibility of reservoir rock takes the value of laboratory measured data, the total compressibility of the reservoir is 3.83x10^{-5}1/psi, by which the calculated investigation radius is **601.4 m** for t=100ks using Eqn. 7.8.

Accurate formation compressibility data and application of that data in MBE analysis and reservoir simulation can significantly improve reservoir development in these types of fields. This observation is consistent with the speculation raised in the MBE analysis in this chapter. Therefore, it is important to utilize knowledge of the geological setting as well as knowledge of reservoir rock properties to evaluate and confidently predict gas-in place from pressure performance of over-pressured gas reservoirs. Correct partitioning of drive energies, therefore, is dependent in many cases on accurate measurements or estimates of formation compressibility. Underestimation of formation compressibility may suggest a water drive where one does not exist and vice versa.

Natural drive energy is often overestimated in reservoir numerical simulation; reserves of reservoirs and investigation radius of wells are frequently underestimated. To increase the accuracy of reservoir engineer calculation, I state that rock compressibility should be one of the routine core measurements in laboratory.

Incorporation of accurate formation compressibility measurements in reservoir performance analysis can allow for the correct partitioning of drive energies and estimates of remaining reserves, which can aid in the most efficient development of the reservoir. The use of variable formation compressibility in material balance analysis for initial reserves leads to accurate estimates of reserves. Applying accurate laboratory-measured pore compressibility data will allow accurate reserve estimates from early time data in overpressured systems, for both gas and oil reservoirs.

CHAPTER 8
8. CONCLUSIONS

1. **My study is the first time measurement results have been published for such a wide range of porosity and rock types with samples obtained from Hungarian's hydrocarbon fields.**

2. Proper practice in petroleum engineering should include the laboratory measurement of pore volume change with inner reservoir pressure changes.

3. **I developed a simple method for using the CoreLab compressibility apparatus, for equipment composite correction, calibration and rock compressibility measurement and calculations, rather than the procedure written in the manual of the Corelab apparatus.**

4. **Plotting the volume change (ΔV_p's) and pore compressibility of Algyo sandstone as a function of confining pressure gives the same shape and behavior as the plot published by Carpenter and Spencer [1940].**

5. **The measurement data of Zsana limestone and Algyo sandstone rocks show that the correlation formula that are available in the literature (i.e., Hall's and Horne's correlations) cannot be reliably applied to estimate the compressibility of these reservoir rocks.**

6. **I found that the pore volume compressibility values in this study are in poor agreement with published compressibility correlations. This is also confirmed by values in the literature. Therefore, there is a need for laboratory compressibility measurements in evaluating rock compressibility for a given reservoir.**

7. **According to the obtained measurement results, I found the pore volume compressibility for a given porosity could vary widely according to rock forming minerals and/or porosity structure type. Therefore, pore volume compressibility depends not only on porosity value; it is also influenced by porosity structure and mineral composition** The pore volume compressibility is a parameter which is associated with large uncertainty. Besides pressure and rock type, it depends strongly on porosity and it is subject to hysteresis if the elastic stress limit is exceeded. Therefore, more investigation of pore size and porosity structure and mineral composition is necessary to consider their effect on the pore volume compressibility.

8. **The measurements I performed in this study on samples of various limestones and sandstones confirmed the theoretical framework of poroelasticity theory.** As an example, Sample Zs-005 demonstrates typical elastic behavior with no irreversible change in the internal structure of the

rock. This is supported by the same values of compressibility in the second and third cycle runs.

9. **Based on my laboratory observations, I state that one of the key questions of correct compressibility measurement is to reach the true stress equilibrium for the samples in the laboratory in any practical time. However, the most significant volume changes take place in the first few minutes of applied stress**. During my measurements, I assumed the true equilibrium is always reached. Investigation of the time effect on the stress was out of the scope of my work. I only point out that they exist.

10. **For heterogeneous reservoir rocks, representative samples should be collected in order to represent all types of reservoir rocks. Using these representative samples to measuring the rock compressibility will result in better characterization of reservoir pore volume changes**. Using the measured data and the formula that are presented in this study with specific constants for the examined reservoir, compressibility can be estimated.

11. **Using the same shape and type as Horne's equation, I constructed modified Horne formulas, which give better compressibility estimations. The two modified formulas Eqns. 6.4 and 6.5 for limestone and sandstone rocks are presented in Chapter 6 with a detailed discussion.**

12. **I developed a new rock compressibility correlation for limestone and sandstone rocks, based on the available published rock compressibility data in the literature and on my own laboratory measurements.**

13. **To increase the accuracy of reservoir engineer calculations, rock compressibility should be one of the routine core measurements in the laboratory.** I found that incorporation of accurate formation compressibility measurements in the reservoir performance analysis can allow for the correct partitioning of drive energies and estimates of remaining reserves, which can aid in the most efficient development of the reservoir. Reliable compressibility is essential for oil and gas reserves estimation, production forecasting, and for history matching. I demonstrated the importance of improving the reservoir analysis and the optimal economic production of the oil and gas reserve in Chapter 7. Applying accurate laboratory data on pore compressibility will allow accurate reserve estimates from early data in overpressured systems.

14. **Accurate formation compressibility measurements in reservoir performance analysis allow:**

- **the correct partitioning of drive energies**
- **estimates of remaining reserves.**

These can aid in the most efficient development of the reservoir.

LIST OF REFERENCES

1. *API Recommended Practice for Core-Analysis Procedure.* 1 ed. Vol. RP-40, API. 1960, NY, USA: American Petroleum Institute

2. Andersen, M.A., *Predicting Reservoir-Condition Pore Volume Compressibility from Hydrostatic-Stress Laboratory Data.* SPE, Reservoir Engineering, 1988. **3**: p. 1078-1082.

3. Bates, D.M., and Watts, D. G, *Nonlinear Regression Analysis and Its Applications.* 1988, NY, USA: Wiley & Sons Inc. 432.

4. Berryman, J.G., *Seismic wave attenuation in fluid porous media.* Pure and Applied Geophysics, 1988. **128**(1): p. 423-432.

5. Billington, E.W., and Tate, A., *The Physics of Deformation and Flow.* 1981, NY, USA: McGraw-Hill. 626.

6. Biot, M.A., *General theory of three dimensional consolidation.* J. Appl. Phys., 1941. **12**: p. 155-164.

7. Biot, M.A., *Theory of propagation of elastic waves in a fluid-saturated porous solid, part I: low frequency range.* J. Acoust. Soc. Am., 1956a. **28**(2): p. 168-178.

8. Biot, M.A., *Theory of propagation of elastic waves in a fluid-saturated porous solid, part II: higher frequency range.* J. Acoust. Soc. Am., 1956b. **28**(2): p. 179-191.

9. Biot, M.A., *Nonlinear and semilinear rheology of porous solids.* J. Geophys. Res., 1973. **78**(23): p. 4924-4937.

10. Biot, M.A., *Exact simplified nonlinear stress and fracture analysis around cavities in rock.* Int. J. Rock Mechanics and Mining Sciences, 1974. **11**(7): p. 261-266.

11. Black, A.D., Dearing, H. L., and DiBona, B. G., *Effects of pore pressure and mud filtration on drilling rates in a permeable sandstone.* SPE, JPT, 1985. **37**(10): p. 1671-1681.

12. Brace, W.F., *Some new measurements of linear compressibility of rocks.* J. of Appl. Mechs., 1965. **22**(4): p. 479-486.

13. Bradley, H.B., (Editor-in-Chef), and Gipson, F. W. , *Petroleum Engineering Handbook.* 1987, Richardson, Texas, USA: Society of Petroleum Engineers.

14. Brandt, H., *A study of the speed of sound in porous granular media.* J. Appl. Mechs., ASME, 1955. **22**(4): p. 479-486.

15. Brown, R.J.S., and Korringa, J., *On the dependence of the elastic properties of a porous rock on the compressibility of the pore fluid.* Geophysics, 1975. **40**: p. 608-616.

16. Carpenter, C.B., and Spencer, G. B., *Measurements of Compressibility of*

Consolidated Oil-Bearing Sandstones. Vol. RI 3540, USBM. 1940.

17.   Carroll, M.M., and Katsube, N., *The role of Terzaghi effective stress in linearly elastic deformation*. J. Energy Res. Tech., ASME, 1983. **105**(4): p. 509-511.

18.   Chierici, G.L., Ciucci, G. M., Eva, F., and Long, G. *effect of Overburden Pressure on some Petrophysical Parameters of Reservoir Rocks*. in *Seventh World Petroleum Congress*. 1967: Elsevier, London.

19.   Chilingarian, G.V., and Wolf, K. H., *Compaction of Course - Grained Sediments*. Vol. 1. 1975, Amsterdam: Elsevier.

20.   Clark, N.J., *Elements of Petroleum Reservoirs*. 1969, Dallas: SPE. 250.

21.   Clark, S.P., (Editor), *Handbook of Physical Constants*. 1966, NY, USA: Geological Society of America. 587.

22.   Cleary, M.P., *Elastic and dynamic response regimes of fluid-impregnated solids with diverse microstructures*. Int. J. Solids Struct, 1978. **14**(10): p. 795-819.

23.   Contreras, E., Iglesias, E., and Bermejo, F. *Effects of Temperature and Stress on the Compressibilities, thermal expansivities, and porosities of Cerro Prieto and Berea sandstones to 9000 psi and 280 C*. in *Eight Workshop on Geothermal Reservoir Engineering*. 1982. Stanford University.

24.   CoreLab, *Operations Manual: Rock Compressibility Apparatus*. Material Code No. 7544-041 ed, ed. M.C.N. 7544-041. Vol. Material Code No. 7544-041. 1980, Dallas, Texas, USA: Core Laboratories Inc.

25.   Coussy, O., *Thermo-mechanics of saturated porous solid in finite deformation*. Eur. J. Mech., A/Solids, 1989. **8**(1): p. 1-14.

26.   Craft, B., C., and Hawkins M. F., *Applied Petroleum Reservoir Engineering*. 1959, NY, USA: Prentice-Hall, Inc., Englewood Cliffs. 132.

27.   Detournay, E., and Cheng,, A. H. D., *Poroelastic response of a borehole in a non-hydrostatic stress field*. Int J. of Rock Mechanics and Mining Sciences, 1988. **25**(3): p. 171-182.

28.   Dewey, J.M., *The elastic constant of materials loaded with non-rigid filters*. J. of Appl. Phys., 1947. **18**(6): p. 578-581.

29.   Digby, J.M., *The effective elastic moduli of porous granular rocks*. ASME J. of Appl.Mech., 1981. **48**(4): p. 803-808.

30.   Domenico, S.N., *Elastic properties of unconsolidated porous and reservoirs*. Geophysics, 1977. **42**(7): p. 1339-1368.

31.   Dropek, R.K., Johnson, J. N., and Walsh, J. B., *The Influence of Pore Pressure on the Mechanical Prperties of Kayenta sandstone*. J. of Geophy Res., 1978. **83**: p. 2817-2824.

32. Economides, M.J., and Nolte, K. G, *Reservoir Stimulation*. 2nd Ed ed. 1989, Huston: Schlumberger. 426.

33. Fatt, I., *Pore Volume Compressibilities of Sandstone Reservoir Rocks*. Transaction, AIME, 1958: p. 213, 362.

34. Fatt, I., *The Biot-Willis elastic coefficients for a sandstone*. J. Appl. Mech., ASME, 1958. **26**: p. 296-297.

35. Fatt, I., *Compressibilities of Sandstones at Low to Moderate Pressure*. Bulletin of the AAPG, 1958a. **42**: p. 1924-1957.

36. Fatt, I., *Pore volume compressibilities of sandstone reservoir rocks*. Petroleum Transaction of the AIME, 1958b. **213**: p. 362-364.

37. Fetkovich, M.J., Reese, D.E., and Whitson, C.H., *Application of a General Material Balance for High-Pressure Gas Reservoirs*, in *SPE Annual Technical Conference and Exhibition*. 1991: Dallas, USA.

38. Gassmann, F., *Über die Elastizität Porbser Medien (On the elasticity of porous media)*. Vierteljahrsschrift der Naturforschenden Gesellschaft, 1951a. **96**(1): p. 1-23.

39. Gassmann, F., *Elastic waves through a packing of spheres*. Geophysical, 1951b. **15**(4): p. 673-685.

40. Geertsma, J., *The effect of fluid pressure decline on volumetric changes of porous rocks*. Petroleum Trans., AIME, 1957. **210**: p. 331-339.

41. Geertsma, J., *Land Subsidence above Compaction Oil and Gas Reservoirs*. JPT, 1973: p. 734-744.

42. Gilluly, I., and Grant, U. S., *Subsidence in the Long Beach harbor area, California*. Bulletin of Geological Society of America, 1949(60): p. 461-530.

43. Green, D.H., and Wang, H. F., *Fluid Pressure Response to Undrained Compression in Saturated Sedimentary Rocks*. Geophysics, 1986. **51**: p. 948-956.

44. Hall, H.N., *Compressibility of Reservoir Rocks*. Trans., AIME, 1953. **198**: p. 309-31.

45. Hamilton, J.M., and J. L. Shafer., *Measurement of Pore Compressibility Characteristics in Rock Exhibiting Pore Collapse and Volumetric Creep*, in *SCA Conference, Paper # 9124*. 1991.

46. Hammerlindl, D.J., *Predicting Gas Reserves in Abnormally Pressured Reservoirs*, in *SPE of AIME 46th Annual Meeting*. 1971, SPE: New Orleans, USA.

47. Harai Zaki, W., Shu-Teh, and Saner, S., *Pore-Compressibility Study of Arabian Carbonate Reservoir Rocks*. SPE Formation Evaluation, 1995: p. 207-214.

48. Harville, D.W., and Hawkins M. F., *Rock Compressibility and Failure as Reservoir*

Mechanisms in Geopressured Gas Reservoirs. JPT, 1969.

49. Hashin, Z., and Shtrikman, S., *Note on a variational approach to the theory of composite elastic materials.* J. of the Franklin Institute, 1961. **271**(4): p. 336-341.

50. Hill, R. *The elastic behavior of a crystalline aggregate.* in *Proceedings of the Physical Society of London.* 1952. London.

51. Horne, N.R., *Modern Well Test Analysis, A Computer-Aided Approach.* 1990: Petroway, Inc.

52. Hughes, D.S., and Cooke, C. E. Jr., *The Effect of Pressure on the Reduction of Pore-Volume of Consolidated Sandstones.* Geophysics, 1953. **18**: p. 298-309.

53. Jaeger, J.C., and Cook, N. G. W., *Rock Mechanics of the Ekofisk reservoir in the evaluation of sandstone.* JPT, 1979. **41**(7): p. 717-722.

54. Jalalh, A.A., *Pore Volume Compressibility Measurement*, in *Intellectual Services for Oil & Gas Industry: Analysis, Solutions and Perspectives.* 2004, University of Miskolc/UFA State Petroleum Technological University.

55. Jalalh, A.A., and Bódi, *Effect of Compressibility In Calculation of Original Gas In Place (O.G.I.P.)*, in *International Scientific conference (MicroCad).* 2004, University of Miskolc: University of Miskolc, Hungary.

56. Jalalh, A.A., *Compressibility measurements of porous rocks. Part-I – measurements of Hungarian rock samples*, in *Acta. Geophysica, Warsaw, Poland.* 2006a. p. (To be issued).

57. Jalalh, A.A., *Compressibility measurements of porous rocks. part II – new relationships.* Acta Geophysica, Warsaw, Poland, 2006b: p. (To be issued).

58. Johnson, J.P., Rhett, D. W. and Siemers, W. T., *Rock Mechanics of the Ekofisk Reservoir in the Evaluation of Subsidence.* JPT, 1989: p. 717-722.

59. Katsube, N., *The constitutive theory for fluid-filled porous materials.* J. Appl. Mech., ASME, 1985. **52**: p. 185-189.

60. King, M.S. *Static and dynamic moduli of rocks under pressure.* in *Rock and Mechanics Theory and Practice: Proceedings of the Eleventh U.S. Symposium on Rock Mechanics.* 1969. NY, USA: Society of Mining Engineers.

61. Knopoff, L., *The theory of finite strain and compressibility of solids.* J, of Geophy. Rese., 1963. **68**(10): p. 2929-2932.

62. Kohlaas, C.A.a.M., F. G. *Rock-Compaction and Pressure-Transient Analysis with Pressure-Dependent Rock Properties.* in *SPE 44th Annual Fall Meeting.* 1969. Denver, Colorado, USA.

63. Laurent, J., Bouteca, M. J., and Sarda, J. P., Bary, D., *Pore Pressure Influence in the Poroelastic Behaviour of Rocks: Experimental Studies and Result.* SPE, Formation Evaluation, 1993: p. 117-124.

64. Lo. T. W, C., C. B., and Toksos, M. N., *Experimental determination of elastic anisotropy of Berea sandstone, Chicopee shale, and Chelmsford granite.* Geophysical, 1986. **51**(1): p. 164-171.

65. Mackenzie, J.K., *The elastic constants of a solid containing spherical holes.* Physical Society of London, 1950. **63**(B1): p. 2-11.

66. Mann, R.L., and Fatt, I., *Effect of pore fluids on the elastic properties of sandstone.* Geophysics, I960. **52**(2): p. 433-444.

67. Marek, B.F., *Predicting pore compressibility of reservoir rock.* JPT, 1971. **11**(3): p. 340-341.

68. Matthews, C., S., and Russell, D. G., *Pressure Build-up and Flow Tests in Wells.* SPE Monograph, Dallas, 1967.

69. Mavko, G., and Nur, A., *Melt squirt in the asthenosphere.* J. of Geophy.l Rese., 1975. **80**(11): p. 1444-1448.

70. Mesri, G., Adachi, K., and Ullrich, C. R.:, *Pore Pressure Response in Rock to Undrained Change in all-round Stress.* Geotechnique, 1976. **26**: p. 317-330.

71. Motulsky, H.J., and Christopouls, A., *Fitting models to biological data using linear and nonlinear regression, (A practical guide to curve fitting).* second edition ed. 2003, San Diego, CA., USA: GraphPad software Inc.

72. Mumaghan, F.D., *Finite Deformation of an Elastic Solid.* 1951, NY, USA: John Wiley & Sons. 140.

73. Newman, G.H., *Pore-volume Compressibility of Consolidated, Friable, and Unconsolidated Reservoir Rocks under Hydrostatic Loading.* JPT, 1973: p. 129-134.

74. Norris, A.N., *Stonely-wave attenuation and dispersion in permeable formations.* Geophysics, 1989. **34**(3): p. 330-341.

75. Nunziato, J.W., and Cowin, S. C., *A nonlinear theory of elastic materials with voids.* Archive for Rational Mechanics and Analysis 1979. **72**(2): p. 175-201.

76. Osif, T.L., *The Effects of Salt, Gas, Temperature, and Pressure on the Compressibility of Water*, in *59th SPE Annual Technical Conference and Exhibition*. 1984, SPE: Houston, Texas, USA.

77. Palciauskas, V.V., and Domenico, P. A., *Fluid pressure in deforming porous rocks.* Water Resources Research 1989. **25**(2): p. 203-213.

78. Pettijohn, F.J., *Sedimentary Rock.* 2nd ed. 1957, NY, USA: Harper & Row. 718.

79. Plona, T.J., *Observation of a second bulk compressional wave in a fluid-saturated porous solid at ultrasonic frequencies.* Applied Physics Letters, 1980. **36**(4): p. 259-261.

80. Raghavan, R., and Miller, F. G., ed. *Mathematical analysis of sand compaction*. ed. G.V. Chilingarian, and Wolf, K. H. Vol. 1. 1975, Elsevier, : Amsterdam.

81. Rice, J.R., and Cleary, M. P., *Some basic stress diffusion solutions for fluid-saturated elastic porous media with compressible constituents*. Reviews of Geophysics and Space Physics, 1976. **14**(2): p. 227-241.

82. Ruddy, I., Andersen, M. A., Pattillo, P. D., Bishiawi, M., and Foged, N., *Rock Compressibility, Compaction, and Subsidence in a High-Porosity Chalk Reservoir: A Case Study of Valhall Field*. Society of Petroleum Engineers 1989. **41**(7): p. 741-746.

83. Sampath, K., *A New Method To Measure Pore Volume Compressibility of Sandstones* Society of Petroleum Engineers, 1982: p. 1360-1362.

84. Santarelli, F.J., Brown, E. T., and Maury, V., *Analysis of borehole stresses using pressure-dependent.* Int J. of Rock Mechanics and Mining Sciences, 1986. **23**(6): p. 445-449.

85. Sawabini, C.T., Chilingar, G. V., and Allen, D. R., *Design and Operation of a Triaxial, High Temperature, High Pressure compaction Apparatus.* J. of Sedimentary Research, 1971. **41**(3): p. 871-881.

86. Schmoker, J.W., and Gautier, D. L, *Compaction of Basin Sediments: Modeling Based on Time-temperature history.* J, of Geophy. Res., 1989. **94**: p. 7379-7386.

87. Sokolnikoff, I.S., *Mathematical Theory of Elasticity*. 2 ed. 1956, NY, USA: McGraw-Hill. 476.

88. Somerton, W.H., *Porous Rock-Fluid System at Elevated Temperatures and pressures," In: Recent Trends in Hydrogeology*. Geological Society of America, Boulder, Colorado, 1982: p. 183-197.

89. Sprunt, E.S., and Nur, A., *Destruction of Porosity through Pressure Solution.* Geophysics, 1977. **42**: p. 726-741.

90. Teeuw, D., *Prediction of Formation Compaction from Laboratory Compressibility Data* JPT, 1971. **11**: p. 263-271.

91. Terzaghi, K. *The Shearing resistance of saturated soils and the angle between the planes of shear*. in *International Conference on Soil Mechanics and Foundation Engineering*. 1936. Cambridge, Mass: Harvard University Press.

92. Toth, J., and Bauer, K., *Pórusos tárlókőzetek deformációja, 1. A deformáció elmélete*, in *Kőolaj és földgáz*. 1988. p. 33 – 39.

93. Toth, J., and Bauer, K., *Pórusos tárlókőzetek deformációja 2. A Pórustérfogat deformáció, pórustér-kompresszibilitás*, in *Kőolaj és földgáz*. 1988. p. 65 – 69.

94. Van der Kamp, G., and Gale, J. E, *Theory of earth tide and barometric effects in porous formations with compressible grains.* Water Resources Research, 1983. **19**(2): p. 538-544.

95.   Van der Knaap, W., *Nonlinear Behavior of Elastic Porous Media.* Trans., AIME, 1959. **216**: p. 179-187.

96.   Von Gonten, W.D., and Choudhary, B. K., *The Effect of Pressure and Temperature on Pore Volume Compressibility* in *Fall Meeting of the Society of Petroleum Engineers of AIME (44th Annual).* 1969, American Institute of Mining, Metallurgical and Petroleum Engineers Inc.: Denver, Colorado.

97.   Walder, J., and Nur, A., *Permeability measurements by the pulse-decay method: Effects of Poroelastic phenomena and non-linear pore pressure diffusion.* Int J. of Rock Mechanics and Mining Sciences, 1986. **23**(3): p. 225-232.

98.   Wilhelmi, B.D., and Somerton, W. H., *Simultaneous Measurement of Pore and Elastic Properties of Rocks Under-Triaxial Stress Conditions.* JPT, 1967. **7**(3): p. 283-294.

99.   Wissa, A.E.Z., *Pore Pressure Measurement in Saturated Stiff Soils.* Journal of the Soil Mechanics and Foundations Division, 1969. **95**(4): p. 1063-1074.

100.   Yale, D.P., Nabor, G. W., and Russell, J. A., *Application of Variable Formation compressibility for improved reservoir Analysis*, in *SPE Annual Technical Conference and Exhibition*. 1993, Society of Petroleum Engineers, Inc.: Houston, Texas.

101.   Zhang, J., Wong, T. F., and Davis, D. M., *Micromechanics of Pressure-induced Grain Crushing in Porous Rocks.* J, of Geophy. Res., 1990. **94**: p. 341-352.

102.   Zimmerman, R.W., Somerton W.H, King M.S., *Compressibility of porous rocks.* J, of Geophy. Res., 1986. **91**(12): p. 765-777.

103.   Zimmerman, R.W.K., M.S.; and Monteiro, P.J.M., *The Elastic Moduli of Mortar as a Porous-Granular Material.* Cement and Concrete Research, 1986. **16**(2): p. 239-245.

NOMENCLATURES

A	=	Area, ft^2 [m^2]
B	=	Formation volume factor, reservoir per standard volume
C	=	Standard "traditional" compressibility
$\overline{C}$		Effective compressibility of heterogeneous solid
C$_{bp}$	=	Bulk compressibility
C$_{bc}$	=	Bulk compressibility
C$_f$	=	Compressibility of the pore fluid is approximately equal to the pore compressibility C$_{pp}$
C$_{pc}$	=	Pore compressibility
C$_{pp}$	=	pore compressibility
C$_r$	=	Compressibility of the rock mineral phase
C$_t$	=	Total compressibility of the rock/fluid system
C$_\phi$	=	Additional compressibility
DVP	=	Pore volume change ($= \Delta V_P$)
dVp	=	Incremental change in pore volume resulting from an incremental change in effective pressure (P$_c$ – P$_f$).
dP$_{eff}$	=	Incremental change in effective pressure.
ΔV_P (calc)		Calculated pore volume change
ΔV_P (correct)		Corrected pore volume change
G	=	Original free gas-in-place, Bscf [std m^3]
G$_p$	=	Cumulative gas production, Bscf [std m^3
G$_s$	=	Initial solution gas in place, Bscf [std m^3]
G$_{inj}$	=	Cumulative gas injection, Bscf [std m^3]
h	=	Thickness, ft [m]
K	=	Bulk modulus
k	=	Formation permeability
M	=	Volume ratio, dimensionless
n$_b$	=	Effective stress coefficient for bulk strain
n$_p$	=	Effective stress coefficient for pore strain
P	=	Reservoir pressure, psia [kPa]
P$_c$	=	Confining pressure
P$_d$ = P$_{eff}$	=	Differential pressure, = Pc – Pp = Effective stress
P$_f$	=	Pore fluid pressure
P$_c$	=	Confining pressure
P$_i$	=	Initial reservoir pressure, psia [kPa]
r$_R$	=	Radius of reservoir, ft [m]
r$_{AQ}$	=	Radius of aquifer, ft [m]
R$_{sw}$	=	Solution gas water ratio. scf/STB [std m^3/ m^3]
S$_{wi}$	=	Initial water saturation, fraction
V	=	Volume, ft^3 [m^3]

V_b	=	Bulk volume
V_f	=	Pore fluid completely fills the pore space,
V_L	=	Wave-speed of the longitudinal "P-wave"
V_p	=	Volume of pore space
V_r	=	Poisson ratio for the rock matrix material
V_s	=	Volume occupied by the mineral grains
V_T	=	Velocity of the transverse "S-wave"
χ	=	Volume fraction of mineral
W	=	Total water in place, bbl [m^3]
We	=	Cumulative water influx, bbl [m^3]
W_{in}j	=	Cumulative water injection, bbl [m^3]
W_p	=	Cumulative water production, bbl [m^3]
Z	=	Gas compressibility factor, dimensionless
ϕ^1		Initial porosity
ϕ	=	Porosity
ε	=	Strain matrix
ε_b	=	Bulk strain, $=\Delta V_b/V_b$
ε_p	=	Pore strain, $=\Delta V_p/V_p$
ΔV_P	=	Pore volume change (= DVP)
ΔV_P (meas)	=	Measured pore volume change
ΔV_P (calc)	=	Calculated pore volume change
ΔV_P (correct)	=	Corrected pore volume change

Subscripts

A	=	Associated water
AQ	=	Limited aquifer
E	=	Effective
F	=	PV ("formation")
G	=	Gas
T	=	Gross interval thickness
I	=	Initial
inj	=	Injection
NNP	=	Nonnet pay
R	=	Reservoir
Sc	=	Standard conditions
Tw	=	Total water
u	=	Displacement vector
W	=	Water

SI Metric Conversion Factor

^{o}F (^{o}F−32)/1.8	= ^{o}C
In.^{3} x1.638 706	E+01 = cm^3
Ft^3 x 2.831 685	E−02 = m^3
Psi x 6.894 757	E-03 = MPa

LABORATORY DATA SHEETS OF COMPRESSIBILITY MEASUREMENTS AND CALCULATION

F1 – SAMPLE DATA SHEET

Sample name:- F1
Pore Volume (Vp):- 0.276728 in3
Rubber sleeve:- Thin

Location:- Főldes's gas reservoir field
Rod cross section (A):- 0.012272 in2
System correction data:-
$\qquad$ Slope = n1** = 0.546770
$\qquad$ Constant = a1** = 1.48E-05

Pc-1	Pi-1	Rod L, inch	Pi-2	Pi-2	Peff	ΔVp-meas	ΔVp-correct	ΔVp-actu	Correction
3563	526	0.3250	3562	445	3117	0.00399	0.00278	0.00292	0.00121
4359	559	0.5125	4358	441	3913	0.00629	0.00492	0.00454	0.00136
5752	576	0.7750	5750	419	5305	0.00951	0.007899	0.00820	0.00161
5743	466	0.8000	5744	441	5299	0.00982	0.008207	0.00818	0.00161

LN (Peff)	ΔVp-correct	
3.49373680	-2.555444	
3.59250985	-2.307623	
3.72468539	-2.102430	
3.72419392	-2.085829	
b		a
1.944488	-9.328676	4.6916E-10
0.160230	0.582450	
0.986602	0.031133	
147.272341	2.000000	
0.142748	0.001939	

LN (Peff)	ΔVp-actu	Cpc_F1
3.4937368	-2.5351466	6.57460E-06
3.5925098	-2.3430836	8.15003E-06
3.7246854	-2.0860698	1.08642E-05
3.7241939	-2.0870255	1.08526E-05
b		a
1.944488	-9.328676198	4.692E-10
4.686E-15	1.7033E-14	
1	9.10451E-16	
1.7221E+29	2	
0.14274836	1.65784E-30	
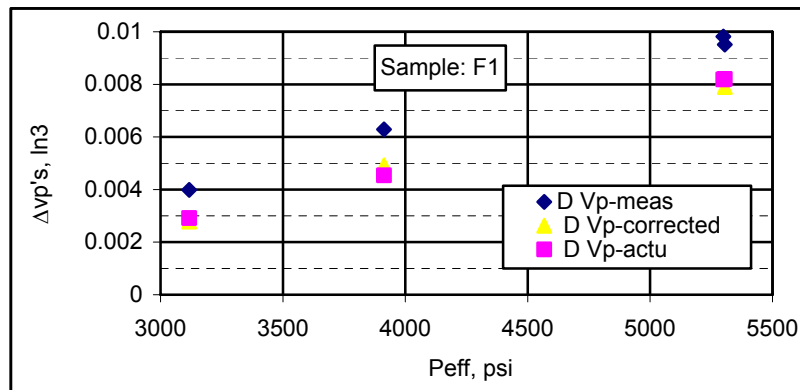
F2 – SAMPLE DATA SHEET

Sample name:- F2
Pore Volume (V_p):- 0.331534 in^3
Rubber sleeve:- Thin

Location:- Főldes's gas reservoir field
Rod cross section (A):- 0.012272 in^2
System correction data:-
        Slope = n1** = 0.546770
        Constant = a1** = 1.48E-05

#	Pc (psi)	Pi-1 (psi)	Rod Position (L, inch)	Pi-2 (psi)	Peff (psi)	ΔVp-meas (inch3)	Correction	ΔVp-corrected (inch3)
1	644	431	0					
2	1023	494	0.15	407	615	0.001345	0.000496	0.001281
3	2054	535	0.31	434	1646	0.002985	0.000850	0.003395
4	3111	565	0.54	436	2701	0.005482	0.001114	0.005543
5	4226	596	0.79	436	3817	0.008318	0.001346	0.007806
6	5640	585	1.04	434	5231	0.011133	0.001599	0.010664
7	6375	525	1.19	436	5967	0.012854	0.001719	0.012148
8	8145	599	1.45	432	7738	0.015813	0.001981	0.015712
9	9480	507	1.56	434	9071	0.017014	0.002161	0.018389

#	LOG Peff (psi)	LOG ΔVp-correct (inch3)
1	6.421622	-6.611642
2	7.406103	-5.814154
3	7.901377	-5.206317
4	8.247220	-4.789353
5	8.562358	-4.497873
6	8.694000	-4.354095
7	8.953899	-4.146925
8	9.112838	-4.073738

#	LOG Peff (psi)	LOG ΔVp-actu (inch3)	Cpc-F2 (1/psi)
1	6.421622	-2.892367	6.22E-06
2	7.406103	-2.469146	6.16E-06
3	7.901377	-2.256232	6.13E-06
4	8.247220	-2.107557	6.11E-06
5	8.562358	-1.972081	6.09E-06
6	8.694000	-1.915490	6.08E-06
7	8.953899	-1.803761	6.06E-06
8	9.112838	-1.735434	6.05E-06

Fitting Results
b = 0.989863586
a =10^ (-13.01645139) = 2.2234E-06
R^2 = 0.99
Polynomial: Linear equation

$$\Delta V_p - actu = a + b * P_{eff}$$

$$Cpc = \left(\frac{ab}{V_p} \right) \left(P_{eff} \right)^{b-1}$$
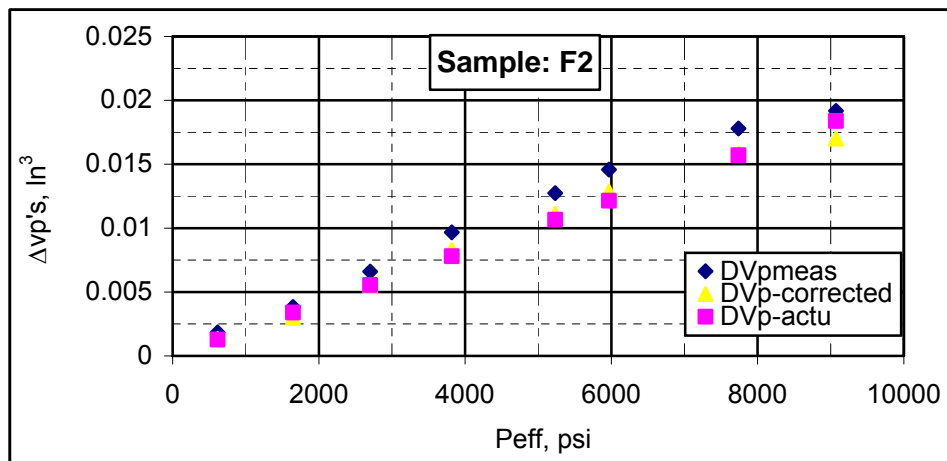
H – SAMPLE (1st Run) DATA SHEET

Sample name:- H
Pore Volume (Vp):- 1.407857in^3
Rubber sleeve:- Thin

Location:-Hajduszoboszlo field
Rod cross section (A):- 0.012272 in^2
System correction data:-
        Slope = n1** = 0.546770
        Constant = a1** = 1.48E-05

Pc	Pi-1	Rod L, inch	Pi-2	Pi-2	Peff-1st	ΔVp -meas	ΔVp-Correct	ΔVP-actu
683	387	0	683	387	296	0		
1023	642	1.3000	958	412	546	0.015953400	0.015488501	0.011961887
2538	1296	4.1000	2430	415	2015	0.050314570	0.049365228	0.058336626
4023	1088	6.0625	3958	405	3553	0.074398068	0.073103566	0.078480141
5598	1119	8.1000	5522	426	5096	0.099401955	0.097825267	0.091289339

LN Peff	ΔVp -correct
6.302619	0.015486
7.608374	0.049365
8.175548	0.073104
8.536211	0.097825

LN Peff	ΔVP-actu	C$_{pc}$-H Sample (1st Run)
6.302619	0.011543	2.8211E-05
7.608374	0.057288	7.6444E-06
8.175548	0.077158	4.3353E-06
8.536211	0.089794	3.0227E-06

b	a
0.035034	-0.209262
0.005260	0.040515
0.956860	0.008924
44.360737	2
0.003533	0.000159

b	a
0.035034	-0.20926
5.78381E-18	4.455E-17
1	9.81308E-18
3.66897E+31	2
0.003533	1.92593E-34

$$C_{pc} - H = \left(\frac{b}{V_p}\right)\left(\frac{1}{P_{eff}}\right) * 0.619 \qquad \Delta V_P - actu(H\text{-}Sample) = a + b * \ln(P_{eff})$$
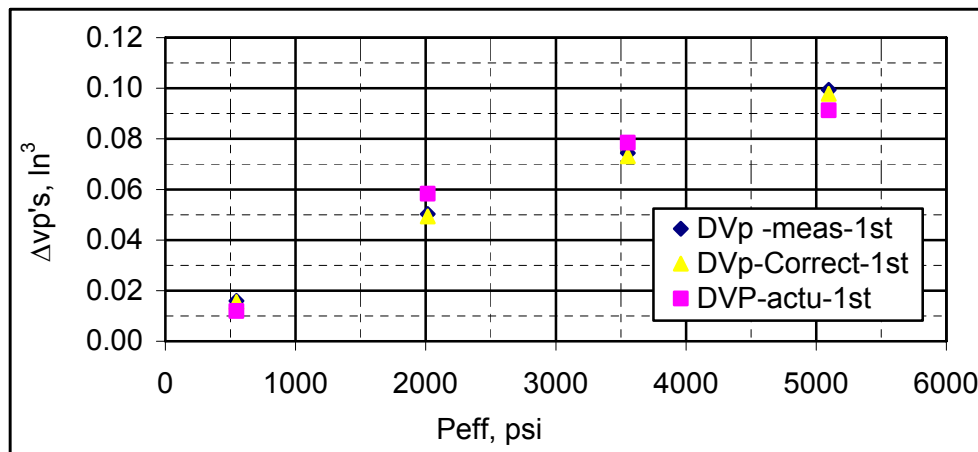
H - SAMPLE (2nd RUN) DATA SHEET

Sample name:- H   Location:-Hajduszoboszlo field
Pore Volume (Vp):- 1.407857in^3 Rod cross section (A):- 0.012272 in^2
Rubber sleeve:- Thin   System correction data:-
                                                        Slope = n1** = 0.546770
                                                        Constant = a1** = 1.48E-05

Pc-1	Pi-1	Rod L, inch	Pc-2	Pi-2	Peff-2nd	ΔVp - meas-2nd	ΔVp- correct-2nd	ΔVp-actu- 2nd
885	578	0.9500	837	416	421	0.011658	0.011255	0.003185
1192	677	2.2125	1125	419	706	0.027151	0.026616	0.024879
1543	687	3.3000	1485	422	1063	0.040497	0.039828	0.042052
2049	745	4.4625	1995	425	1570	0.054763	0.053935	0.058416
2224	553	4.8875	2206	420	1786	0.059979	0.059089	0.063825
2526	570	5.3750	2505	426	2079	0.065961	0.064996	0.070199
2957	667	6.1250	2930	416	2514	0.075165	0.074094	0.078172
3391	605	6.6875	3364	422	2942	0.082068	0.080900	0.084769
3700	559	7.1250	3677	432	3245	0.087437	0.086205	0.088883
4036	571	7.5500	4018	425	3593	0.092652	0.091349	0.093158
4428	586	8.0375	4405	434	3971	0.098635	0.097259	0.097355
4693	538	8.4000	4677	427	4250	0.103084	0.101655	0.100205
4850	501	8.6125	4840	424	4416	0.105691	0.104233	0.101812
5003	488	8.8250	4996	424	4572	0.108299	0.106813	0.103269
5115	466	8.9750	5107	425	4682	0.110139	0.108635	0.104267
5298	566	9.3750	5287	416	4871	0.115048	0.113510	0.105927
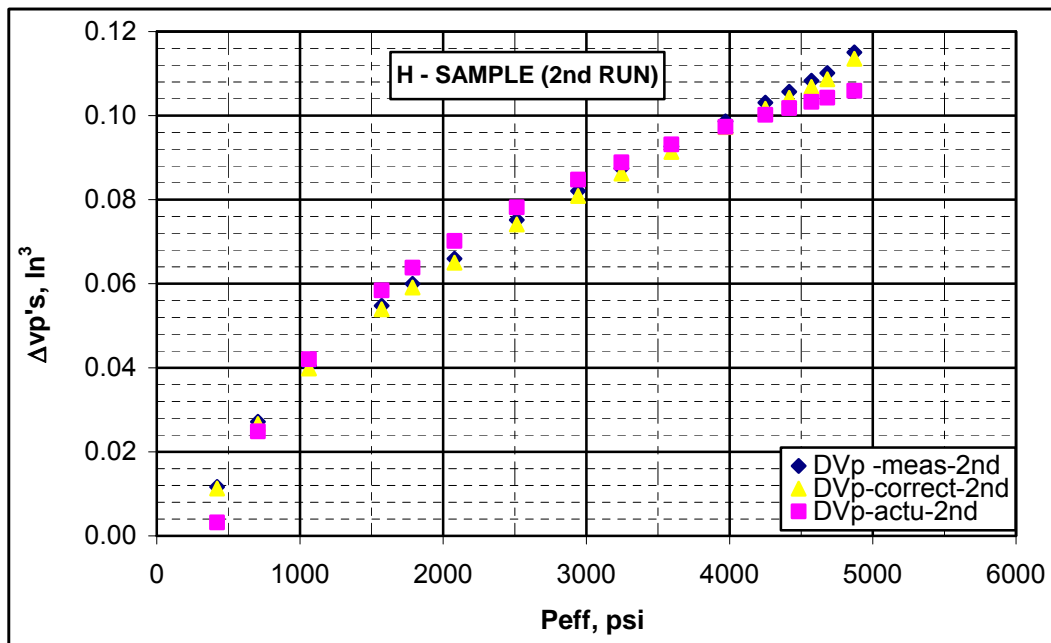
LN Peff-2nd	ΔVp -correct	LN Peff-2nd	ΔVp-actu
6.042632834	0.01125496	6.042633	0.00318499
6.559615237	0.02661642	6.559615	0.02487898
6.968850378	0.03982788	6.96885	0.04205161
7.358830898	0.05393486	7.358831	0.05841625
7.487733761	0.05908991	7.487734	0.06382537
7.639642288	0.06499546	7.639642	0.07019987
7.829630389	0.07409363	7.82963	0.07817228
7.986844901	0.08090037	7.986845	0.08476943
8.084870629	0.08620502	8.084871	0.08888286
8.186742787	0.09134999	8.186743	0.09315770
8.286773231	0.09725929	8.286773	0.09735525
8.354674262	0.10165581	8.354674	0.10020456
8.392989588	0.10423335	8.39299	0.10181237
8.427706025	0.10681318	8.427706	0.10326917
8.451480648	0.10863451	8.451481	0.10426682
8.491054534	0.11351032	8.491055	0.10592745
b	a	b	a
0.041962728	-0.250380369	0.041963	-0.2503804
0.001577432	0.012330455	4.3E-18	3.361E-17
0.980600351	0.004486792	1	1.223E-17
707.6625491	14	9.53E+31	14
0.014246167	0.000281838	0.014246	2.094E-33

$$C_{pc} - H = \left(\frac{b}{V_p} \right) \left(\frac{1}{P_{eff}} \right) * 0.619$$

$$\Delta V_P - actu(H\text{-}Sample) = a + b * \ln(P_{eff})$$

H - SAMPLE (3rd RUN) DATA SHEET

Sample name:- H   Location:- Hajduszoboszlo field
Pore Volume (Vp):- 1.407857in^3 Rod cross section (A):- 0.012272 in^2
Rubber sleeve:- Thin   System correction data:-
                                                    Slope = n1** = 0.546770
                                                    Constant = a1** = 1.48E-05

Pc-1	Pi-1	Rod L, inch	Pi-2	Pi-2	Peff-52C	Vp - meas-52C	Vp-correct-52C	Vp-actu-52C
883	523	0.8375	833	357	476	0.0102777	0.00984637	0.018035539
1189	603	1.8500	1131	360	771	0.0227029	0.02214148	0.033760289
1529	606	2.7350	1484	361	1123	0.0335635	0.03287389	0.046022319
2042	653	3.7000	1994	361	1633	0.0454058	0.04455956	0.058230373
2286	502	4.1375	2260	362	1898	0.0507748	0.04985597	0.063133674
2521	484	4.5125	2501	362	2139	0.0553767	0.05439585	0.067031281
2953	552	5.1000	2922	360	2562	0.0625864	0.06150385	0.072914965
3399	561	5.6750	3371	366	3005	0.0696427	0.06846152	0.078115222
4025	638	6.4625	3988	369	3619	0.0793068	0.07799921	0.084177272
4428	547	6.9750	4401	369	4032	0.0855961	0.08420894	0.087700796
4924		7.6000	4892	365	4527	0.0932660	0.09178818	0.091476432
5058	435	7.8125	5042	364	4678	0.0958738	0.09436919	0.092546263
5208	434	8.0750	5193	356	4837	0.0990952	0.09756280	0.093636075
5303	401	8.2000	5291	361	4930	0.1006291	0.09908074	0.094257027

LN Peff	ΔVp -correct-52^{0}C
5.717027701	0.0098464
6.165417854	0.0221415
6.647688374	0.0328739
7.023758955	0.0445596
7.398174093	0.0498560
7.548555979	0.0543959
7.668093709	0.0615039
7.848543482	0.0684615
8.008032847	0.0779992
8.193953024	0.0842089
8.302017810	0.0917882
8.417814747	0.0943692
8.450625947	0.0975628
8.484049973	0.1006291
b	a
0.032605662	-0.182992
0.001715074	0.0130518
0.967865170	0.0054556
361.4265871	12
0.010757381	0.000357164

LN Peff	ΔVp- actu - 520C
6.165418	0.0180355
6.647688	0.0337603
7.023759	0.0460223
7.398174	0.0582304
7.548556	0.0631337
7.668094	0.0670313
7.848543	0.0729150
8.008033	0.0781152
8.193953	0.0841773
8.302018	0.0877008
8.417815	0.0914764
8.450626	0.0925463
8.484050	0.0936361
8.503094	0.0942570
b	a
0.032606	-0.182992
5.86E-18	4.56651E-17
1	1.55502E-17
3.1E+31	12
0.007488	2.9017E-33

Zs – 001 - SAMPLE DATA SHEET

Sample name:- Zs-001
Pore Volume (Vp):- 0.792386 in3
Rubber sleeve:- Thin

Location:-   Zsana's Field
Rod cross section (A):- 0.012272 in2
System correction data:-

$$\text{Slope} = n1^{**} = 0.546770$$
$$\text{Constant} = a1^{**} = 1.48E\text{-}05$$

Pc-1	Pi-1	Rod L, inch	Pc-2	Pi-2	Peff	ΔVp-meas	ΔVp-actu	ΔVp-Correct	Correction
632	203	0.000	632	203	429	0.00000	0.00216	0.00041	0.0004075
1027	219	0.258	1026	203	823	0.00316	0.00403	0.00258	0.0005818
1510	223	0.563	1510	204	1306	0.00690	0.00626	0.00615	0.0007489
2511	230	1.000	2510	203	2307	0.01227	0.01077	0.01125	0.0010223
3515	225	1.350	3514	203	3311	0.01657	0.01520	0.01532	0.0012455
4564	225	1.700	4562	203	4359	0.02086	0.01976	0.01941	0.0014476
5494	222	2.000	5494	203	5291	0.02454	0.02377	0.02293	0.0016094
6977	241	2.563	6976	203	6773	0.03145	0.03008	0.02960	0.0018420
8470	243	3.150	8469	203	8266	0.03866	0.03638	0.03660	0.0020540
9471	232	3.575	9470	203	9267	0.04387	0.04057	0.04169	0.0021865

LOG (P_{eff})	LOG ΔVp-correct
2.9154	-2.5887
3.115943	-2.2108
3.363048	-1.9489
3.519959	-1.8147
3.639387	-1.7119
3.723538	-1.6395
3.830781	-1.5286
3.917295	-1.4365
3.966939	-1.38
b = n1	0.954079
$a1=(10)^{-5.1766} = 6.7E\text{-}06$	
R^2	0.998299

| LOG Peff	LOG ΔVp actu	Cpc_Zs_OO1
2.9154	-2.39505	3.647E-06
3.115943	-2.20372	3.570E-06
3.363048	-1.96796	3.478E-06
3.519959	-1.81826	3.421E-06
3.639387	-1.70431	3.378E-06
3.723538	-1.62403	3.348E-06
3.830781	-1.52171	3.310E-06
3.917295	-1.43916	3.280E-06
3.966939	-1.3918	3.263E-06
b = n1	0.954079	
$a1 =-5.17658=6.66E\text{-}06$		
R^2	1	

Zs – 002 - SAMPLE DATA SHEET

Sample name:- Zs-002
Pore Volume (Vp):- 0.900879819 in3
Rubber sleeve:- Thin

Location:- Zsana's Field
Rod cross section (A):- 0.012272 in2
System correction data:-
 Slope = n1** = 0.546770
 Constant = a1** = 1.48E-05

#	Pc (psi)	Pi-1 (psi)	Rod Position (L, inch)	Pc-2 (psi)	Pi-2 (psi)	Peff (psi)	ΔVp-meas (inch^3)	ΔVp-actu (inch^3)	ΔVp-corrected (inch^3)
1	682	387	0						0
2	1070	528	0.3500	1065	390	675	0.004295	0.004192208	0.003773
3	2176	670	0.9750	2164	389	1775	0.011965	0.009868133	0.011079
4	3125	567	1.3750	3119	391	2728	0.016874	0.014437737	0.015753
5	4387	597	1.8000	4381	389	3992	0.022089	0.020225698	0.020709
6	5259	525	2.0875	5256	388	4868	0.025617	0.024109778	0.024079
7	6124	509	2.3500	6121	385	5736	0.028839	0.027879727	0.027157
8	7079	521	2.6125	7076	389	6687	0.032060	0.031935857	0.030231
9	8074	539	2.9000	8070	390	7680	0.035588	0.036101071	0.033615
10	8797	557	3.5000	8790	274	8516	0.042951	0.039559772	0.040864

LOG Peff	LOG ΔVp-correct
2.82930	-2.4233
3.24920	-1.9555
3.43584	-1.8026
3.60119	-1.6838
3.68735	-1.6183
3.75861	-1.5661
3.82523	-1.5195
3.88536	-1.4735
3.93024	-1.3887

LOG Peff	LOG ΔVp-aactu	Cpc_ZS-OO2
2.829304	-2.3775572	3.77853E-06
3.249198	-2.0057650	3.38236E-06
3.435844	-1.8405009	3.21987E-06
3.601191	-1.6940965	3.08245E-06
3.687351	-1.6178068	3.01319E-06
3.758609	-1.5547115	2.95708E-06
3.825231	-1.4957214	2.90557E-06
3.885361	-1.4424799	2.85985E-06
3.930236	-1.4027462	2.82619E-06

b		a
0.885442	-4.88274	1.309E-05
0.033614	0.120799	
0.990013	0.033842	
693.8816	7	
0.794704	0.008017	

b		a
0.885442	-4.882740606	1.3100E-05
2.0789E-16	7.47104E-16	
1	2.09304E-16	
1.8141E+31	7	
0.79470392	3.06656E-31	

$$\Delta Vp\text{-}actu = a * (P_{eff})^b$$

$$Cpc = \left(\left(\frac{ab}{V_p} \right) (P_{eff})^{b-1} \right) (0.619)$$
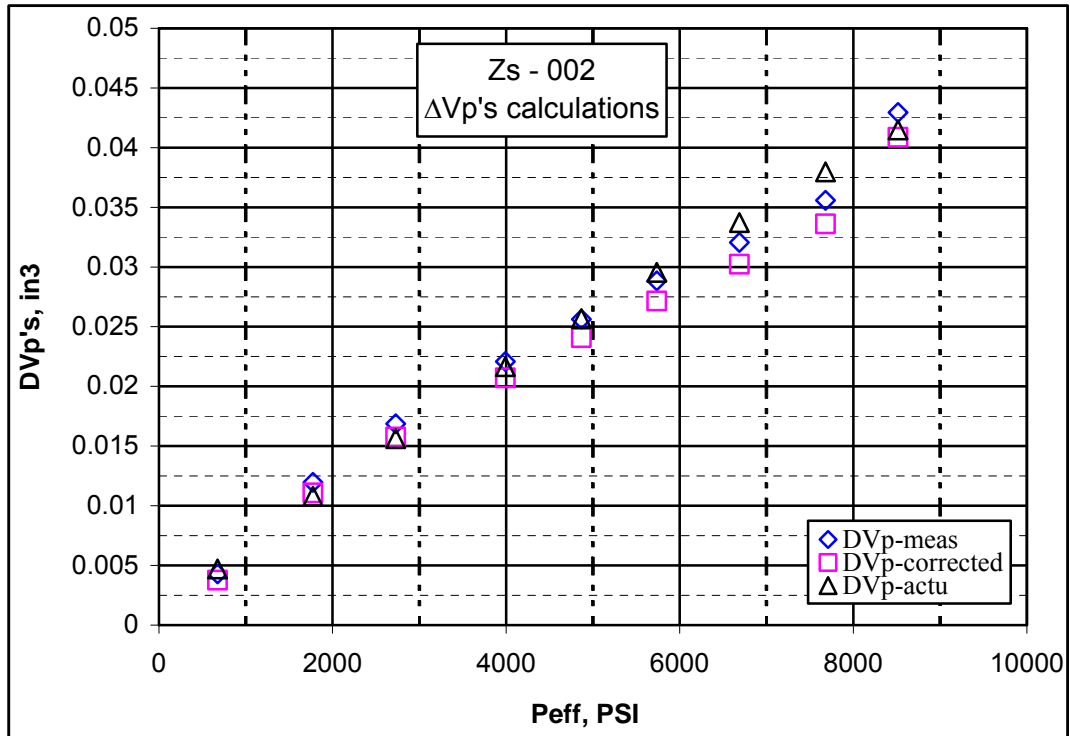
Zs – 005 – SAMPLE (1st Run) DATA SHEET

Sample name:- Zs-005   Location:- Zsana field
Pore Volume (Vp):- 0.979126 in^3 Rod cross section (A):- 0.012272 in^2
Rubber sleeve:- Thin   System correction data:-
                                                                          Slope = n1** = 0.54676967
                                                                          Constant = a1** = 1.48165E-05

Pc	Pi-1	Rod L, inch	Pc-2	Pi-2	Peff	ΔVp-meas	ΔVp-Calc	ΔVp-correct
	325	0			0			
1014	650	0.7875	1014	325	689	0.009664	0.007473	0.009136123
2029	587	1.4	2020	331	1689	0.017181	0.015438	0.016318569
3093	550	1.9	3078	337	2741	0.023317	0.022842	0.022193224
4057	571	2.425	4047	331	3716	0.029759	0.029220	0.028432584
5084	561	2.9	5074	333	4741	0.035588	0.035586	0.034072703
6085	564	3.425	6075	330	5745	0.042031	0.041571	0.040347582
7066	582	4.025	7056	331	6725	0.049394	0.047221	0.047559287
8103	575	4.575	8093	330	7763	0.056144	0.053037	0.054158995
9057	574	5.125	9035	354	8681	0.062893	0.058057	0.06078344

LOG Peff	LOG ΔVp-correct	
2.838219	-2.039238039	
3.22763	-1.787317921	
3.437909	-1.653779601	
3.570076	-1.546183672	
3.67587	-1.467593414	
3.75929	-1.394182485	
3.827692	-1.322764669	
3.89003	-1.266329405	
3.93857	-1.216214726	
b		a
0.809177	-4.423143619	3.8E-05
0.02764	0.101518507	
0.993048	0.017758927	
857.0737	6	
0.270303	0.001892277	

LOG Peff	LOG ΔVp act	
2.83822	-2.1265223	
3.22763	-1.8114204	
3.43791	-1.6412672	
3.57008	-1.534321	
3.67587	-1.4487147	
3.75929	-1.3812131	
3.82769	-1.3258636	
3.89003	-1.2754217	
3.93857	-1.2361441	
b		a
0.80918	-4.4231436	4E-05
5.3E-16	1.942E-15	
1	3.397E-16	
2.3E+30	6	
0.2703	6.926E-31	

Cpc_ZS-OO5 (1st Run)
5.54822E-06
4.67569E-06
4.26304E-06
4.02252E-06
3.83982E-06
3.70162E-06
3.59203E-06
3.49498E-06
3.42122E-06

$$\Delta Vp\text{-}actu = a*\left(P_{eff}\right)^b$$

$$Cpc = \left(\frac{ab}{V_p}\right)\left(P_{eff}\right)^{b-1}*0.619$$

DVp's calculations Zs - 005 (1st Run)

Legend:
DVp-meas
DVp-Calc
DVp-correct

Y-axis: ΔVp's, in³
X-axis: Peff, PSI
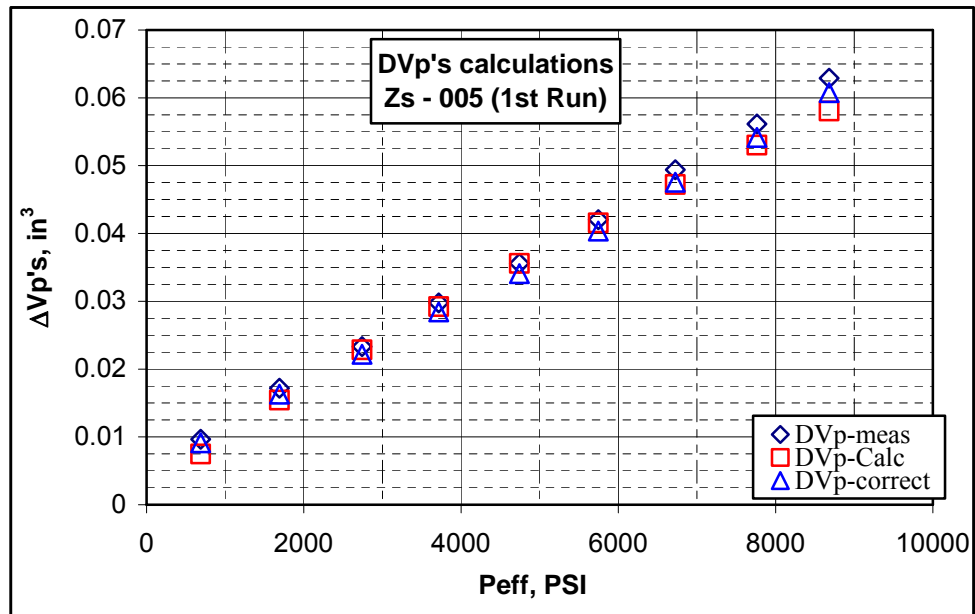
Zs – 005 – SAMPLE (2nd Run) DATA SHEET

Sample name:- Zs-005
Location:- Zsana field
Pore Volume (Vp):- 0.979126 in^3
Rod cross section (A):- 0.012272 in^2
Rubber sleeve:- Thin
System correction data:-

          Slope = n1** = 0.54676967
          Constant = a1** = 1.48165E-05

#	Pc-1	Pi-1	Rod L, (inch)	Pi-2	Pi-2	Peff	ΔVp-meas. (inch)	ΔVp-actu (inch)	ΔVp-correct (inch)
1	1502	492	0.7125	1500	359	1141	0.008744	0.008401	0.00804806
2	2990	536	1.500	2981	359	2622	0.018408	0.016723	0.01731142
3	4477	482	2.200	4472	358	4114	0.026998	0.024277	0.02559552
4	6099	468	2.750	6094	358	5736	0.033748	0.031963	0.03206553
5	7065	414	3.100	7063	358	6705	0.038043	0.036369	0.03621081
6	8048	412	3.500	8047	358	7689	0.042951	0.040733	0.04097713
7	10027	496	4.00	10023	358	9665	0.049087	0.049220	0.04685004

#	LOG Peff	LOG (ΔVp-correct)		LOG (Peff)	LOG (ΔVp actu)		Cpc-ZS--005 (2nd Run)
1	3.057286	-2.0943		3.057286	-2.07567		3.85E-06
2	3.418633	-1.7617		3.418633	-1.77667		3.34E-06
3	3.614264	-1.5918		3.614264	-1.61480		3.09E-06
4	3.758609	-1.4940		3.758609	-1.49536		2.91E-06
5	3.826399	-1.4412		3.826399	-1.43926		2.84E-06
6	3.885870	-1.3875		3.885870	-1.39006		2.77E-06
7	3.985202	-1.3293		3.985202	-1.30786		2.66E-06
	Linear regression fitting			Linear regression fitting			
	b		a	b		a	
	0.827457	- 4.6055	2.5E-05	0.827457	-4.60545	2.5E-05	
	0.022567	0.08263		3.964E-16	1.451E-15		
R	0.996295	0.01773		1	3.1137E-16		
	1344.465	5		4.358E+30	5		
	0.422467	0.00157		0.4224667	4.84757E-31		

$$\Delta Vp\text{-}actu = a * (P_{eff})^b$$

$$Cpc = \left(\left(\frac{ab}{V_p} \right)(P_{eff})^{b-1} \right)(0.619)$$

Zs – 005 – SAMPLE (3rd RUN) DATA SHEET

Sample name:- Zs-005
Pore Volume (Vp):- 0.979126 in3
Rubber sleeve:- Thin

Location:- Zsana field
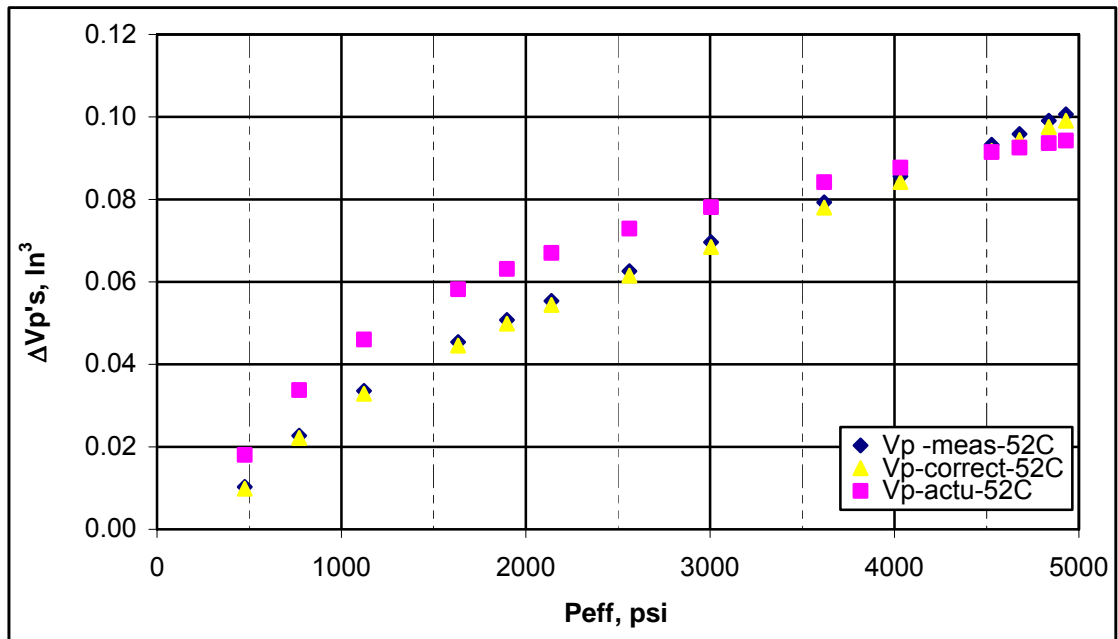Rod cross section (A):- 0.012272 in2
System correction data:-
$\qquad$ Slope = n1** = 0.54676967
$\qquad$ Constant = a1** = 1.48165E-05

Pc	Pi-1	Rod L, inch	Pi-2	Pi-2	Peff	ΔVp - meas	ΔVp-correct	ΔVp-actu
0	0							
1517	627	0.6875	1505	375	1130	0.008437	0.00774494	0.008318636
3052	735	1.625	3036	340	2696	0.019942	0.01882859	0.017007488
4650	630	2.2125	4641	373	4268	0.027151	0.02572045	0.024815384
6023	591	2.7	6016	372	5644	0.033134	0.03146674	0.031227315
7067	518	3.0375	7061	375	6686	0.037276	0.03544666	0.035896275
8058	520	3.36	8054	372	7682	0.041233	0.03926005	0.040239181
10161	695	4.0375	10150	376	9774	0.049548	0.04729647	0.049054055

LOG Peff	LOGΔVp -correct		LOG Peff	LOG ΔVp actu	Cpc_ZS-OO5 (3rd Run)
3.05308	-2.11098		3.05308	-2.07995	3.82764E-06
3.43072	-1.72518		3.43072	-1.76936	3.28003E-06

3.63022	-1.58972
3.75159	-1.50215
3.82517	-1.45042
3.88547	-1.40605
3.99007	-1.32517

b		a
0.822442	-4.59093	2.56E-05
0.033990	0.12455	
0.991532	0.02670	
585.4725	5.00000	
0.417245	0.00356	

3.63022	-1.60528	3.02311E-06
3.75159	-1.50547	2.87677E-06
3.82517	-1.44495	2.79152E-06
3.88547	-1.39535	2.72353E-06
3.99007	-1.30933	2.60951E-06

b		a
0.822442	-4.59093	2.56E-05
1.32E-16	4.9E-16	
1.0	1.0E-16	
3.9E+31	5	
0.417245	5.4E-32	

$$\Delta Vp\text{-}actu = a * \left(P_{eff}\right)^{b}$$

$$Cpc = \left(\left(\frac{ab}{V_p}\right)\left(P_{eff}\right)^{b-1}\right)(0.619)$$
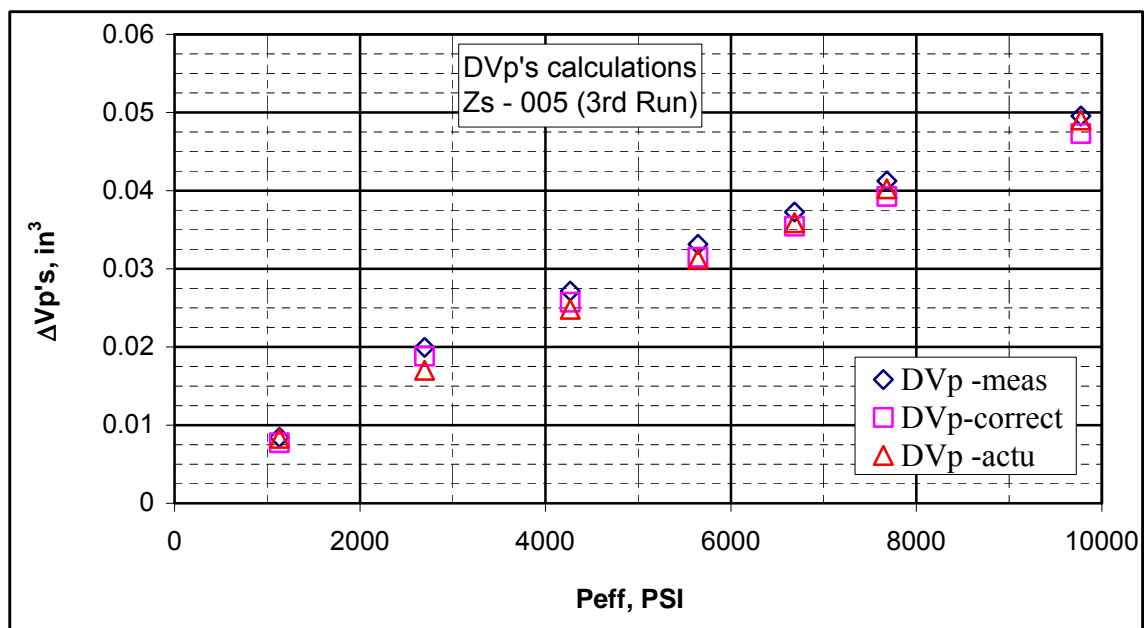
Zs – 006 – SAMPLE DATA SHEET

Sample name:- Zs – 006   Location:- Zsana field
Pore Volume (Vp):- 0.628368in^3 Rod cross section (A):- 0.012272 in^2
Rubber sleeve:- Thin   System correction data:-

<div align="right">

Slope = n1** = 0.546770
Constant = a1** = 1.48E-05

</div>

#	Pc-1 (PSI)	Pi-1 (PSI)	Rod position (L, inch)	Pc-2 (PSI)	Pi-2 (PSI)	Peff (PSI)	ΔVp-meas (inch3)	Correction	ΔVp-corrected (inch3)
1	661	362	0			299			0
2	914	500	0.4	902	362	540	0.0046115	0.0002973	0.00461146
3	1215	498	0.7125	1207	367	840	0.0082811	0.0004626	0.00828112
4	1503	476	0.9375	1499	366	1133	0.0109188	0.0005861	0.01091879
5	1877	479	1.175	1874	365	1509	0.0137011	0.0007183	0.01370110
6	2090	427	1.3125	2087	361	1726	0.0153207	0.0007861	0.01532068
7	2086	376	1.3375	2086	362	1724	0.0156281	0.0007855	0.01562808
8	2528	453	1.5125	2526	364	2162	0.0176517	0.0009095	0.01765168
9	3490	557	1.875	3486	364	3122	0.0218682	0.0011415	0.02186818
10	4522	552	2.225	4519	365	4154	0.0259513	0.0013536	0.02595131
11	5010	457	2.4	5008	364	4644	0.0280074	0.0014451	0.02800737
12	5558	474	2.625	5555	363	5192	0.0306716	0.001542	0.03067157
13	5956	412	2.725	5954	360	5594	0.0318307	0.0016101	0.03183072
14	6462	443	2.875	6461	365	6096	0.0335898	0.0016918	0.03358975
15	7486	543	3.2	7482	365	7117	0.0374212	0.0018487	0.03742118
16	8463	579	3.6	8460	360	8100	0.0421886	0.00199	0.04218864

#	Log (Peff) (PSI)	Log (ΔVp-corrected) (inch3)
1	2.732394	-2.33616
2	2.924279	-2.08191
3	3.05423	-1.96183
4	3.178689	-1.86324
5	3.237041	-1.81472
6	3.236537	-1.80609
7	3.334856	-1.75321
8	3.494433	-1.66019
9	3.618466	-1.58584
10	3.666892	-1.55273
11	3.715335	-1.51326
12	3.747722	-1.49715
13	3.785045	-1.47379
14	3.852297	-1.42688
15	3.908485	-1.37480

Fitting Results

b = 0.737788

a = 10$^{(-4.24498)}$ = 5.68886E-05

R2 = 0.98

#	Peff (PSI)	ΔVp-actu (inch3)	Cpc-Zs-006 (1/PSI)
1	540	0.003254	9.81E-06
2	840	0.005909	7.94E-06
3	1133	0.008133	7.09E-06
4	1509	0.010702	6.43E-06
5	1726	0.012087	6.16E-06
6	1724	0.012075	6.16E-06
7	2162	0.014715	5.74E-06
8	3122	0.019995	5.15E-06
9	4154	0.025162	4.74E-06
10	4644	0.027485	4.60E-06
11	5192	0.030002	4.46E-06
12	5594	0.031802	4.37E-06
13	6096	0.033999	4.26E-06
14	7117	0.038322	4.09E-06
15	8100	0.042326	3.94E-06

$$Cpc = \left(\left(\frac{ab}{V_p} \right) \left(P_{eff} \right)^{b-1} \right) (0.619)$$

$$\Delta Vp\text{-}actu = a * \left(P_{eff} \right)^b$$

DVp's calculations
Zs - 006

◇ DVp-meas
□ DVp-actu
△ DVp-actu

Zs – 007 – SAMPLE DATA SHEET

Sample name:- Zs-007
Pore Volume (Vp):- 1.168366633 in3
Rubber sleeve:- Thick

Location:- Zsana field
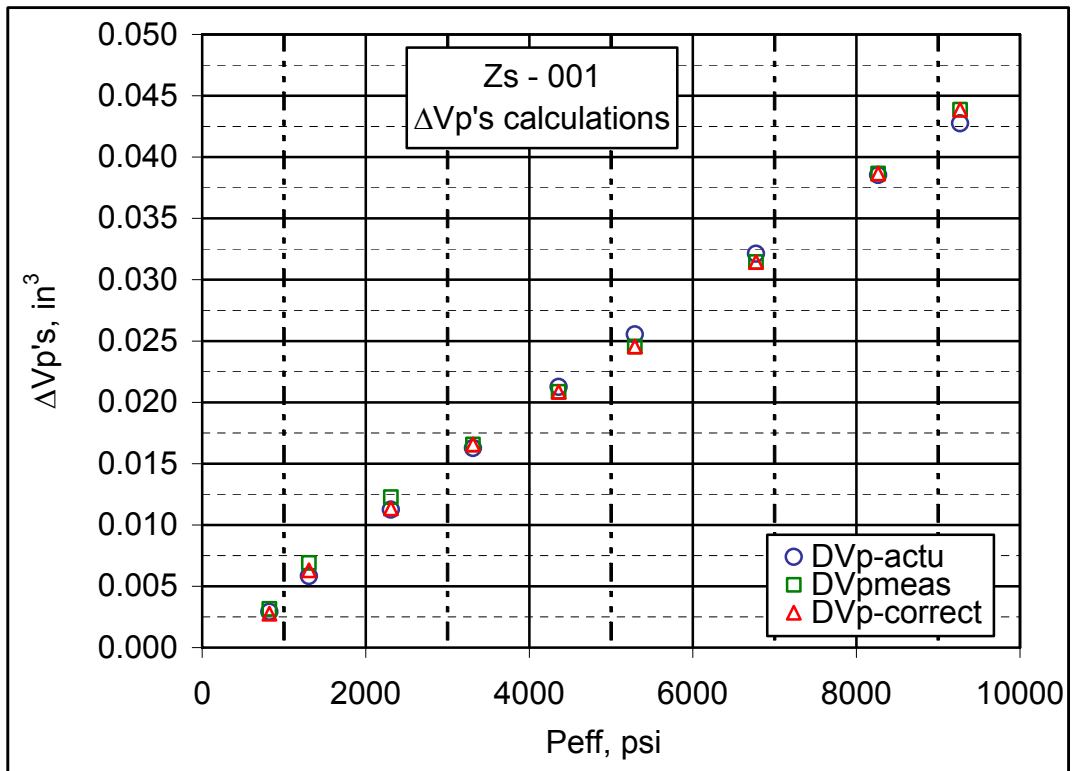Rod cross section (A):- 0.012272 in2
System correction data:-
$\quad$ Slope = n1* = 0.390642602
$\quad$ Constant = a1* = 4.61632E-05

#	Pc-1 (PSI)	Pi-1 (PSI)	Rod position (L, inch)	Pc-2 (PSI)	Pi-2 (PSI)	Peff (PSI)	ΔVp-meas (inch3)	Correction	ΔVp-corrected (inch3)
1	658	361	0	0	0	0	0	0	0
2	1293	613	0.625	1305	374	931	0.00767	0.000667	0.007002952
3	2531	703	1.4	2516	368	2148	0.017181	0.0009246	0.016256034
4	3735	643	2	3725	366	3359	0.024544	0.001101	0.023442701
5	5050	618	2.5375	5040	368	4672	0.03114	0.0012524	0.029887361
6	6226	593	3.025	6219	358	5861	0.037122	0.0013684	0.035753893
7	7216	535	3.375	7209	364	6845	0.041417	0.001454	0.039963508
8	8856	644	3.95	8844	368	8476	0.048474	0.0015806	0.046893219

#	Log (Peff) (PSI)	Log (ΔVp-corrected) (inch3)
1	2.968949681	-2.15472
2	3.332034277	-1.78899
3	3.526210004	-1.62999
4	3.669502834	-1.52451
5	3.767971721	-1.44668
6	3.835373452	-1.39834
7	3.928190948	-1.32889
Fitting Results		
b = 0.851918436		
a = 10(-4.6563) = - 0.00194		
R2 = 0.99		

#	Peff (PSI)	ΔVp-actu (inch3)	Cpc-Zs-007 (1/PSI)
1	931	0.0074645	3.62E-06
2	2148	0.0152166	3.20E-06
3	3359	0.022271	2.99E-06
4	4672	0.0294994	2.85E-06
5	5861	0.035785	2.76E-06
6	6845	0.0408434	2.69E-06
7	8476	0.0489998	2.61E-06

$$\Delta Vp - actu = a * \left(P_{eff} \right)^{b}$$

$$Cpc = \left(\left(\frac{ab}{V_p} \right) \left(P_{eff} \right)^{b-1} \right) (0.619)$$

30. S - SAMPLE DATA SHEET

Sample name:- 30.S
Pore Volume (Vp):- 0.7671 in3
Rubber sleeve:- Thick

Location:-Algyo field
Rod cross section (A):- 0.012272 in2
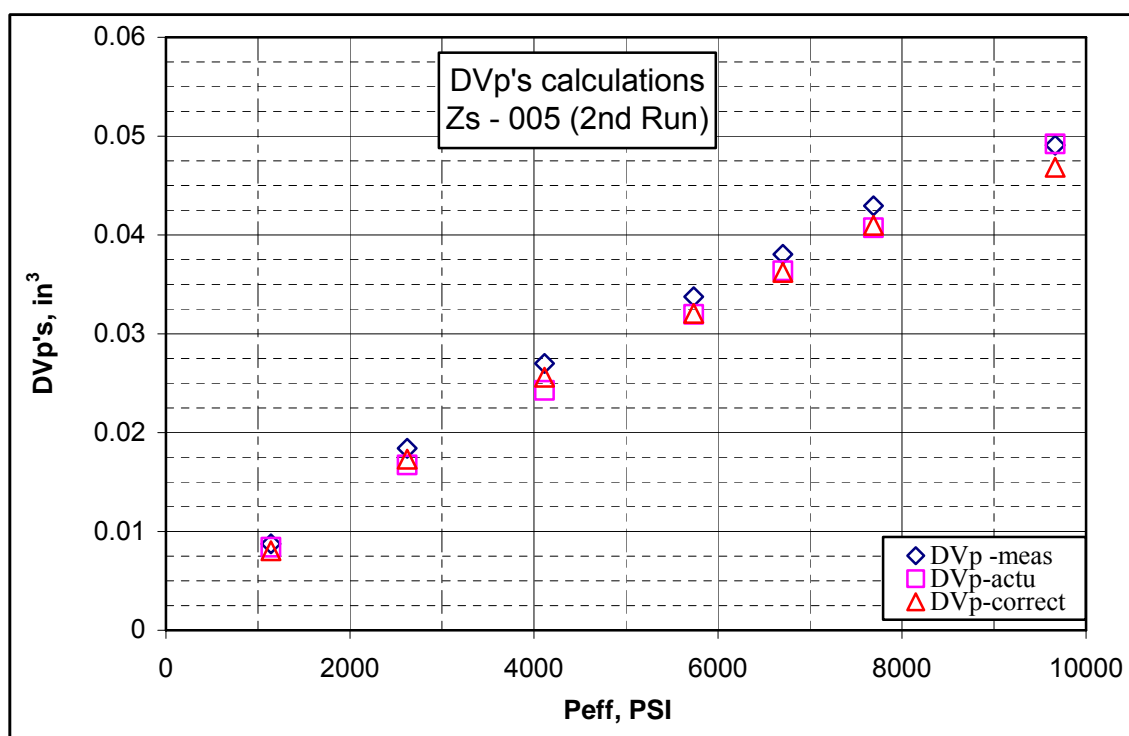System correction data:-

Slope = n1* = 0.390642
Constant = a1* = 4.616E-05

#	Pc-1 (psi)	Pi-1 (psi)	Rod position (L, inch)	Pc-2 (psi)	Pi-2 (psi)	Peff (psi)	ΔVp-meas (inch3)	Correction	ΔVp-corrected (inch3)
1	440	6	0						
2	604	64	0.4375	594	6	588	0.005369	0.0005574	0.004811577
3	799	70	0.8580	783	8	775	0.010529	0.0006208	0.009908403
4	1022	64	1.2375	1011	8	1003	0.015186	0.0006866	0.014499765
5	1513	159	1.7500	1496	7	1489	0.021476	0.0008012	0.020674489
6	1860	39	2.0250	1853	7	1846	0.024850	0.0008714	0.023979073
7	2102	17	2.2250	2095	5	2090	0.027305	0.0009147	0.026390141
8	2512	20	2.4000	2509	7	2502	0.029452	0.0009813	0.028471108
9	2900	19	2.5750	2892	7	2885	0.031600	0.0010375	0.030562532
10	3213	15	2.6875	3207	8	3199	0.032981	0.0010802	0.031900388
11	3598	17	2.8725	3591	5	3586	0.035251	0.0011295	0.034121399
12	3904	9	2.9250	3900	7	3893	0.035895	0.0011663	0.034728840
13	4505	20	3.0750	4498	8	4490	0.037736	0.0012332	0.036502768
14	5021	17	3.2250	5015	7	5008	0.039577	0.0012869	0.038289811
15	5514	14	3.3250	5508	8	5500	0.040804	0.0013348	0.039469013
16	5817	12	3.4250	5811	6	5805	0.042031	0.0013633	0.040667754
17	6022	9	3.4500	6019	7	6012	0.042338	0.0013821	0.040955762
18	6606	17	3.5750	6502	7	6495	0.043872	0.0014246	0.042447385
19	7004	13	3.6500	6999	8	6991	0.044792	0.0014660	0.043326229
20	7503	14	3.7500	7497	8	7489	0.046019	0.0015059	0.044513472

132
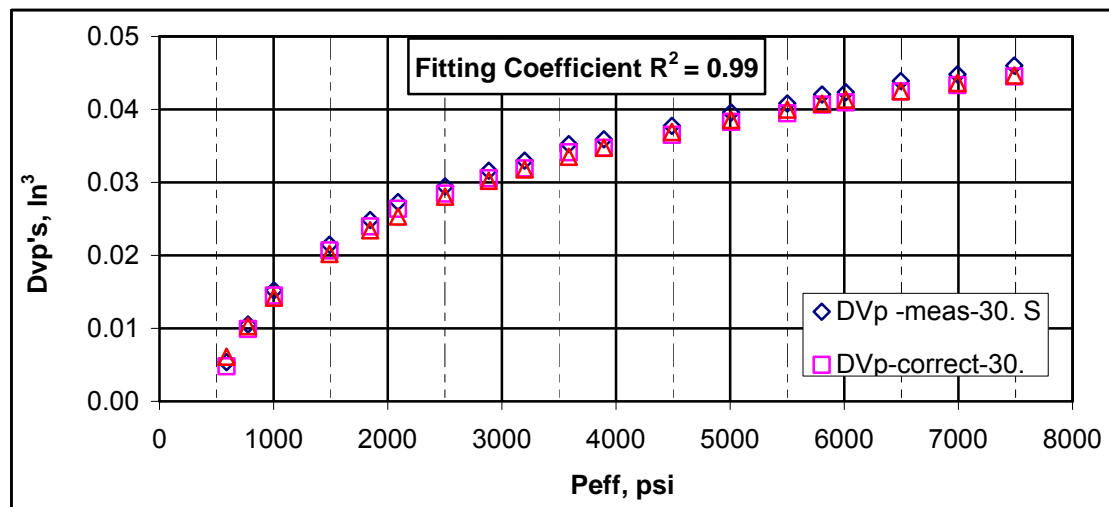
#	LN Peff (psi)	ΔVp-correct (inch^3)
1	6.37673	0.00481
2	6.65286	0.00991
3	6.91075	0.01450
4	7.30586	0.02067
5	7.52078	0.02398
6	7.64492	0.02639
7	7.82485	0.02847
8	7.96728	0.03056
9	8.07059	0.03190
10	8.18479	0.03412
11	8.26694	0.03473
12	8.40961	0.03650
13	8.51879	0.03829
14	8.61250	0.03947
15	8.66647	0.04067
16	8.70151	0.04096
17	8.77879	0.04245
18	8.85238	0.04333
19	8.92119	0.04451
Fitting Results		
b = 0.015147	a=-0.09047	
R^2 = 0.99		

	LN Peff (psi)	ΔVp-actu (inch^3)	C$_{pc}$-30. S (1/psi)
1	6.37673	0.00612	2.0785E-05
2	6.65286	0.01030	1.5770E-05
3	6.91075	0.01421	1.2185E-05
4	7.30586	0.02019	8.2080E-06
5	7.52078	0.02345	6.6206E-06
6	7.64492	0.02533	5.8477E-06
7	7.82485	0.02805	4.8848E-06
8	7.96728	0.03021	4.2363E-06
9	8.07059	0.03177	3.8205E-06
10	8.18479	0.03350	3.4082E-06
11	8.26694	0.03475	3.1394E-06
12	8.40961	0.03691	2.7220E-06
13	8.51879	0.03856	2.4404E-06
14	8.61250	0.03998	2.2221E-06
15	8.66647	0.04080	2.1054E-06
16	8.70151	0.04133	2.0329E-06
17	8.77879	0.04250	1.8817E-06
18	8.85238	0.04361	1.7482E-06
19	8.92119	0.04466	1.6320E-06
Fitting Results			
b =0.0151465		a=-0.0905	
R^2 = 1			

$$C_{pc} - 30.S = \left(\frac{b}{V_p}\right)\left(\frac{1}{P_{eff}}\right) * 0.619$$

$$\Delta V_P - \text{actu}\,(30.S\text{-}Sample) = a + b*\ln(P_{eff})$$

43. S SAMPLE DATA SHEET

Sample name:- 43.S   Location:- Algyo field
Pore Volume (Vp):- 0.7544 in^3 Rod cross section (A):- 0.012272 in^2
Rubber sleeve:- Thick   System correction data:-
                                             Slope = n1* = 0.390642
                                             Constant = a1* = 4.616E-05

#	Pc-1 (psi)	Pi-1 (psi)	Rod position (L, inch)	Pc-2 (psi)	Pi-2 (psi)	Peff (psi)	ΔVp-meas (inch^3)	Correction	ΔVp-corrected (inch^3)
1	355	19	0						
2	651	129	0.5210	638	20	618	0.006394	0.00056830	0.005825
3	1272	302	1.2750	1241	19	1222	0.015647	0.00074172	0.014905
4	1614	70	1.5720	1605	20	1585	0.019291	0.00082104	0.018470
5	1920	49	1.8000	1916	19	1897	0.022089	0.00088074	0.021209
6	2525	80	2.1250	2517	19	2498	0.026078	0.00098071	0.025097
7	3008	44	2.3250	3002	19	2983	0.028532	0.00105110	0.027481
8	4003	90	2.6500	3997	19	3978	0.032520	0.00117619	0.031344
9	5486	231	3.0500	5485	18	5467	0.037429	0.00133174	0.036097
10	6556	135	3.3250	6555	18	6537	0.040804	0.00142806	0.039376
11	7500	46	3.4625	7489	19	7470	0.042491	0.00150446	0.040987
12	8054	38	3.5750	8057	19	8038	0.043872	0.00154815	0.042324
13	8526	31	3.6500	8521	20	8501	0.044792	0.00158239	0.0432098

#	LN Peff (psi)	(ΔVp-corrected) (inch^3)
1	6.42649	0.005825335
2	7.10824	0.014904888
3	7.36834	0.018470303
4	7.54803	0.021208581
5	7.82325	0.025096964
6	8.00068	0.027480944
7	8.28853	0.031344200
8	8.60649	0.036097389
9	8.78523	0.039375832
10	8.91865	0.040986810
11	8.99194	0.042323700
12	9.04794	0.043209846
Fitting Results		
b = 0.014338996	a= -.0869434	
R^2 = 0.99		

#	LN Peff (psi)	ΔVp-actu (inch^3)	Cpc-43. S (1/psi)
1	6.42649	0.00521	1.903897E-05
2	7.10824	0.01498	9.628546E-06
3	7.36834	0.01871	7.423396E-06
4	7.54803	0.02129	6.202469E-06
5	7.82325	0.02523	4.710201E-06
6	8.00068	0.02778	3.944379E-06
7	8.28853	0.03191	2.957789E-06
8	8.60649	0.03646	2.152201E-06
9	8.78523	0.03903	1.799921E-06
10	8.91865	0.04094	1.575112E-06
11	8.99194	0.04199	1.463807E-06
12	9.04794	0.04279	1.384082E-06
Fitting Results		
b = 0.014338996		a= -.0869434
R^2 = 1		

$$C_{pc} - 43.S = \left(\frac{b}{V_p}\right)\left(\frac{1}{P_{eff}}\right) * 0.619$$

$$\Delta V_P - actu\,(43.S\text{-}Sample) = a + b * \ln(P_{eff})$$

69. S – SAMPLE   DATA SHEET

Sample name:- 69.S   Location:- Algyo field
Pore Volume (Vp): 0.4058 in^3 Rod cross section (A):- 0.012272 in^2
Rubber sleeve:- Thick   System correction data:-

                                                         Slope = n1* = 0.390642
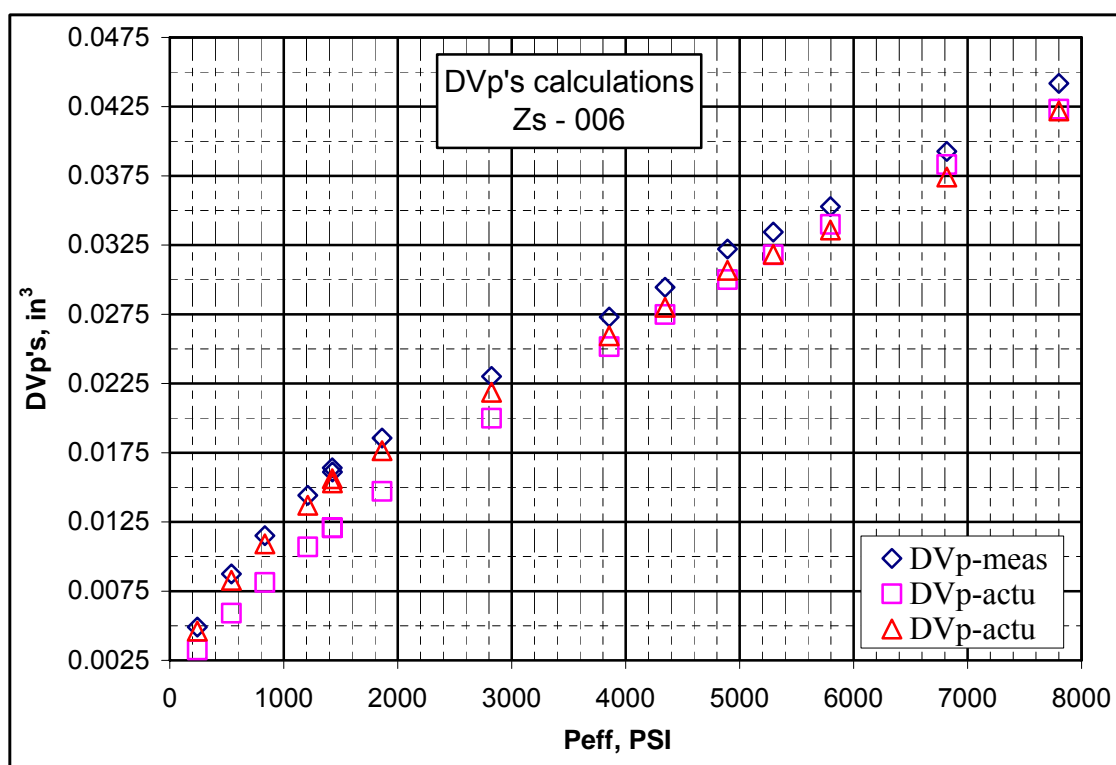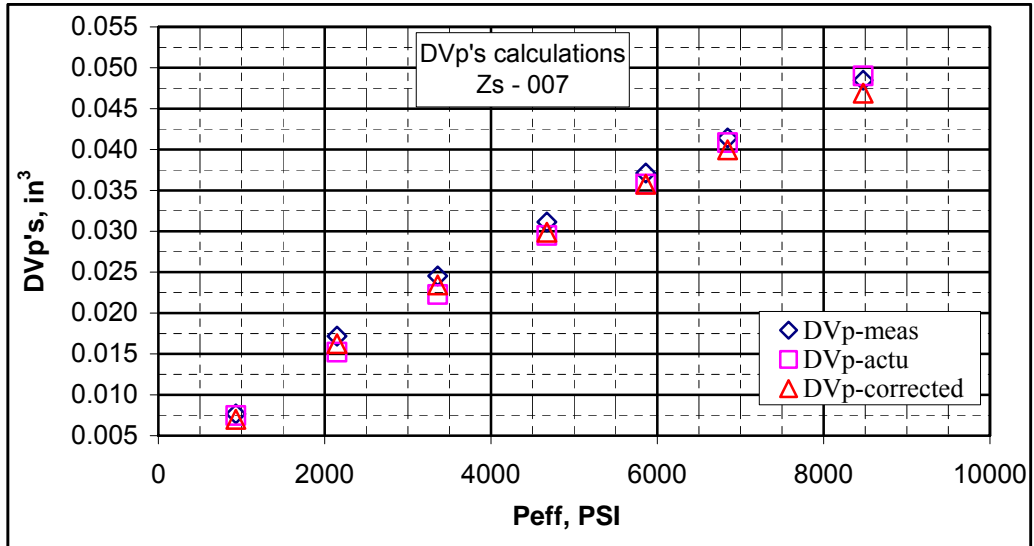   Constant = a1* = 4.616E-05

#	Pc-1 (psi	Pi-1 (psi)	Rod position (L, inch)	Pc-2 (psi)	Pi-2 (psi)	Peff (psi)	ΔVp-meas (inch3)	Correction	ΔVp-corrected (inch3)
1	370	32	0	670					
2	676	37	0.2750	1631	33	637	0.003375	0.000575	0.0027997
3	1635	40	0.6750	3049	33	1598	0.008283	0.000824	0.0074598
4	3054	38	1.0000	5501	32	3017	0.012272	0.001056	0.0112161
5	5510	38	1.2500	7016	33	5468	0.015340	0.001332	0.0140079
6	7016	37	1.5250	8479	32	6984	0.018715	0.001465	0.0172492
7	8484	35	1.6750	670	32	8447	0.020555	0.001578	0.0189768

#	LN Peff (psi)	(ΔVp-corrected) (inch³)
1	6.45677	0.00280
2	7.37651	0.00746
3	8.01202	0.01122
4	8.60667	0.01401
5	8.85138	0.01725
6	9.04157	0.01898
Fitting Results		
b = 0.006085236		a = - 0.0370801
$R^2 = 0.99$		

#	LN Peff (psi)	ΔVp-actu (inch³)	Cpc-69. S (1/psi)
1	6.45677	0.002210881	1.4573E-05
2	7.37651	0.0078077	5.8091E-06
3	8.01202	0.0116749	3.0769E-06
4	8.60667	0.0152935	1.6977E-06
5	8.85138	0.0167826	1.3292E-06
6	9.04157	0.0179399	1.0990E-06
Fitting Results			
b = 0.006085236		a = - 0.037080046	
$R^2 = 1$			
$C_{pc} - 69.S = \left(\dfrac{b}{V_p}\right)\left(\dfrac{1}{P_{eff}}\right) * 0.619$			

$$\Delta V_P - actu \ (69.S - Sample) = a + b * \ln(P_{eff})$$

74. S – SAMPLE   DATA SHEET

Sample name:- 74.S   Location:- Algyo field
Pore Volume (Vp): 2.80132 in^3 Rod cross section (A):- 0.012272 in^2
Rubber sleeve:- Thick   System correction data:-
                                              Slope = n1* = 0.390642
                                              Constant = a1* = 4.616E-05

#	Pc-1 (PSI)	Pi-1 (PSI)	Rod position (L, inch)	Pc-2 (PSI)	Pi-2 (PSI)	Peff (PSI)	ΔVp-meas (inch3)	Correction	ΔVp-corrected (inch3)
1	653	32	0						
2	1192	56	0.1500	1190	32	1158	0.001841	0.00072629	0.001114485
3	1774	167	0.4500	1773	32	1741	0.005522	0.00085171	0.004670624
4	2494	103	0.6875	2493	32	2461	0.008437	0.00097501	0.007461885
5	3518	122	0.9375	3518	32	3486	0.011505	0.00111707	0.010387787
6	4496	114	1.1875	4496	32	4464	0.014573	0.00123036	0.013342453
7	5613	120	1.4375	5612	32	5580	0.017641	0.00134243	0.016298351
8	6492	51	1.5375	6491	32	6459	0.018868	0.00142138	0.017446588
9	8227	65	1.7000	8226	32	8194	0.020862	0.00155982	0.019302319

#	LN(Peff) (psi)	(ΔVp-corrected) (inch3)
1	7.05445	0.001114485
2	7.46221	0.004670624
3	7.80832	0.007461885
4	8.15651	0.010387787
5	8.40380	0.013342453
6	8.62694	0.016298351
7	8.77323	0.017446588
8	9.01116	0.019302319

Fitting Results		
b = 0.00954674	a = -0.066668181	
R^2 = 0.98		

#	LN Peff (PSI)	ΔVp-actu (inch3)	C$_{pc}$-74. S (1/psi)
1	7.05445	0.001361676	2.98521E-05
2	7.46221	0.005427586	1.98557E-05
3	7.80832	0.008878700	1.40466E-05
4	8.15651	0.012350545	9.91645E-06
5	8.40380	0.014816327	7.74390E-06
6	8.62694	0.017041336	6.19512E-06
7	8.77323	0.018499981	5.35203E-06
8	9.01116	0.020872406	4.21879E-06

Fitting Result	
b = 0.00954674	a = -0.066668181
R^2 = 1	

$$C_{pc} - 74.S = \left(\frac{b}{V_p}\right)\left(\frac{1}{P_{eff}}\right) * 0.619$$

$$\Delta V_P - actu\ (74.S - Sample) = a + b * \ln(P_{eff})$$

76. S – SAMPLE DATA SHEET

Sample name:- 76.S   Location:- Algyo field
Pore Volume (Vp): 2.94089 in^3 Rod cross section (A):- 0.012272 in^2
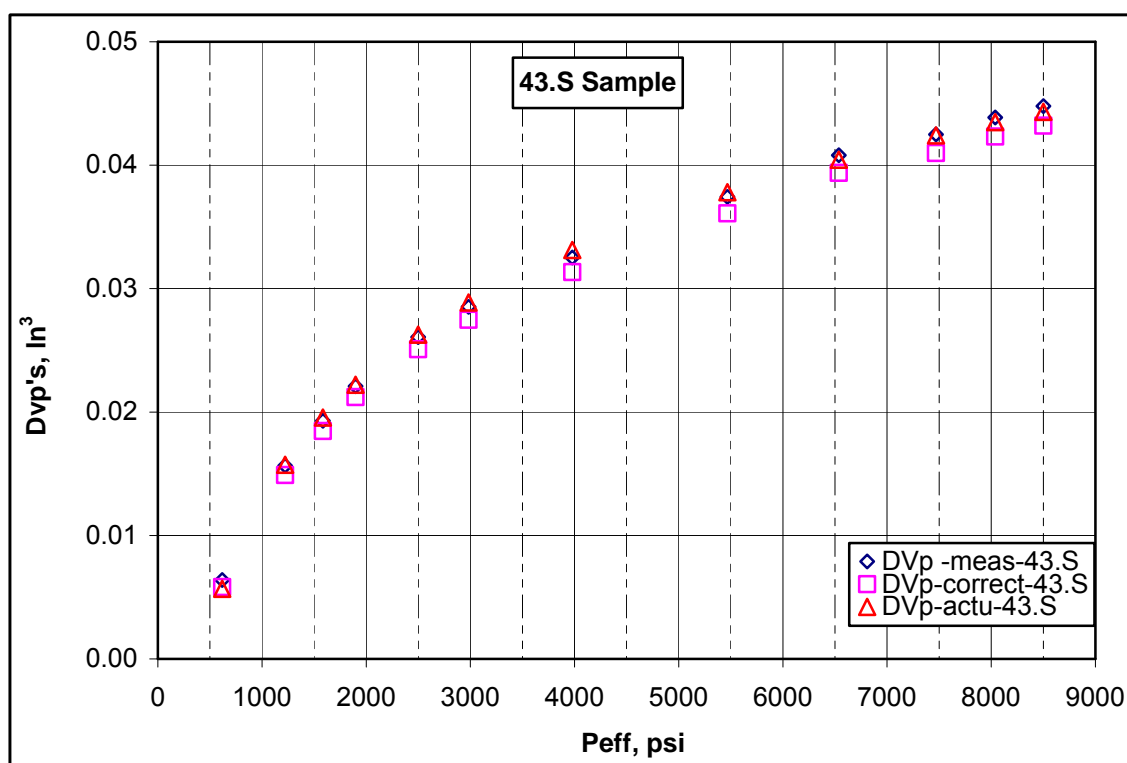Rubber sleeve:- Thick   System correction data:-
                                                        Slope = n1* = 0.390642
                                                        Constant = a1* = 4.616E-05

#	Pc-1 (PSI)	Pi-1 (PSI)	Rod position (L, inch)	Pc-2 (PSI)	Pi-2 (PSI)	Peff (PSI)	ΔVp-meas (inch3)	Correction	ΔVp-corrected (inch3)
1	663	68	0						
2	1198	226	0.0750	1195	60	1135	0.00092	0.00072062	0.000199766
3	2027	652	0.2500	2018	62	1956	0.003068	0.00089134	0.002176618
4	2742	1066	0.4750	2736	68	2668	0.005829	0.00100626	0.004822867
5	3508	1275	0.7000	3501	30	3471	0.00859	0.00111519	0.007475104
6	4465	1457	0.9750	4459	35	4424	0.011965	0.00122605	0.010739004
7	5172	1047	1.1500	5169	32	5137	0.014113	0.00129974	0.012812881
8	6165	1568	1.4250	6161	62	6099	0.017487	0.00138989	0.016097495

#	Peff (psi)	ΔVp-actu (inch3)	Cpc-76. S (1/psi)
1	7.03439	-0.00179154	2.8746E-05
2	7.57866	0.00335696	1.6681E-05
3	7.88908	0.00629345	1.2229E-05
4	8.15220	0.00878237	9.4000E-06
5	8.39480	0.01107725	7.3751E-06
6	8.54422	0.01249074	6.3514E-06
7	8.71588	0.01411451	5.3496E-06

$$C_{pc} - 76.S = \left(\frac{b}{V_p} \right) \left(\frac{1}{P_{eff}} \right) * 0.619$$

#	LN (Peff) (psi)	(ΔVp-corrected) (inch3)
1	7.03439	0.00020
2	7.57866	0.00218
3	7.88908	0.00482
4	8.15220	0.00748
5	8.39480	0.01074
6	8.54422	0.01281
7	8.71588	0.01610
Fitting Results		
b = 0.009459488		a = -0.0683
$R^2 = 0.93$		

$$\Delta V_P - actu\ (76.S\text{ - Sample}) = a + b * \ln(P_{eff})$$

77. S – SAMPLE   DATA SHEET

Sample name:- 77.S
Pore Volume (Vp): 2.80132 in^3
Rubber sleeve:- Thick

Location:- Algyo field
Rod cross section (A):- 0.012272 in^2
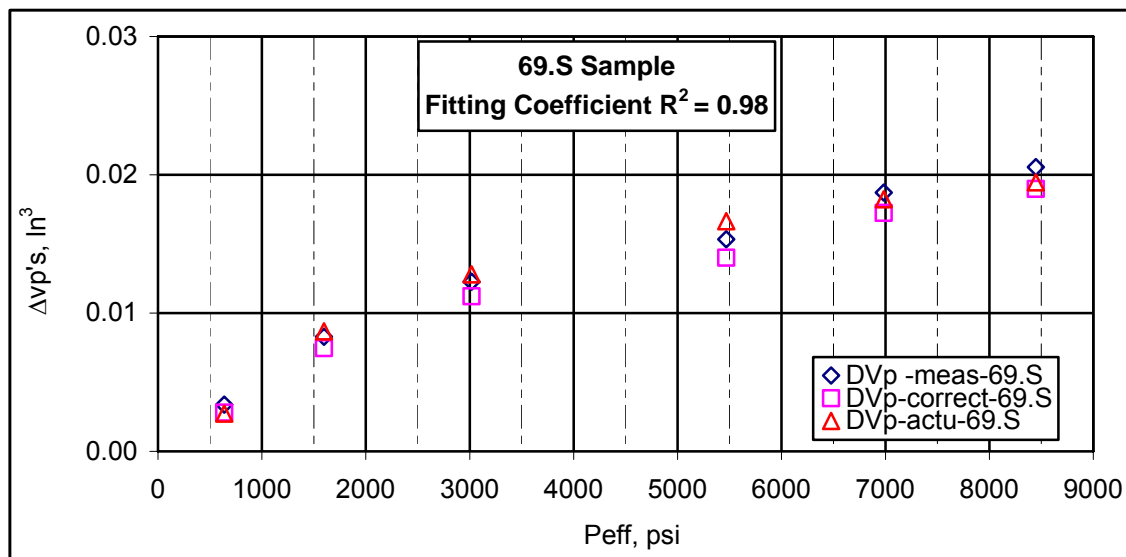System correction data:-
        Slope = n1* = 0.390642
        Constant = a1* = 4.616E-05

#	Pc	Pi-1	Rod L, inch	Pi-2	Pi2	Peff	ΔVp-meas	Correction	ΔVp-corrected
1	638	42	0						
2	1182	190	0.2250	1177	42	1135	0.002761	0.00072062	0.002040543
3	1864	438	0.5500	1853	42	1811	0.00675	0.00086492	0.005884592
4	2506	629	0.8875	2498	43	2455	0.010891	0.00097408	0.009917184
5	3326	832	1.2500	3315	42	3273	0.01534	0.00108989	0.014249915
6	4206	842	1.6000	4197	40	4157	0.019635	0.00119659	0.018438363
7	5034	825	1.8500	5027	43	4984	0.022703	0.00128448	0.021418435
8	6079	755	2.1375	6073	40	6033	0.026231	0.00138399	0.024847080
9	7124	685	2.4250	7119	42	7077	0.029759	0.00147303	0.028286199

#	Peff (PSI)	ΔVp-actu (inch3)	Cpc-77. S (1/PSI)
1	7.03439	-0.000021332	2.315836667E-05
2	7.50163	0.006834550	1.451394046E-05
3	7.80588	0.011298758	1.070661759E-05
4	8.09346	0.015518407	8.030780988E-06
5	8.51399	0.019026512	6.323008461E-06
6	8.70500	0.021688758	5.273825476E-06
7	8.86461	0.024491461	4.356828472E-06
8	7.03439	0.026833346	3.714108545E-06

$$C_{pc} - 77.S = \left(\frac{b}{V_p}\right)\left(\frac{1}{P_{eff}}\right) * 0.619$$

#	(Peff) (PSI)	(ΔVp-corrected) (inch3)
1	7.03439	0.00204
2	7.50163	0.00588
3	7.80588	0.00992
4	8.09346	0.01425
5	8.51399	0.02142
6	8.70500	0.02485
7	8.86461	0.02829
8	7.03439	0.00204
Fitting Results		
b = 0.014673		a = -0.103237
R^2 = 0.98		

$$\Delta V_P - actu\,(77.S\text{-}Sample) = a + b * \ln(P_{eff})$$
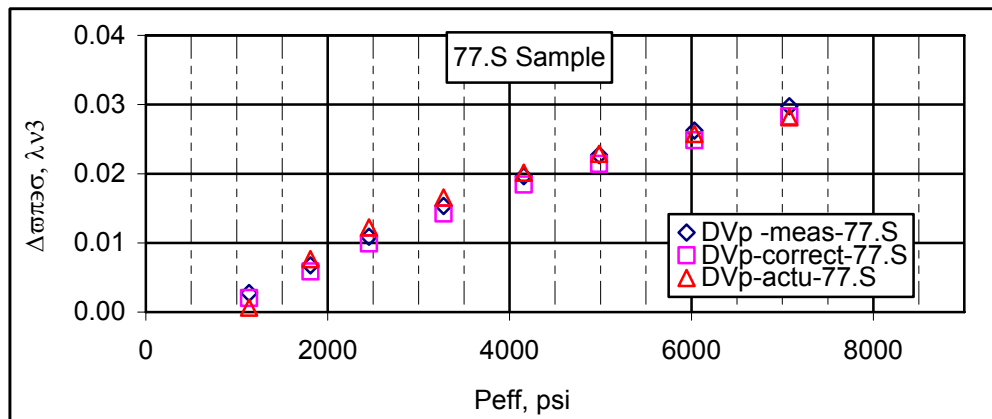
82. S – SAMPLE   DATA SHEET

Sample name:- 82.S
Pore Volume (Vp): 0.9241 in^3
Rubber sleeve:- Thick

Location:- Algyo field
Rod cross section (A):- 0.012272 in^2
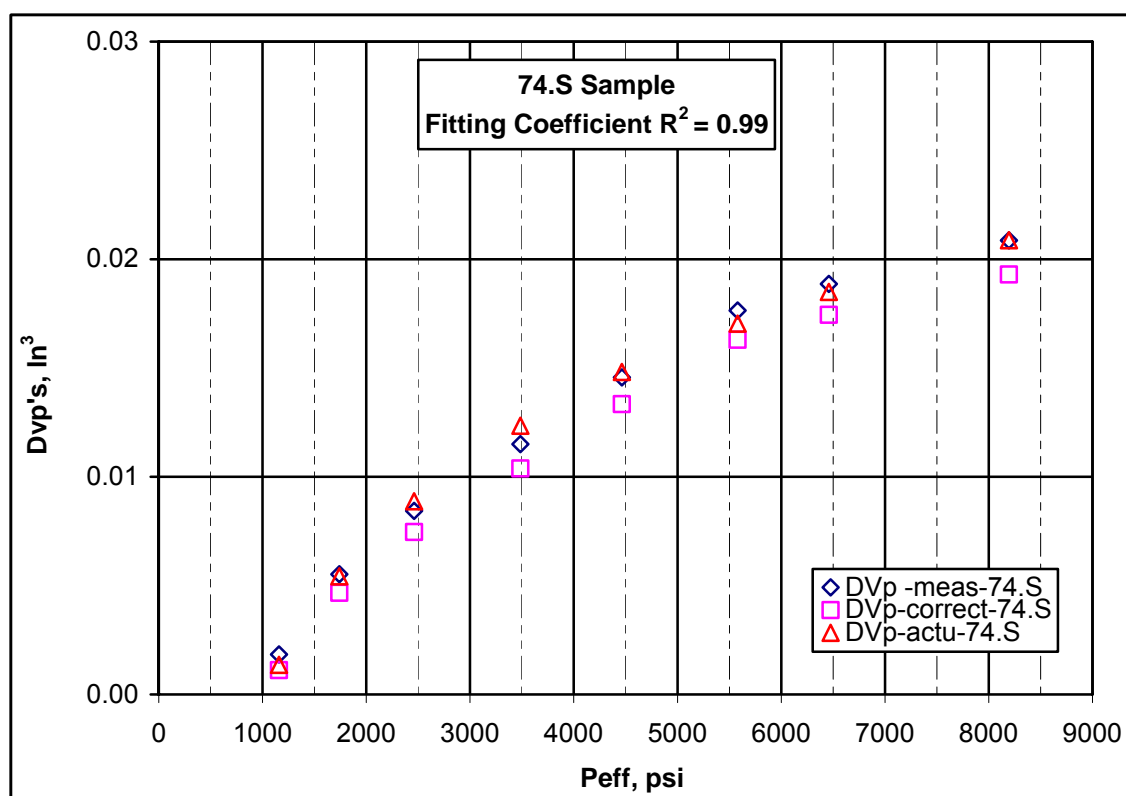System correction data:-
Slope = n1* = 0.390642
Constant = a1* = 4.616E-05

#	Pc-1 (PSI)	Pi-1 (PSI)	Rod position (L, inch)	Pc-2 (PSI)	Pi-2 (PSI)	Peff (PSI)	ΔVp-meas (inch3)	Correction	ΔVp-corrected (inch3)
1	393	51	0						
2	728	329	0.9000	676	62	614	0.011045	0.00056686	0.0104778
3	1527	820	2.2250	1424	67	1357	0.027305	0.00077271	0.0265322
4	2542	920	3.0750	2474	85	2389	0.037736	0.00096377	0.0367722
5	4037	1055	3.8000	3981	57	3924	0.046633	0.00116993	0.0454631
6	5530	786	4.2750	5491	45	5446	0.052462	0.00132974	0.0511324
7	7220	730	4.6750	7185	51	7134	0.057371	0.00147765	0.0558932
8	8230	400	4.8750	8204	60	8144	0.059825	0.00155609	0.0582692

#	LN Peff (psi)	ΔVp-actu (inch3)	Cpc-82.S (1/psi)
1	6.41999	0.011298	1.9965E-05
2	7.21303	0.025811	9.0334E-06
3	7.77863	0.036161	5.1311E-06
4	8.27487	0.045243	3.1239E-06
5	8.60264	0.051241	2.2509E-06
6	8.87263	0.056182	1.7183E-06
7	9.00504	0.058605	1.5052E-06

$$C_{pc} - 82.S = \left(\frac{b}{V_p}\right)\left(\frac{1}{P_{eff}}\right) * 0.619$$

#	LN (Peff) (psi)	(ΔVp-corrected) (inch3)
1	6.41999	0.01048
2	7.21303	0.02653
3	7.77863	0.03677
4	8.27487	0.04546
5	8.60264	0.05113
6	8.87263	0.05589
7	9.00504	0.05827
Fitting Results		
b = 0.01831	a = -.1061881	
R^2 = 0.99		

$$\Delta V_P - actu\,(82.S\text{-}Sample) = a + b * ln(P_{eff})$$

83. S – SAMPLE DATA SHEET

Sample name:- 83.S
Location:- Algyo field
Pore Volume (Vp):0.5992 in^3
Rod cross section (A):- 0.012272 in^2
Rubber sleeve:- Thick
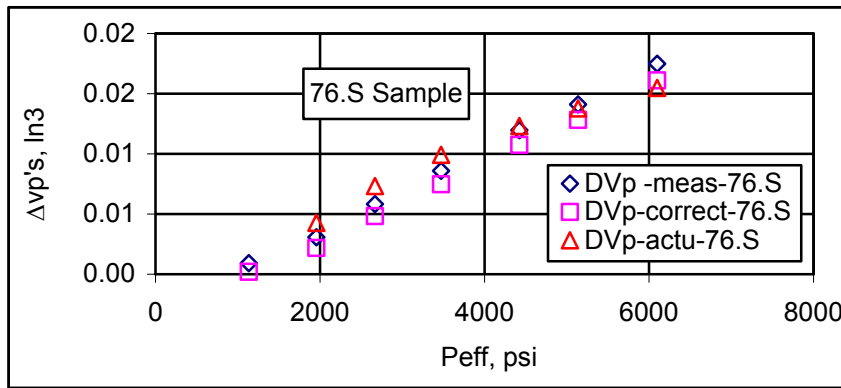System correction data:-

Slope = n1* = 0.390642
Constant = a1* = 4.616E-05

#	Pc-1 (psi)	Pi-1 (psi)	Rod position (L, inch)	Pc-2 (psi)	Pi-2 (psi)	Peff (psi)	ΔVp-meas (inch^3)	Correction	ΔVp-corrected (inch^3)
1	467	226	0						
2	695	440	0.8500	642	239	403	0.010431	0.000481	0.0099502
3	1018	597	1.8000	952	230	722	0.022089	0.000604	0.0214854
4	1572	780	2.6250	1507	240	1267	0.032214	0.000752	0.0314613
5	2510	1018	3.3750	2446	250	2196	0.041417	0.000933	0.0404849
6	3225	806	3.8000	3230	232	2998	0.046633	0.001053	0.0455799
7	4069	715	4.1000	4030	251	3779	0.050315	0.001153	0.0491617
8	5030	745	4.4000	5002	207	4795	0.053996	0.001265	0.0527309
9	5800	575	4.5750	5716	241	5475	0.056144	0.001333	0.0548112
10	6540	576	4.7250	6502	242	6260	0.057984	0.001404	0.0565804
11	7900	813	4.9750	7760	204	7556	0.061052	0.001511	0.0595412

#	LN Peff (psi)	ΔVp-actu (inch3)	Cpc-83.S (1/psi)
1	5.99894	0.011371	4.3753E-05
2	6.58203	0.021119	2.4422E-05
3	7.14441	0.030520	1.3917E-05
4	7.69439	0.039715	8.0294E-06
5	8.00570	0.044919	5.8814E-06
6	8.23721	0.048789	4.6659E-06
7	8.47533	0.052769	3.6773E-06
8	8.60795	0.054986	3.2206E-06
9	8.74194	0.057226	2.8167E-06
10	8.93010	0.060372	2.3336E-06

$$C_{pc} - 83.S = \left(\frac{b}{V_p}\right)\left(\frac{1}{P_{eff}}\right) * 0.619$$

#	LN (Peff) (psi)	(ΔVp-corrected) (inch3)
1	5.99894	0.00995
2	6.58203	0.02149
3	7.14441	0.03146
4	7.69439	0.04048
5	8.00570	0.04558
6	8.23721	0.04916
7	8.47533	0.05273
8	8.60795	0.05481
9	8.74194	0.05658
10	8.93010	0.05954
Fitting Results		
b = 0.01672	a =-0.088913	
R^2 = 0.99		

$$\Delta V_P - actu\,(83.S\text{-}Sample) = a + b * \ln(P_{eff})$$

A 985 / 1.2 – SAMPLE   DATA SHEET

Sample name:- A 985 / 1.2   Location:- Algyo field
Pore Volume (Vp):1.4722 in^3 Rod cross section (A):- 0.012272 in^2
Rubber sleeve:- Thick   System correction data:-
                Slope = n1* = 0.390642
                Constant = a1* = 4.616E-05

#	Pc-1 (psi)	Pi-1 (psi)	Rod position (L, inch)	Pc-2 (psi)	Pi-2 (psi)	Peff (psi)	ΔVp-meas (inch^3)	Correction	ΔVp-corrected (inch^3)
1	1423	617	0						
2	1920	985	0.6250	1870	626	1244	0.00767	0.00074690	0.006923000
3	2528	1102	1.3250	2470	613	1857	0.01626	0.00087344	0.015386756
4	3260	1144	1.9750	3208	622	2586	0.024237	0.00099406	0.023242833
5	4094	1176	2.6250	4042	606	3436	0.032214	0.00111078	0.031102814
6	5108	1244	3.3500	5047	610	4437	0.041111	0.00122745	0.039883233
7	6030	1246	3.8500	5958	626	5332	0.047247	0.00131880	0.045927811

#	LN Peff (psi)	ΔVp-actu (inch3)	Cpc-A 985 / 1.2 (1/ psi)
1	7.12609	0.0052639	9.0734127E-06
2	7.52672	0.0160190	6.0782581E-06
3	7.85787	0.0249089	4.3647817E-06
4	8.14206	0.0325382	3.2850190E-06
5	8.39773	0.0394018	2.5439093E-06
6	8.58148	0.0443347	2.1169027E-06

$$C_{pc} - A\ 985\ /\ 1.2 = \left(\frac{b}{V_p}\right)\left(\frac{1}{P_{eff}}\right) * 0.619$$

#	LN (Peff) (psi)	(ΔVp-corrected) (inch^3)
1	7.12609	0.00692
2	7.52672	0.01539
3	7.85787	0.02324
4	8.14206	0.03110
5	8.39773	0.03988
6	8.58148	0.04593
Fitting Results		
b = 0.0268456	a =-0.18603957	
R^2 = 0.99		

$$\Delta V_P - actu\ (A\ 985\ /\ 1.2\ \text{-}\ Sample) = a + b * ln(P_{eff})$$

A 985 / 5.2 – SAMPLE   DATA SHEET

Sample name:- A 985 / 5.2
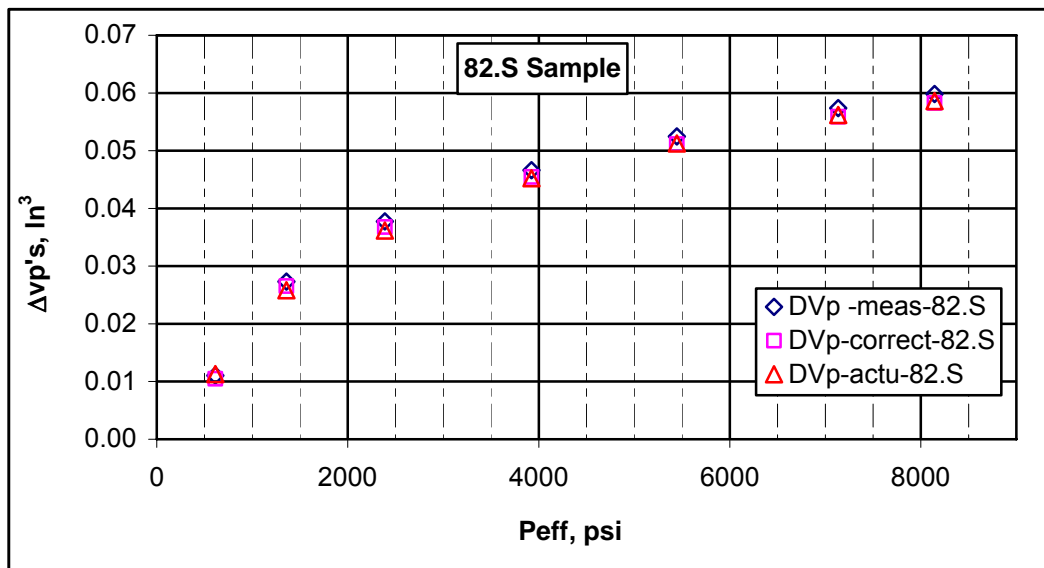Pore Volume (Vp):1.4467 in^3
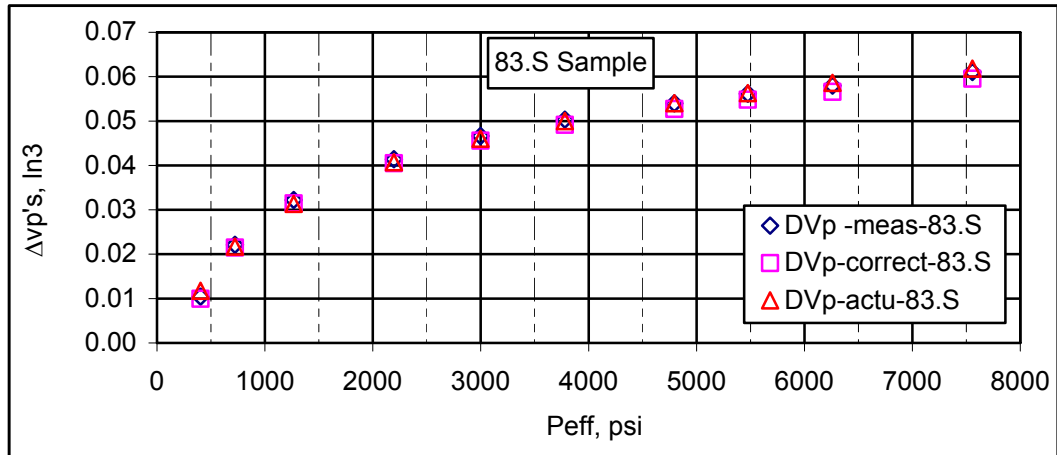Rubber sleeve:- Thick

Location:- Algyo field
Rod cross section (A):- 0.012272 in^2
System correction data:-
Slope = n1* = 0.390642
Constant = a1* = 4.616E-05

#	Pc-1 (psi)	Pi-1 (psi)	Rod position (L, inch)	Pc-2 (psi)	Pi-2 (psi)	Peff (psi)	ΔVp-meas (inch³)	Correction	ΔVp-corrected (inch³)
1	1246	633	0						
2	1768	1080	1.0000	1685	648	1037	0.012272	0.00069565	0.011576
3	2118	1001	1.6750	2064	642	1422	0.020555	0.00078696	0.019768
4	2977	1343	2.7500	2888	641	2247	0.033748	0.00094097	0.032807
5	3980	1421	3.8000	3895	640	3255	0.046633	0.00108755	0.045545
6	4528	1058	4.3250	4481	646	3835	0.053076	0.00115949	0.051916
7	5116	1056	4.8250	5071	641	4430	0.059212	0.00122670	0.057985
8	8100	1056	5.5500	6744	645	6099	0.068109	0.00138989	0.066718

#	LN Peff (psi)	ΔVp-actu (inch3)	Cpc- A 985 / 5.2 (1/psi)
1	6.877296	0.015683	1.25322E-05
2	7.276556	0.027226	8.40683E-06
3	7.711997	0.039816	5.43905E-06
4	8.093462	0.050845	3.71411E-06
5	8.318010	0.057337	2.96712E-06
6	8.561019	0.064363	2.32701E-06

$$C_{pc} - A\ 985\ /\ 5.2 = \left(\frac{b}{V_p}\right)\left(\frac{1}{P_{eff}}\right) * 0.619$$

#	LN (Peff) (psi)	(ΔVp-corrected) (inch³)
1	6.877296	0.016503
2	7.276556	0.027433
3	7.711997	0.038730
4	8.093462	0.049531
5	8.318010	0.056887
6	8.561019	0.066187
Fitting Results		
b = 0.026845507	a =-0.18603957	
R^2 = 0.99		

$$\Delta V_P - actu \ (A \ 985 \ / \ 5.2 \ - Sample) = a + b * \ln(P_{eff})$$

A 1.1 – SAMPLE DATA SHEET

Sample name:- A 1.1
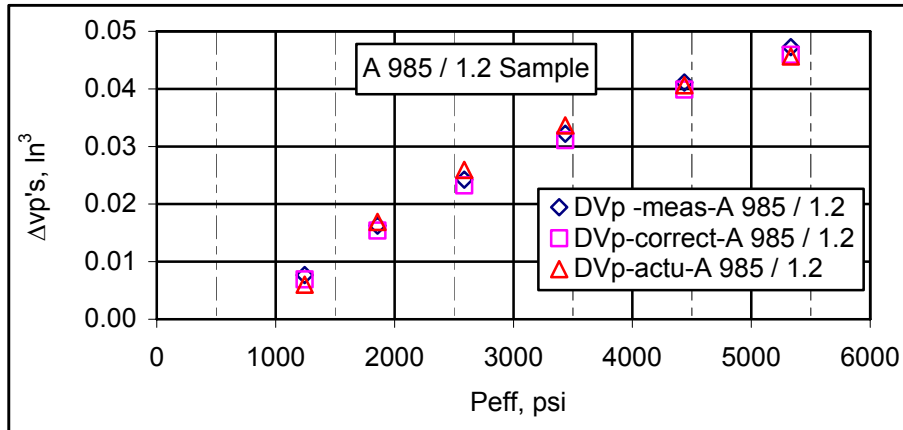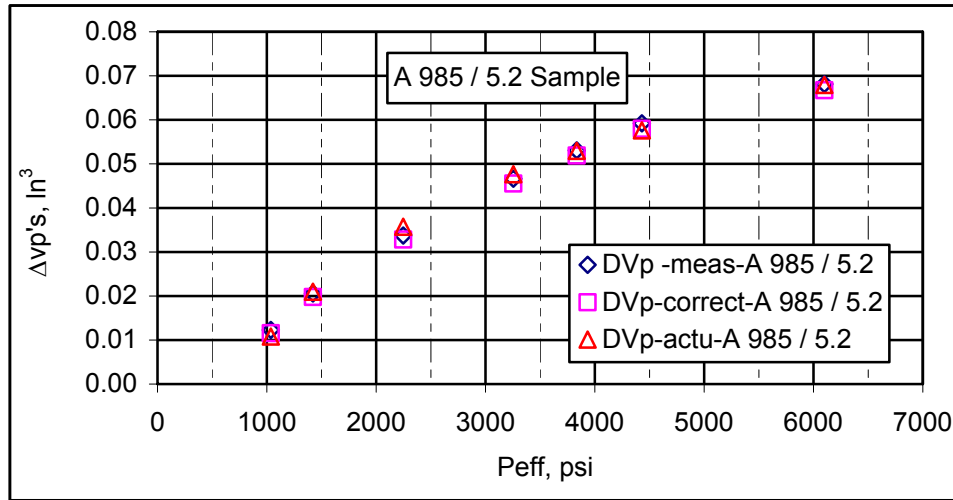Pore Volume (Vp): 1.4722 in^3
Rubber sleeve:- Thick

Location:- Algyo field
Rod cross section (A):- 0.012272 in^2
System correction data:-

Slope = $n1*$ = 0.390642
Constant = $a1*$ = 4.616E-05

#	Pc-1 (psi)	Pi-1 (psi)	Rod position (L, inch)	Pc-2 (psi)	Pi-2 (psi)	Peff (psi)	ΔVp-meas (inch^3)	Correction	ΔVp-corrected (inch^3)
1	1213	723	0						
2	1831	1288	1.4000	1693	723	970	0.017181	0.00067773	0.016763
3	2293	1255	2.3000	2170	724	1446	0.028225	0.00079212	0.026905
4	3035	1413	3.2325	2959	724	2235	0.039669	0.0009390	0.035221
5	4068	1508	4.1250	3997	724	3273	0.050621	0.00108989	0.042779
6	4871	1318	4.7325	4821	724	4097	0.058077	0.00118981	0.050489
7	6030	1478	5.5000	5948	724	5224	0.067495	0.00130830	0.058815

#	LN Peff (psi)	ΔVp-actu (inch3)	Cpc- A 1.1 (1/psi)
1	7.0466	0.01540	1.175E-05
2	7.4877	0.02736	7.558E-06
3	7.8244	0.03649	5.397E-06
4	8.1008	0.04398	4.094E-06
5	8.3540	0.05084	3.178E-06
6	8.5779	0.05692	2.541E-06

$$C_{pc} - A \ 1.1 = \left(\frac{b}{V_p}\right)\left(\frac{1}{P_{eff}}\right) * 0.619$$

#	LN (Peff) (psi)	(ΔVp-corrected) (inch3)
1	7.0466	0.016763
2	7.4877	0.026905
3	7.8244	0.035221
4	8.1008	0.042779
5	8.3540	0.050489
6	8.5779	0.058815
Fitting Results		
b =0.0289122	a =-0.183155	
R^2 = 0.99		

$$\Delta V_P - \text{actu (A 1.1 - Sample)} = a + b * \ln(P_{eff})$$

A 1.2 – SAMPLE   DATA SHEET

Sample name:- A 1.2   Location:- Algyo field
Pore Volume (Vp): 1.2435 in^3 Rod cross section (A):- 0.012272 in^2
Rubber sleeve:- Thick   System correction data:-
$\qquad\qquad\qquad\qquad\qquad\qquad\qquad\qquad$ Slope = n1* = 0.390642
$\qquad\qquad\qquad\qquad\qquad\qquad\qquad\qquad$ Constant = a1* = 4.616E-05

#	Pc-1 (psi)	Pi-1 (psi)	Rod position (L, inch)	Pc-2 (psi)	Pi-2 (psi)	Peff (psi)	ΔVp-meas ($inch^3$)	Correction	ΔVp-corrected ($inch^3$)
1	1225	733	0						
2	2047	1442	1.4250	1883	734	1149	0.017487	0.000724	0.016763
3	2605	1324	2.2625	2515	729	1786	0.027765	0.000860	0.026905
4	3300	1318	2.9500	3228	727	2501	0.036202	0.000981	0.035221
5	4094	1327	3.5750	4027	730	3297	0.043872	0.001093	0.042779
6	5053	1400	4.2125	4980	733	4247	0.051695	0.001207	0.050489
7	6112	1467	4.9000	6041	728	5313	0.060132	0.001317	0.058815

#	Peff (PSI)	ΔVp-actu ($inch3$)	Cpc- A 1.2 (1/ psi)
1	7.0466	0.01540	1.175E-05
2	7.4877	0.02736	7.558E-06
3	7.8244	0.03649	5.397E-06
4	8.1008	0.04398	4.094E-06
5	8.3540	0.05084	3.178E-06
6	8.5779	0.05692	2.541E-06

$$C_{pc} - A\ 1.2 = \left(\frac{b}{V_p}\right)\left(\frac{1}{P_{eff}}\right) * 0.619$$

#	(Peff) (psi)	(ΔVp-corrected) ($inch3$)
1	7.0466	0.01676
2	7.4877	0.02690
3	7.8244	0.03522
4	8.1008	0.04278
5	8.3540	0.05049
6	8.5779	0.05882
Fitting Results		
b =0.027114904	a =-0.175673999	
R^2 = 0.99		

$$\Delta V_P - actu\ (A\ 1.2 - Sample) = a + b * \ln(P_{eff})$$

SA-5 – SAMPLE DATA SHEET

Sample name:- SA-5
Pore Volume (Vp): 1.2435 in^3
Rubber sleeve:- Thick

Location: Algyo field
Rod cross section (A):- 0.012272 in^2
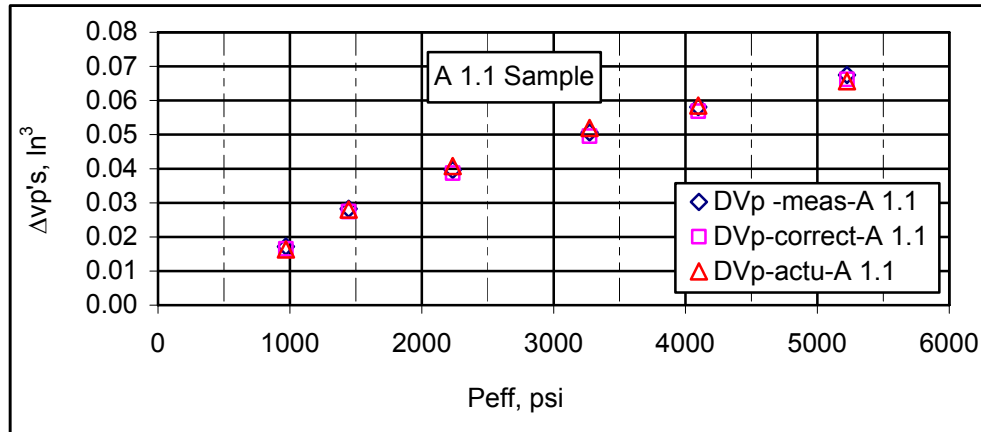System correction data:-
Slope = $n1^* = 0.390642$
Constant = $a1^* = 4.616E-05$

#	Pc-1 (psi)	Pi-1 (psi)	Rod position (L, inch)	Pc-2 (psi)	Pi-2 (psi)	Peff (psi)	ΔVp-meas (inch3)	Correction	ΔVp-corrected (inch3)
1	652	359	0						
2	1256	888	0.8500	1159	356	803	0.010431	0.00062951	0.0098012
3	2070	1096	1.7000	1982	360	1622	0.020862	0.00082847	0.0200337
4	2809	960	2.1500	2730	359	2371	0.026384	0.00096092	0.0254236
5	3633	960	2.5625	3590	359	3231	0.031447	0.00108441	0.0303622
6	4135	742	2.8000	4110	358	3752	0.034361	0.00114962	0.0332115
7	5026	888	3.1125	4930	350	4580	0.038196	0.00124276	0.0369534

#	Peff (psi)	ΔVp-actu (inch3)	Cpc SA-5 (1/psi)
1	6.68835	0.00938	2.845431E-05
2	7.39142	0.02021	1.408681E-05
3	7.77107	0.02606	9.636781E-06
4	8.08055	0.03082	7.071745E-06
5	8.23004	0.03313	6.089768E-06
6	8.42945	0.03620	4.988823E-06

$$C_{pc} - SA - 5 = \left(\frac{b}{V_p}\right)\left(\frac{1}{P_{eff}}\right) * 0.619$$

#	(Peff) (psi)	(ΔVp-corrected) (inch3)
1	6.68835	0.00980
2	7.39142	0.02003
3	7.77107	0.02542
4	8.08055	0.03036
5	8.23004	0.03321
6	8.42945	0.03695
Fitting Results		
b =0.0154	a =-0.093656	
R^2 = 0.99		

$$\Delta V_P - actu\ (SA\ \text{-}\ 5\ \text{-}\ Sample) = a + b*\ln(P_{eff})$$

SA-7 – SAMPLE   DATA SHEET

Sample name:- SA-7

Pore Volume (Vp): 0.4173 in^3

Rubber sleeve:- Thick

Location:- Algyo field

Rod cross section (A):- 0.012272 in^2

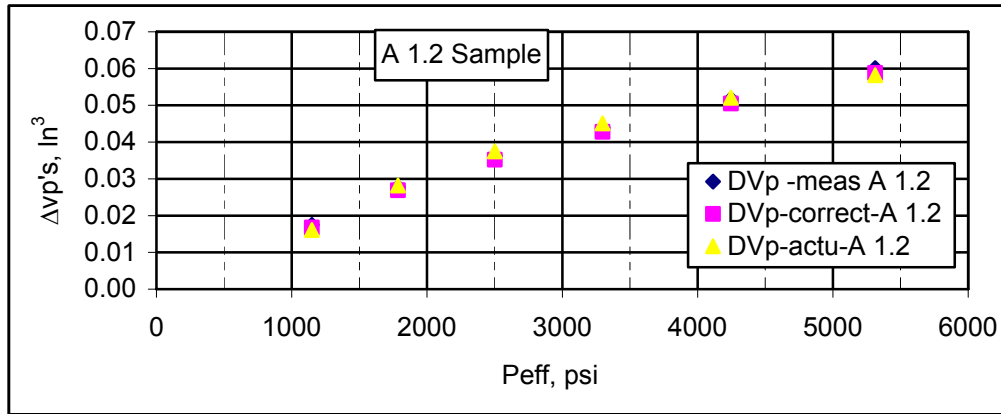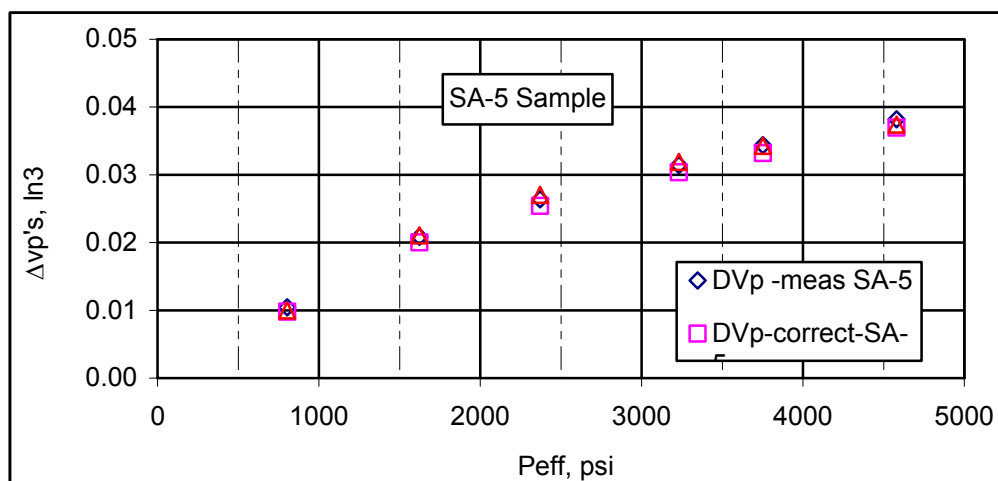System correction data:-

Slope = n1* = 0.390642

Constant = a1* = 4.616E-05

#	Pc-1 (psi)	Pi-1 (psi)	Rod position (L, inch)	Pc-2 (psi)	Pi-2 (psi)	Peff (psi)	ΔVp-meas (inch3)	Correction	ΔVp-corrected (inch3)
1	680	327	0						
2	1116	695	0.8600	1084	327	757	0.010554	0.00061517	0.009938
3	1870	1215	1.7500	1801	327	1474	0.021476	0.00079808	0.020678
4	2580	1376	2.2500	2512	327	2185	0.027612	0.00093074	0.026681
5	3127	1191	2.6500	3092	324	2768	0.03252	0.00102083	0.031499
6	4112	1328	3.0000	4063	327	3736	0.036816	0.00114771	0.035668

#	LN (Peff) (psi)	(ΔVp-corrected) ($inch^3$)
1	6.62936	0.00994
2	7.29574	0.02068
3	7.68937	0.02668
4	7.92588	0.03150
5	8.22577	0.03567
Fitting Results		
b =0.016249	a =-0.097837	
R^2 = 0.99		

#	LN Peff (psi)	ΔVp-actu (inch^3)	Cpc- SA-7 (1/ psi)
1	6.62936	0.00988	3.18371E-05
2	7.29574	0.02071	1.63505E-05
3	7.68937	0.02711	1.10301E-05
4	7.92588	0.03095	8.70689E-06
5	8.22577	0.03582	6.45093E-06
$C_{pc} - SA - 7 = \left(\dfrac{b}{V_p} \right)\left(\dfrac{1}{P_{eff}} \right) * 0.619$			

$$\Delta V_P - actu \ (SA - 7 \ - Sample) = a + b * \ln(P_{eff})$$
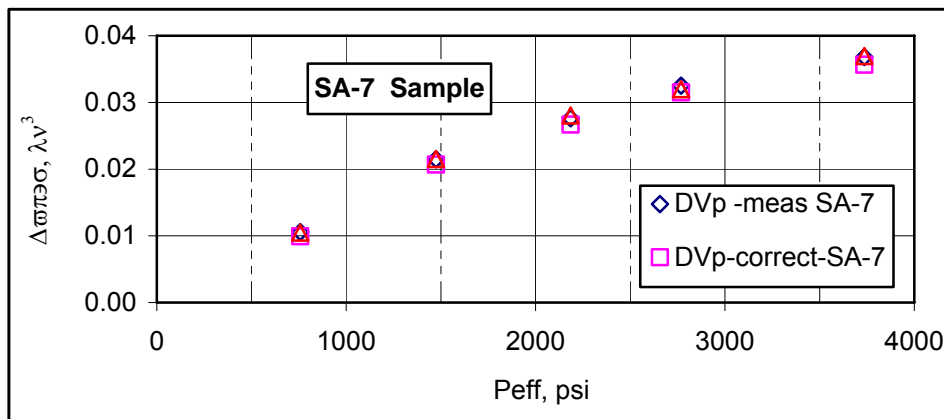
TWELVE FITTING FORMULAS WITH TWO PARAMETERS USED IN THE RESEARCH

λ = Pore volume compressibility, 1/psi

T = Porosity, %

A and B = fitting parameters

$$\lambda = AT + B \tag{B.1}$$

$$\lambda = \frac{A + T}{B + T} \tag{B.2}$$

$$\lambda = AT^2 + B \tag{B.3}$$

$$\lambda^2 = AT + B \tag{B.4}$$

$$\lambda = \frac{A}{T} + B \tag{B.5}$$

$$\lambda = \frac{1}{AT + B} \tag{B.6}$$

$$\lambda = BT^A \tag{B.7}$$

$$\lambda = A\ln T + B \tag{B.8}$$

$$\lambda = B\exp(AT) \tag{B.9}$$

$$\lambda = \frac{T^2}{AT + B} \tag{B.10}$$

$$\lambda = \frac{T}{AT + B} \tag{B.11}$$

$$\lambda = \frac{T + A}{T + B} \tag{B.12}$$

DATA MODELING EQUATIONS USED BY CurveExpert 1.38 PROGRAM

There are two types of curve fitting used by CurveExpert 1.3. The first group falls under the category of regression curves (which can be further subdivided into linear and nonlinear), which attempt to minimize the difference between themselves and the data

points. The second group, interpolations, ensure that the curve fit passes exactly through each data point.

In CurveExpert, the regression models are divided into families according to their typical behavior. Of course, you are not limited to only these models in CurveExpert! If the model that you would like to use does not appear below, simply define a custom model and let CurveExpert apply that model to your data set.

1. Regressions

Linear Family	(B.13)
Linear Fit, y=a+bx	(B.14)
Quadratic Fit, y=a+bx+cx^2	(B.15)
nth order Polynomial Fit, y=a+bx+cx^2	(B.16)

2. Exponential Family

Exponential Fit, y=a*exp(bx)	(B.17)
Modified Exponential Fit, y=a*exp(b/x)	(B.18)
Logarithm Fit, y=a+b*ln(x)	(B.19)
Reciprocal Logarithm Fit, y=1/(a+b*ln(x))	(B.20)
Vapor Pressure Model, y=exp(a+b/x+c*ln(x))	(B.21)

3. Power Law Family

Power Fit, y=a*x^b	(B.22)
Modified Power Fit, y=ab^x	(B.23)
Shifted Power Fit, y=a*(x-b)^c	(B.24)
Geometric Fit, y=ax^(bx)	(B.25)
Modified Geometric Fit, y=ax^(b/x)	(B.26)
Root Fit, y=a^(1/x)	(B.27)
Hoerl Model, y=a*(b^x)*(x^c)	(B.28)
Modified Hoerl Model, y=a*b^(1/x)*(x^c)	(B.29)

4. Yield-Density Models

Reciprocal Model, y=1/(a+bx)   (B.30)

Reciprocal Quadratic, y=1/(a+bx+cx^2)   (B.31)

Bleasdale Model, y=(a+bx)^(-1/c)   (B.32)

Harris Model, y=1/(a+bx^c)   (B.33)

5. Growth Models

Exponential Association Fit, y=a*(1-exp(-bx))   (B.34)

Three-Parameter Exponential Association Fit, y=a*(b-exp(-cx))   (B.35)

Saturation-Growth Rate Model, y=a*x/(b+x)   (B.36)

6. Sigmoidal Models

Gompertz Relation, y=a*exp(-exp(b-cx))   (B.37)

Logisitic Model, y=a/(1+exp(b-cx))   (B.38)

Richards Model, y=a/(1+exp(b-cx))^(1/d)   (B.39)

MMF Model, y=(ab+cx^d)/(b+x^d)   (B.40)

Weibull Model, y=a-b*exp(-cx^d)   (B.41)

7. Miscellaneous Models

Sinusoidal Function, y=a+b*cos(cx+d)   (B.42)

Gaussian Model, y=a*exp((-(b-x)^2)(2*c^2))   (B.43)

Hyperbolic Fit, y=a+b/x   (B.44)

Heat Capacity Model, y=a+bx+c/x^2   (B.45)

Rational Function, y= (a+bx)/(1+cx+dx^2)   (B.46)

8. Interpolations

Lagrangian Interpolation, y=a+bx+cx^2+.   (B.47)

Linear Spline, y=a+bx, piecewise   (B.48)

Quadratic Spline, y=a+bx+cx^2, piecewise   (B.49)

Cubic Spline, y=a+bx+cx^2+dx^3, piecewise   (B.50)

Tension Spline   (B.51)

APPENDIX C

DERIVATION OF GENERAL GAS MATERIAL BALANCE

The derivation that follows is based on the following assumptions:

1. Any pressure change caused by production or injection into the reservoir will be felt immediately throughout the total system including (a) *net pay reservoir* (R); (b) *nonnet pay* (NNP), including interbedded shales and poor quality rock assumed to be 100% water-saturated; and (c) *limited aquifer* (AQ), when present, also assumed to be water-saturated. The canonnet pay and aquifer volumes are referred to as "associated" water volumes and both contribute to water influx during depletion.

2. Simple modifications to the material balance equations can be made to generalize for nonnet pay that has initial free gas saturation.

3. All water in the system is initially saturated with solution gas. Practically, the assumption of equal pressure throughout the system is reasonable and any transient effects caused by a large aquifer may be treated by a conventional water influx term (We) as shown below.

For the sake of brevity we have chosen to omit explicit reference to pressure dependence—i.e., $\overline{C}_e$ $\overline{C}_f$, and $\overline{C}_{tw}$, should actually read $\overline{C}_e$(p), $\overline{C}_f$(p), and $\overline{C}_{tw}$(p).

Derivation. The volumetric balance at any pressure states that the total PV (VpR + VpA) equals the net reservoir PV occupied by gas and water ($V_{gR} + V_{wR}$) plus the associated (nonnet pay and aquifer) PV, which also is occupied by gas and water ($V_{gA} + V_{wA}$):

$$(V_{pR} + V_{pA}) = (V_{gR} + V_{wR}) + (V_{gA} + V_{wA}) \qquad (C.1)$$

The initial volume V_{pRi} less the change in PV ΔV_{pR} gives the net-pay reservoir PV V_{pR}

$$VpR = VpRi - \Delta V_{pR} \qquad (C.2)$$

$$V_{pRi} = V_{pRi} + V_{wRi} \qquad (C.3)$$

$$V_{pRi} = GB_{gi} + \frac{Gb_{gi}}{1 - S_{wi}} S_{wi}$$

and

$$\Delta V_{pR} = \frac{GB_{gi}}{1-S_{wi}}\overline{C}_f(p_i-P) \quad ; \; \overline{C}_f = \overline{C}_f ,$$ (C.4)

yielding

$$V_{pRi} = GB_{gi} + \frac{Gb_{gi}}{1-S_{wi}}S_{wi} - \frac{Gb_{gi}}{1-S_{wi}}\overline{C}_f(p_i-p)$$ (C.5)

PV of the associated rock is given by the initial PV less the change in PV, i.e.,

$$V_{pR} = \frac{GB_{gi}}{1-S_{wi}}M - \frac{GB_{gi}}{1-S_{wi}}M\overline{C}_f(p_i-p)$$ (C.6)

The net reservoir gas volume is given by the sum of unproduced free gas, gas released from solution, and any injected gas,

$$V_{pA} = \left(V_{gR}\right)_{FreeGas}^{Unproduced} + \left(V_{gR}\right)_{FromSolution}^{Released} + \left(V_{gR}\right)_{Injected},$$ (C.7)

resulting in

$$V_{gR} = \lfloor G - (G_p - W_p R_{sw})\rfloor B_g$$

$$+ \frac{GB_{gi}}{1-S_{wi}}\frac{S_{wi}}{B_{wi}}(R_{swi}-R_{sw})\frac{B_g}{5.615} + G_{inj}B_g$$ (C.8)

Pressure/volume/temperature properties B_g and R_{sw}, are evaluated at current reservoir pressure. Value G_p for a gas condensate is the wet gas volume calculated by adding separator gas to liquid condensate convened to an equivalent surface gas volume. Also, the two-phase Z-factor must be used to calculated B_g for gas condensate reservoirs. Strictly speaking the cumulative water production term W_P represents "free" water production and not the water condensed out of solution from the produced gas wellstream.

The gas volume in the associated PV is a function of the amount of gas that has come out of solution,

$$V_{gA} = \frac{GB_{gi}}{1-S_{wi}}M\frac{1}{B_{wi}}(R_{swi}-R_{sw})B_g\frac{1}{5.615}$$ (C.9)

The water volume in the net-pay reservoir equals the unproduced initial water plus injected water plus water encroachment from an external aquifer,

$$V_{wR} = \left(V_{wR}\right)_{Unproduced} + \left(V_{wR}\right)_{Injected} + \left(V_{wR}\right)_{Encroachment}$$ (C.10)

yielding

$$V_{wR} = \left(\frac{GB_{gi}}{1-S_{wi}}\frac{S_{wi}}{B_{wi}}B_w - \frac{W_p B_w}{5.615}\right) + 5.615W_{inj}B_w + 5.615W_e$$ (C.11)

The aquifer encroachment term W_e represents any external water volume that is not already included in the M term. Later in the derivation, we show the conditions required so that water encroachment (treated rigorously by the method of superposition) can be included as part of the M term used in the cumulative effective compressibility $\overline{C}_e$

The water volume in the associated PV is given by simple expansion.

$$V_{wA} = \left(\frac{GB_{gi}}{1 - S_{wi}} M \frac{1}{B_{wi}} B_w \right) \tag{C.12}$$

Inserting the appropriate equations above in Eq. 1., rearranging, and grouping terms yields.

$$G(B_g - B_{gi}) + \frac{GB_{gi}}{1 - S_{wi}} \left\{ \begin{array}{l} S_{wi} \left[\dfrac{\left(B_w + \left((R_{swi} - R_{sw})B_g\right)/5.615\right)}{B_{wi}} - \dfrac{B_{wi}}{B_i} \right] \\[4ex] + \overline{C}_f (p_i - p) + M \left[\dfrac{\left(B_w + \left((R_{swi} - R_{sw})B_g\right)/5.615\right)}{B_{wi}} - \dfrac{B_{wi}}{B_i} \right] \\[4ex] + M\overline{C}_f (p_i - p) \end{array} \right\}$$

$$\equiv (G_p - W_p R_{sw} - G_{inj})B_g + 5.615 \left(W_p - W_{inj} - \frac{W_e}{B_w} \right) B_w \tag{C.13}$$

Defining the total water/gas formation volume factor B_{tw},

$$B_{tw} \equiv B_w + \frac{(R_{swi} - R_{sw})B_g}{5.615} \tag{C.14}$$

Nothing that $B_{twi} = B_{wi}$ and defining the cumulative total water/gas compressibility $\overline{C}_{tw}$,

$$\overline{C}_{tw} \equiv \frac{(B_{tw} - B_{twi})}{B_{twi}} \frac{1}{(p_i - p)} \tag{C.15}$$

Now, defining a cumulative effective compressibility $\overline{C}_e$

$$\overline{C}_e \equiv \frac{S_{wi} \overline{C}_{tw} + \overline{C}_f + M(\overline{C}_{tw} + \overline{C}_f)}{1 - S_{wi}} \tag{C.16}$$

$$G(B_g - B_{gi}) + GB_{gi} \left[\overline{C}_e (p_i - p) \right]$$

$$= B_g \left[G_p - G_{inj} + W_p R_{sw} + \frac{5.615}{B_g} \left(W_p B_w - W_{inj} B_w - W_e \right) \right] \tag{C.17}$$

Deriving through by GB_{gi} and expressing $B_g \equiv \left(P_{sc} / T_{sc} \right) \left(zT / P \right)$ gives the final form of the material balance

$$\frac{P}{Z} \left[1 - \overline{C}_e (p_i - p) \right] = \left(\frac{P}{Z} \right) \left\{ 1 - \frac{1}{G} \left[G_p - G_{inj} + W_p R_{sw} + \frac{5.615}{B_g} \left(W_p B_w - W_{inj} B_w - W_e \right) \right] \right\} \tag{C.18}$$

The p/z vs. cumulative plot, including all terms, would consider

$$(p/z) \left[1 - \overline{C}_e (p_i - p) \right] = \left(\frac{p}{z} \right)_i - \frac{(p/z)}{G} Q \tag{C.19}$$

with

$$Q = G_p - G_{inj} + W_p R_{sw} + \frac{5.615}{B_g} \left(W_p B_w - W_{inj} B_w - W_e \right) \tag{C.20}$$

where the intercept is given by p/z, and the slope equals (p/z)i/G. Setting $G_{inj} = W_{inj} = W_p = W_e = 0$ gives the common form of the gas material balance,

$$\frac{P}{Z} \left[1 - \overline{C}_e (p_i - p) \right] = \left(\frac{P}{Z} \right)_i \left(1 - \frac{G_p}{G} \right) \tag{C.21}$$

Treating Limited Aquifers in $\overline{C}_e$ Terms. The material balance thus far has considered any associated water volume expressed in terms of M parameter. In fact M may include a limited aquifer with up to 2.5 times the reservoir PV for system permeability greater than about 100 md, and even larger aquifer volumes for higher permeabilities. The condition that determines when a limited aquifer can be treated as art of the $\overline{C}_e$ term is outlined below. We start with the general material balance equation including a water encroachment term W_e and a $\overline{C}_e$ term that considers only nonnet pay.

$$\frac{P}{Z} \left[1 - \overline{C}_e (p_i - p) \right] = \left(\frac{P}{Z} \right)_i \left(1 - \frac{G_p}{G} + 5.615 \frac{W_e}{GB_g} \right) \tag{C.22}$$

and

$$\overline{C}_e \equiv \frac{S_{wi} \overline{C}_{tw} + \overline{C}_f \left(V_{pNNP} / V_{pR} \right) \left(\overline{C}_{tw} + \overline{C}_f \right)}{1 - S_{wi}} \tag{C.23}$$

The water encroachment term calculated by superposition is expressed,

$$W_p = B \sum_j Q_D \left(\Delta t_j \right)_D \Delta p_j \tag{C.24}$$

where $Q_D(t_D)$ is the dimensionless cumulative influx given as a function of dimensionless time tD and water aquifer to reservoir radius $r_D = r_{AQ}/r_R$. Value Δp_j is given by $p_j - p_{j-1}$ (in the limit for small time steps), and $\Delta t_j = t - t_{j-1}$. Assuming that permeability is reasonably high and the ratio r_{AQ}/r_R is not too large, Q_D for the smallest time step will approach the limiting value Q_D, and the summation can be closely approximated by

$$\sum_j Q_D(\Delta t_j)_D \Delta p_j \equiv Q_D^\infty (p_i - p) \tag{C.25}$$

giving a simple expression for W_p that is independent of time and only dependent on reservoir pressure.

$$W_e = BQ_D^\infty (p_i - p); \quad W_e \text{ (bbl)} \tag{C.26}$$

$$B = \frac{2\pi}{5.615} \Phi r_R^2 h(\overline{C}_{tw} + \overline{C}_f)$$

$$Q_D^\infty = \frac{1}{2}\left[\left(\frac{r_{AQ}}{r_R}\right)^2 - 1\right] \tag{C.27}$$

Expressing We in terms of aquifer PV V_{pAQ},

$$W_e = \pi(\eth_{AQ}^2 - \eth_R^2)\varnothing h(\overline{C}_{tw} - \overline{C}_f)(p_i - p);$$

and

$$W_e(ft^3) = V_{pAQ}(\overline{C}_{tw} + \overline{C}_f)(p_i - p) \tag{C.28}$$

The material balance equation can then be written

$$\frac{P}{Z}[1 - \overline{C}_e(p_i - p)] = \left(\frac{P}{Z}\right)_i\left(1 - \frac{G_p}{G}\right) + \left(\frac{P}{Z}\right)_i \frac{W_e}{GB_g} 5.615 \tag{C.29}$$

and simplified in a form where the $\overline{C}_e$ term includes the aquifer contribution to pressure support,

$$\left(\frac{P}{Z}\right)_i \frac{W_e}{GB_g} = \left(\frac{P}{Z}\right)_i \frac{W_e}{G} \frac{T_{sc}}{P_{sc}T} \frac{P}{Z} = \frac{P}{Z} \frac{W_e}{GB_{gi}}$$

$$GB_{gi} = V_{pR}(1 - S_{wi}) = \frac{P}{Z} \frac{V_{pAQ}(\overline{C}_{tw} - \overline{C}_f)(p_i - p)}{V_{pR}(1 - S_{wi})} \tag{C.30}$$

Rearranging, we arrive to the general form of material balance (without water production and gas/water injection terms);

$$\frac{P}{Z}[1 - \overline{C}_e(p_i - p)] = \left(\frac{P}{Z}\right)_i\left(1 - \frac{G_p}{G}\right) \tag{C.31}$$

where

$$\overline{C}_e \equiv \frac{S_{wi}\,\overline{C}_{tw} + \overline{C}_f\left(V_{pNNP}/V_{pR}\right) + \left(V_{pAQ}/V_{pR}\right)\left(\overline{C}_{tw} + \overline{C}_f\right)}{1 - S_{wi}} \tag{C.32}$$

$$M \equiv \frac{V_{pNNP} + V_{pAQ}}{V_{pR}} = \frac{V_{pA}}{V_{pR}} \tag{C.33}$$

and

$$\overline{C}_e \equiv \frac{S_{wi}\,\overline{C}_{tw} + \overline{C}_f\,M\left(\overline{C}_{tw} + \overline{C}_f\right)}{1 - S_{wi}} \tag{C.34}$$

DERIVATION OF BLACK OIL MATERIAL BALANCE

Derivation of Material Balance Equation

Starting derive the material balance equation (MBE) for a black oil system, using the modified formation volume factors introduced in chapter 7 (see Eq. 7.39). The system may be comprised of three zones gas cap, oil zone, and pot aquifer. Phases present consist of hydrocarbon vapor, hydrocarbon liquid, and brine, which are more commonly called free gas, oil, and water. Gas is also looked upon as a component, and may be present either in free form or dissolved in oil and water. Oil and water are not soluble in gas or in each other. A common (average) pressure characterizes all zones and phases.

Since the contribution of water-saturated formation to drive energy may be considerable, the distribution of water in the system is of importance.

First, average connate water saturation may be different in the gas cap and oil zone.

Second, we allow for the presence of a pot or "steady state" aquifer, which is in immediate pressure communication with the hydrocarbon zones. This could be underlying water or simply a small aquifer. In the usual analysis, the energy contribution from a small aquifer might be neglected, but the possibility of high and variable formation compressibility enhances the importance of such a contribution, especially in overpressured systems.

Finally, we will allow for water and gas influx from a "transient" aquifer. Precise treatment of such influx requires separate analysis, which is beyond the scope of this work, but the overall effects are easily included in the general formulation.

The analysis begins by relating the pore volumes of the oil, water, and free gas phases to the total pore volume of the system.

$$NB_{oi} + WB_{wi} + G_{Fi}B_{gi} = V_{psc}B_{fj} \tag{C.35}$$

from which

$$V_{psc} = N\tilde{B}_{oi} + W\tilde{B}_{wi} + G_{Fi}\tilde{B}_{gi} \tag{C.36}$$

After some depletion, influx of water and gas, and shrinkage of pore volume, the following will apply:

$$\left(N - N_p\right)B_o + \left(W - W_p + W_e\right)B_w \\ + \left(G_{Fi} + G_{si} - G_s - G_p\right)B_g \approx V_{psc}B_f \tag{C.37}$$

The term (G_{si}- G_s) represents the difference in solution gas content between initial and current conditions and can be written after combining like terms as

$$G_{si} - G_s = N(R_{si} - R_s) + N_p R_s \tag{C.38}$$

We now go through the algebraic steps of solving Eqn. C.37 for V_{psc}, the equating the result to Eqn. C.36, and then gathering all terms dealing with production or influx on the right hand side of the equation with production while all others are gathered on the left we get:

$$\left(N \left\{ \left[\tilde{B}_o + (R_{sj} - R_s) \right] - \tilde{B}_{oi} \right\} \right) +$$
$$W \left\{ \tilde{B}_w - \tilde{B}_{wi} \right\} + G_{Fi} \left(\tilde{B}_g - \tilde{B}_{gi} \right)$$
$$=$$
$$N_p \left(\tilde{B}_o - R_s \tilde{B}_g \right) +$$
$$(W_p - W_e) \tilde{B}_w + G_p \tilde{B}_g \tag{C.39}$$

we can define a modified two-phase formation volume factor by dividing the standard two phase factor by B_t

$$\tilde{B}_t = \tilde{B}_o + (R_{si} - R_s) \tilde{B}_g \tag{C.40}$$

Note that $\tilde{B}_{ti} = \tilde{B}_{oi}$

A final step to reach the form desired requires relating W and G_{Fi} to N. We define two quantities

F_{gc} = Pore volume ratio, gas cap/oil zone

F_{pa} = pore volume ratio, pot aquifer/oil zone

Then

$$B_{ti} V_{psc} = \frac{N B_{oi}}{1 - S_{wi}} \left[1 + F_{gc} + F_{pa} \right] \tag{C.41}$$

and the pore volume of water can be found by multiplying each of the terms within brackets by the appropriate water saturation for each zone:

$$B_{wi} W = \frac{N B_{oi}}{1 - S_{wi}} \left[S_{wi} + F_{gc} S_{wgi} + F_{pa} \right] \tag{C.42}$$

After division by B_{ti}, substitutions and rearrangement:

$$W = \frac{N\,\tilde{B}_{ti}}{B_{wi}}\left[\frac{S_{wi} + F_{gc}S_{wgi} + F_{pa}}{1 - S_{wi}}\right] \tag{C.43}$$

For free gas

$$G_{Fi} = \frac{N\,\tilde{B}_{ti}}{B_{gi}}\left[\frac{F_{gc}\left(1 - S_{wgi}\right)}{1 - S_{wi}}\right] \tag{C.44}$$

When the appropriate substitutions are made in Eqn. C.41, the final result is:

$$N = \frac{N_p\left(\tilde{B}_o - R_s\,\tilde{B}_g\right) + \left(W_p - W_e\right)\tilde{B}_w + G_p\,\tilde{B}_g}{\tilde{B}_{ti}\left\{\left(\dfrac{\tilde{B}_t}{\tilde{B}_{ti}} - 1\right) + \left[\dfrac{S_{wi} + F_{gc}S_{wgi} + F_{pa}}{1 - S_{wi}}\right]\left(\dfrac{\tilde{B}_w}{\tilde{B}_{wi}} - 1\right) + \left[\dfrac{F_{gc}\left(1 - S_{wgi}\right)}{1 - S_{wi}}\right]\left(\dfrac{\tilde{B}_g}{\tilde{B}_{gi}} - 1\right)\right\}} \tag{C.45}$$

while the preceding equation is a very general form, it does require a calculation of W_e by other means, In addition, using the produced gas oil-ratio

$$R_p = G_p / N_p \tag{C.46}$$

we can rearrange terms to yield:

$$N = \frac{N_p\left[\tilde{B}_t + \left(R_p - \tilde{B}_{si}\right)\tilde{B}_g\right] + \left(W_p - W_e\right)\tilde{B}_w}{\tilde{B}_{ti}\left\{\left(\dfrac{\tilde{B}_t}{\tilde{B}_{ti}} - 1\right) + \left[\dfrac{S_{wi} + F_{gc}S_{wgi} + F_{pa}}{1 - S_{wi}}\right]\left(\dfrac{\tilde{B}_w}{\tilde{B}_{wi}} - 1\right) + \left[\dfrac{F_{gc}\left(1 - S_{wgi}\right)}{1 - S_{wi}}\right]\left(\dfrac{\tilde{B}_g}{\tilde{B}_{gi}} - 1\right)\right\}} \tag{C.47}$$

The numerator is sometimes referred to as the "expanded net=production-plus-excess-gas" formulation.

For gas reservoirs with associated aquifers, the same approach may be used to derive the analog of Eqn. C.45.

$$G_{Fi} = \frac{G_p\,\tilde{B}_g + \left(W_p - W_e\right)\tilde{B}_w}{\tilde{B}_{gi}\left\{\left(\dfrac{\tilde{B}_g}{\tilde{B}_{gi}} - 1\right) + \left[\dfrac{S_{wi} + F_{pa}}{1 - S_{wi}}\right]\left(\dfrac{\tilde{B}_{wt}}{\tilde{B}_{wti}} - 1\right)\right\}} \tag{C.48}$$

The terms appearing In the denominator of the Eqns. C.45, C.47, and C.48 are worthy of examination. Each of the terms $\left[\left(\tilde{B}_J \big/ \tilde{B}_{ji}\right) - 1\right]$ represents the expansion of a unit volume of initial fluid, including its dissolved gas, and the contraction of its associated pore space. The factors which multiply $\left[\left(\tilde{B}_J \big/ \tilde{B}_{ji}\right) - 1\right]$ are volume ratios at initial conditions for (water/oil), (free gas/oil) or (water/free gas); the multiplier for the first term is unity of course since the analysis is based on a unit of either oil or of free gas.

The water term is often neglected in material balance formulations, but it should not be. In the general form shown here, its significance becomes more obvious, especially in overpressured reservoirs where formation and gas or oil compressibilities can be comparable in magnitude. The water term may in fact be dominant for quite modest values of $F_{pa.}$

This can be demonstrated by noting that

$$\ln \tilde{B}_w - \ln B_w - \ln B_t$$

and taking the derivative and rearranging:

$$\left(\tilde{B}_w \big/ \tilde{B}_{wi}\right) = e^{\overline{C_w + C_f}(Pi - P)}$$

The exponent is small, since compressibilities are typically 10^{-6} (psi) in order of magnitude while pressure changes are 10^{+3} in magnitude, so:

$$\left(\tilde{B}_w \big/ \tilde{B}_{wti}\right) \doteq 1 + \overline{C_w + C_t}\left(P_i - P\right)$$

or

$$\left(\frac{\tilde{B}_w}{B_{wi}} - 1\right) \doteq \overline{C_w + C_t}\left(Pi - P\right) \tag{C.49}$$

Similar expressions may be developed for oil and its dissolved gas, and also for free gas, and the pore space associated with each.

Some order of-magnitude calculations can now be made. If we choose a system at 10,000 psi and 225°F as typical of an overpressured reservoir setting with a weakly consolidated or unconsolidated formation, we can estimate:

$C_w = 3(10^{-6})\text{psi}^{-1}$ (Osif, 1984)

$C_g = 37(10^{-6})\text{psi}^{-1}$ (Bradley, 1987)

$C_f(\text{frbl}) = 10(10^{-6})\text{ps}i^{-1}$ (friable sand)

$C_f(\text{uc}) = 35(10^{-6})\text{psi}^{-1}$ (unconsoli dated sand)

it follows that

$C_w + C_f(\text{frbl}) = 13(10^{-6})\text{psi}^{-1}$

$C_w + C_f(\text{uc}) = 38(10^{-6})\text{psi}^{-1}$

Compared to

$C_g + C_f(\text{frbl}) = 47(10^{-6})\text{psi}^{-1}$

$C_g + C_f(\text{uc}) = 72(10^{-6})\text{psi}^{-1}$

Thus, the unit expansibility of water and its pore space is nearly 30 % of that of gas and its pore space for weakly consolidated sand and over 50% for unconsolidated sand. if $S_{Wi} = 0.2$, the water term appearing in the denominator of Eqn. C.47, for gas reservoirs, will dominate if $F_{pa} > 2.7$ for a weak sand and for $F_{pa} > 1.3$ for an unconsolidated sand. For oil reservoirs, an estimate of two-phase compressibility will be system-specific, but we can reasonably argue that it will be less than gas compressibility. The water term will then exceed the oil term at even lower values of Fpa.

While the preceding development aimed to illustrate the need to account for water-bearing formation in material balance analysis, the key issue is actually the high formation compressibility. In the example, formation compressibility contributes over 20 percent of the expansion energy associated with gas-bearing rock, and over 75 percent of the energy associated with water bearing rock for weak formations. For unconsolidated formation, formation compressibility contributes nearly 50% of the energy associated with gas-bearing reserves. Formation compressibility effects should be included, and water-bearing rock should not be ignored, even though its total volume may appear to be quite modest.

These facts have long been recognized in analyzing performance of overpressured gas reservoirs [Hammerlindl, 1971; Bass, 1972]. However, these and other investigators [Ramagost and Farshad, 1981; Bernard, 1987] have suggested only approximations for dealing with the problem. The formulation proposed here is by Yale [1993], explicitly includes the effects of all contributing fluids and their assonated pore space, and has the added attraction of allowing variable compressibilities to be included with relative ease.

The Material Balance Equation (MBE) presented in Eqns. C.45 and C.48, is more comprehensive than those usually presented, but it has the same format except for the use of the modified formation volume factors $\tilde{B}_{o,w,g}$ in place of the $B_{o,w,g}$. The modified fluid formation (volume factors) can be calculated independently as a pre-analysis step and used in place of the usual fluid volume factors in MBE's in current use. It is readily apparent this MBE formulation will reduce to conventional presentations of the MBE [see, for example, Dake, 1978; Bradley, 1987] if appropriate simplifying assumptions are made.

As an example, consider the gas material balance Eqn. C.48. If we divide both numerator and denominator on the right hand side by $\tilde{B}_g$, solve the resulting expression for $\dfrac{1}{\tilde{B}_g}$ and then substitute $B_g\left(\dfrac{P}{Z}\right) = \text{constant} * \left(\dfrac{1}{\tilde{B}_g}\right)$, we obtain, after some algebra

$$\left(\frac{P}{Z}\right)\left\{\frac{B_f}{B_{fi}}\left[\frac{F_{pa}+1}{1-S_{wi}}\right] - \frac{B_{wt}}{B_{wti}}\left[\frac{F_{pa}+S_{wi}}{1-S_{wi}}\right]\right\} =$$
$$\left(\frac{P}{Z}\right)_i - \left(\frac{1}{G_{Fi}}\right)\left(\frac{P}{Z}\right)_j\left\{\left(G_p\right)+\left(W_p-W_e\right)\left(\frac{B_w}{B_g}\right)\right\} \tag{C.50}$$

If we assume $W_e = 0.0$, then $G_{Fi} = G$. We also introduce the approximations:
$$B_f = B_{fi}\left[1-C_f\left(Pi-P\right)\right]$$
$$B_w = B_{wi}\left[1-C_w\left(Pi-P\right)\right]$$

where C_f and C_w, are taken to be small and constant, The equation which ultimately results is:

$$\left(\frac{P}{Z}\right)\left[1-\frac{C_w\left(F_{pa}+S_{wi}\right)+C_f\left(F_{pa}+2\right)}{1-S_{wi}}\left(Pi-P\right)\right]$$
$$= \left(\frac{P}{Z}\right)_J - \left(\frac{1}{G}\right)\left(\frac{P}{Z}\right)_J\left(G_p+W_p\frac{B_w}{B_g}\right) \tag{C.51}$$

The preceding equation is that developed by Bass [1972]. If, $F_{pa} = 0$ and $W_p = 0$, then:

$$\left(\frac{P}{Z}\right)\left[1-\frac{\left(C_f+C_wS_{wi}\right)\left(Pi-P\right)}{1-S_{wi}}\right] = \left(\frac{P}{Z}\right)_J - \left(\frac{G_p}{G}\right)\left(\frac{P}{Z}\right) \tag{C.52}$$

which was proposed by Ramagost and Farshad [1981].

Any one of the Eqns. C.50 through C.52 can be plotted as "corrected" $\frac{P}{Z}$ versus "corrected" G_p and the line extrapolated to an intercept to estimate G_{Fi} or G, provided of course that F_{pa} can be estimated with sufficient accuracy to allow an accurate correction to be calculated. Eqn. C.50 has an advantage for cases where Influx can reasonably be taken as zero, and the overpressured gas reservoir may well fit this case. Since all variable effects are properly allowed for, F_{pa} may be determined by trial and error as the value, which leads to the best straight-line fit of the pressure and production data. Eqns. C.51 and, C.52 are not suitable; since C_f will in fact change rather rapidly as $(P_i - P)$ increases.

BIOGRAPHICAL SKETCH

Ali Ahmed Jalalh graduated in 1989 as a geologist from Sebha University, Libya. He then worked as a petrophysicist in Agip Oil Co. Ltd. in Libya from 1990-2001. He got his MSc in geophysics from AGH University of Science and Technology, Krakow, Poland in 1997 and his MSc in petroleum engineering from Miskolc University, Hungary, in 1999.

Ali Jalalh is a professional petroleum geologist and consulting engineer with a strong reservoir/petroleum engineering background and knowledge of Oil and Gas E&P, who integrates geosciences and engineering data to maximize asset value. He is well versed in Geoframe using ELAN and experienced in design, coordinating and overseeing drilling work, production, completion and concentric operations. He has done extensive work on carbonate and sandstone reservoir rocks and directional and horizontal well technology.